

https://dspace.org/

Beneficiation of fine ores using the Longi wet high magnetic separator

Makhula, Mpho Johanna

2014
http://hdl.handle.net/10539/18081

Downloaded from a DSpace repository. https://dspace.org/

BENEFICIATION OF FINE ORES USING THE LONGI WET HIGH MAGNETIC SEPARATOR

Mpho Johanna Makhula

A Dissertation submitted to the Faculty of Engineering and the Built Environment, University of the Witwatersrand, in fulfilment of the requirements of the degree of Master of Science in Engineering.

Johannesburg, 2014

ABSTRACT

Magnetic separation has been used since 1955 for processing a variety of minerals from iron ore in steel production to the desulphurisation of coal. The accumulation of such fines and slimes during mining operations and the increasing global demand for quality products motivated the use of the semi-continuous pilot wet high intensity magnetic separator (WHIMS) introduced in 2008. Its unique features were considered to be favourable for beneficiating a Sishen low grade hematite-rich ore and an ash-rich Witbank coal.

An automated Mineral Liberation Analyser (MLA) was used to characterise the size distribution of the hematite-rich material thereby providing an estimated grade at the same time. This type of analysis characterises mineral types in terms of particle size and elemental composition, specific density, weight percent, area of particle, particle shape, circularity and equivalent circle diameter. However, for this research study only size and elemental composition were considered.

The application of the Longi LGS 500 WHIMS for beneficiating a low grade South African iron ore material was investigated by determining the effects of changing the operating parameters of pulp solids, magnetic field intensity and the pulsation frequency. This was followed by a 3^3 full factorial design which consisted of twenty seven (27) test matrix, with mass yield of concentrate and Fe grade selected as the main responses to the changing of the parameters. The results obtained were validated using the analysis of variance (ANOVA) and the mathematical model, which showed the variables as being significant to the investigation process, thus rejecting the null hypothesis. The significance of the variables was in the order of magnetic field intensity followed by pulsation frequency and lastly the percentage pulp solids. The model predictions and actual data were in good agreement, reporting regression coefficients ranging between 0.83 and 0.94. It was shown that a single stage magnetic separation has the potential to produce a 55% Fe product.

DECLARATION

I declare that the dissertation is my own unaided work. It is being submitted for the Degree of Master of Science in the University of Witwatersrand, Johannesburg. It has not been submitted before for any degree or examination in any other University.

Mpho J. Makhula

29/09/2014

Mpho J. Makhula

Date

DECLARATION

I declare that the dissertation is my own unaided work. It is being submitted for the Degree of Master of Science in the University of Witwatersrand, Johannesburg. It has not been submitted before for any degree or examination in any other University.

....

Mpho J. Makhula Date

DEDICATION

This dissertation is dedicated to the Almighty God and Makhula family.

ACKNOWLEDGEMENTS

I would like to express my sincere gratitude to my supervisor Prof. R.M.S Falcon, thank you for giving me the opportunity to work with you, for your encouragement, your constructive suggestions and support throughout the research. I thank you for always making time to see me, even in your busy schedule. Mr C.P Bergmann for the support you have shown me, your encouragement, your insight and guidance and going beyond the call of duty in ensuring that the funds for the research are available. Dr. S.O Bada, thank you for sacrificing your time in teaching and guiding me throughout the research, insightful and constructive criticisms, your patience, and for ensuring that the experiments and writing of this dissertation are completed. I thank Mintek for funding the research.

I would also like to thank a special set of people for sacrificing their time in assisting me with the experiments: Sipho Mabuza, Unathi Mqala, Lawrence Ndouvhada, Albert Nkonde and Carla da Corte. Gravmax for allowing us to conduct tests at your premises and sharing your technical knowledge.

A special thank you and love to my parents, Mr Samson Makhula and Mrs Maria Makhula and my two brothers Lebohang and Sibusiso Makhula for their support.

TABLE OF CONTENTS

ABSTRACT i

DECLARATION ii

DEDICATION iii

ACKNOWLEDGEMENTS iv

TABLE OF CONTENTS v

LIST OF TABLES viii

LIST OF SYMBOLS xii

LIST OF ACROMYNS xiv

1. INTRODUCTION AND MOTIVATION 1

1.1. Justification of the investigation 3

1.2. Problem Statement 3

1.3. Hypothesis 4

1.4. Objectives of the research 4

1.5. Layout of the thesis 5

2. Literature Survey 6

2.1 Principles of magnetic separation 6

2.2 Classification of materials 9

2.3 Background and Related Work 10

2.4 The history of the development of the magnetic separator 12

2.4.1 Dry Magnetic Separators 13

2.4.1.1 Previous work conducted using dry magnetic separators 16

2.4.2 Wet High Intensity Magnetic Separators (WHIMS) 17

2.4.2.1 Previous work conducted using WHIMS 19

2.5 Modelling of high intensity magnetic separation 22

2.5.1 Analysis Of Variance 23

2.6 Longi LGS 500 24

2.7 Summary 26

3 Material and Methodology 27

3.1. Material 27

3.1.1 Sample Preparation (ISO 3082:2009) 30

3.1.1.1 Iron ore sample preparation 30

3.1.1.2 Coal ore sample preparation 30

3.1.1.3 The operation of the HPGR and the Jones's splitter 31

3.2. Iron ore analyses 32

3.2.1 X -Ray Diffraction (XRD, ISO 17025) 32

3.2.2 Mineral Liberation Analyser (MLA, ISO 17025) 32

3.2.3 Particle Size Distribution on the -1.18 m iron material (PSD, ISO 2395-1990) 33

3.2.4 Particle Size Distribution on the coal material (PSD, ISO 2395-1990) 33

3.2.5 X-ray Fluorescence (XRF, ISO 9001 & ISO 14001) 34

3.2.6 Induced Coupled Plasma Emission Spectroscopy (ICP-OES, ASD-MET-OES-SP005) 34

3.3. Coal analysis 34

3.3.1 Thermogravimetric Analysis (TGA, ASTM D-5142) 34

3.4. Experimental Methods 35

3.4.1 Beneficiation Studies using the Longi LSG 500 Wet High Intensity Magnetic Separator 35

3.4.2 A representation of Longi LGS 500 WHIMS 35

3.5. Comparison testwork with Eriez Wet High Intensity Magnetic Separator (WHIMS) 39

4. RESULTS AND DISCUSSION 40

4.1. Characterisation: Particle Size Distribution for Iron Ore 40

4.2. Scanning Electron Microscope on Iron ore 45

4.3. Head Grade Determination of iron ore feed 46

4.4. X-ray Diffraction 47

4.5. Wet High Intensity Magnetic Separation (Longi LGS 500): Iron ore material 51

4.5.1 Effects of pulp solids 51

4.5.2. Effects of magnetic field intensity 54

4.5.3 Effects of pulsation frequency 58

4.6. Laboratory scale Eriez WHIMS: Iron ore material 61

4.7. Wet High Intensity Magnetic Separation (Longi LGS 500): Coal material 63

4.7.1. Particle Size Distribution Analysis 64

4.8. Analysis of Variance (ANOVA): Statistical analysis 65

4.8.1. Interaction effects 66

4.8.2. The mathematical model 68

4.9. Summary 71

5. CONCLUSION 73

6. RECOMMENDATIONS 75

7. REFERENCES 76

8. APPENDICES 81

8.1. Appendix A: Effects of changing the pulp solids 81

8.2. Appendix B: Effects of changing the magnetic field intensity 83

8.3. Appendix C: Effects of changing pulsation frequency 85

8.4. Appendix D: Regression coefficient data 87

LIST OF TABLES

Table 4-1: PSD determined from SEM analysis for the -1.18 mm 41

Table 4-2: PSD determined from sieve stacking analysis for the -1.18 mm 41

Table 4-3: PSD determined from SEM analysis for the -1000+106 μm size fraction 43

Table 4-4: PSD determined form SEM analysis for the -106+75 μm size fraction 43

Table 4-5: PSD determined form SEM analysis for the -75 μm size fraction 44

Table 4-6: Head grade from the individual size fractions as determined by XRF analysis 47

Table 4-7: Eriez WHIMS results on the -1000+106 μm 62

Table 4-8: Eriez WHIMS results on the -106 +75 μm 62

Table 4-9: Eriez WHIMS results on the -75 μm 62

Table 4-10: Magnetic separation 1st test over 30 seconds retention time 63

Table 4-11: Magnetic separation 2nd test over 1 minute retention time 63

Table 4-12: Particle size distribution from the 1st test 64

Table 4-13: Particle size distribution from the 2nd test 64

Table 4-14: Longi LGS 500 unit parameters 65

Table 4-15: Full factorial design (3^3) investigation matrix on the Longi LGS 500 unit 65

Table 4-16: ANOVA output for mass yield of concentrate 66

Table 4-17: ANOVA output for Fe grade 67

Table 4-18: ANOVA summary output data for mass yield 67

Table 4-19: ANOVA summary output data for Fe grade 67

Table 8-20: -1000+106 μm at 20% pulp solids 81

Table 8-21: -1000+106 μm at 25% pulp solids 81

Table 8-22: -1000+106 μm at 30% pulp solids 81

Table 8-23: -106+75 μm at 20% pulp solids 81

Table 8-24: -106+75 μm at 25% pulp solids 82

Table 8-25: -106+75 μm at 30% pulp solids 82

Table 8-26: -75 μm at 20% pulp solids....82
Table 8-27: -75 μm at 25% pulp solids....82
Table 8-28: -75 μm at 30% pulp solids....82
Table 8-29: -1000+106 μm at 1000 Gauss....83
Table 8-30: -1000+106 μm at 5500 Gauss....83
Table 8-31: -1000+106 μm at 10000 Gauss....83
Table 8-32: -106+75 μm at 1000 Gauss....83
Table 8-33: -106+75 μm at 5500 Gauss....83
Table 8-34: -106+75 μm at 10000 Gauss....84
Table 8-35:-75 μm at 1000 Gauss....84
Table 8-36: -75 μm at 5500 Gauss....84
Table 8-37: -75 μm at 10000 Gauss....84
Table 8-38: -1000+106 μm at 6.5 Hz....85
Table 8-39: -1000+106 μm at 19.5 Hz....85
Table 8-40: -1000+106 μm at 25.2 Hz....85
Table 8-41: -106+75 μm at 6.5 Hz....85
Table 8-42: -106+75 μm at 19.5 Hz....85
Table 8-43: -106+75 μm at 25.2 Hz....86
Table 8-44: -75 μm at 6.5 Hz....86
Table 8-45: -75 μm at 19.5 Hz....86
Table 8-46: -75 μm at 25.2 Hz....86
Table 8-47: Model output for Fe grades....88
Table 8-48: Model output for SiO_2 grades....89
Table 8-49: Model output for Fe recovery....90
Table 8-50: Model output for SiO_2 recovery....91

LIST OF FIGURES

Figure 2-1: Schematic representation of forces acting upon a particle (Svoboda et al., 2003) .7

Figure 2-2: Longi LGS 500 (Longi Magnet Co. LTD, 2010).....25

Figure 3-1: Sample preparation for the hematite material 28

Figure 3-2: Sample preparation for the coal material 29

Figure 3-3: Longi LGS 500 (Longi Magnet Co. LTD, 2010).....36

Figure 3-4: Top view of the Longi LGS 500 (Mintek, 2014).....37

Figure 3-5: Front view of the Longi LGS 500 (Mintek, 2014).....37

Figure 3-6: Side view of the Longi LGS 500 (Mintek, 2014) 38

Figure 3-7: Side view of the Longi LGS 500 (Mintek, 2014) 38

Figure 4-1: SEM and Sieve stacking particle size distribution results 42

Figure 4-2: BSE image from the -1000 μm feed 45

Figure 4-3: BSE image from the -1000 +106 μm feed 45

Figure 4-4: BSE image from the -106 +75 μm feed 46

Figure 4-5: BSE images from the -75 μm feed.....46

Figure 4-6: XRD patterns for the -1000+106μm feed and the different Longi magnetic separation products 48

Figure 4-7: XRD patterns for the -106+75μm feed and the different Longi magnetic separation products. 49

Figure 4-8: XRD patterns for the -75μm feed and the Longi magnetic separation products ..50

Figure 4-9: Effects of changes in pulp solids for the -1000+106 μm size fraction 52

Figure 4-10: Effects of changes in pulp solids for the -106+75 μm size fraction 52

Figure 4-11: Effects of changes in pulp solids for the -75 μm size fraction.....53

Figure 4-12: Effects of changes in magnetic field intensity for the -1000+106 μm size fraction 55

Figure 4-13: Effects of changes in magnetic field intensity for the -106+75 μm size fraction 55

Figure 4-14: Effects of changes in magnetic field intensity for the -75 μm size fraction 56

Figure 4-15: Effects of changes in pulsation frequency for the -1000+106 μm size fraction .58

Figure 4-16: Effects of changes in pulsation frequency for the -106+75 μm size fraction 59

Figure 4-17: Effects of changes in pulsation frequency for the -75 μm size fraction 59

Figure 4-18: Mass yield relationship between the model and actual data for the treatment of the -1000+106μm fraction 68

Figure 4-19: Mass yield relationship between the model and actual data for the treatment of the 106+75μm fraction.....69

Figure 4-20: Mass yield relationship between the model and actual data for the treatment of the -75 μm fraction.....69

Figure 4-21: Fe grade relationship between the model and actual data for the treatment of the -1000+106 μm fraction 70

Figure 4-22: Fe grade relationship between the model and actual data for the treatment of the -106+75μm fraction 70

Figure 4-23: Fe grade relationship between the model and actual data for the treatment of the -75 μm fraction 71

LIST OF SYMBOLS

a	The radius on the spherical magnetic collector
F_m	Magnetic force
F_d	Hydro dynamic drag force
F_g	Force of gravity (m/s)
H	Magnetic field (Am^{-1})
H_o	Applied magnetic field
V	Particle volume (m^3)
$\emptyset$	Potential
J	Magnetic polarisation of a particle (T)
χ	Magnetic susceptibility
μ_m	Permeability of free space
μ_o	Constant
r	Position of a particle (m)
v	Velocity of a particle (m/s)
B	Magnetic induction
I_s	Saturation polarisation of the matrix material
A	Hamaker constant
b	The particle radius
h	The distance between the surfaces of two interacting bodies

(L_{ijk}).	Transfer coefficients known as
(i),	The transferring particle size
(j)	Magnetic susceptibility or specific gravity
(k)	The output flow stream of the separator
S_i	Particle size
a	The constant related to the type of matrix utilised
$P1$	Model parameter
C	The scaling coefficient
df	Degree of freedom
MS	Mean square
F value	Calculated F value
Fcritical	Theoretical F value
T	Tesla
G	Gauss
1T	10^4 Gauss

LIST OF ACROMYNS

ANOVA	Analysis of Variance
ASTM	American Society for Testing and Materials
Bt	Billion tonnes
DRI	Direct Reduced Iron
ECD	Equivalent Circle Diameter
HGMS	High Gradient Magnetic Separator
HPGR	High Pressure Grind Roller
ICP-OES	Induced Coupled Plasma Emission Spectroscopy
ISO	International Organisation for Standardisation
MLA	Mineral Liberation Analyser
Mt	Million tonnes
ROM	Run Of Mine
SEM	Scanning Electron Microscope
SLon (VPHGMS)	Vertically Pulsating High Gradient Magnetic Separator
SOS	Sum Of all Squares
TGA	Thermogravimetric Analysis
VMS	Vertical Magnetic Separator
WHIMS	Wet High Intensity Magnetic Separator
XRD	X-ray Diffraction
XRF	X-ray Florescence

Chapter 1

1. INTRODUCTION AND MOTIVATION

The production of iron ore is largely used to meet the increase in the global demand for steel and pig iron. An estimated 1.5 billion tonnes (Bt) of steel were produced globally in 2011 of which 683 million tonnes (Mt) was produced in China (Kumba, 2012). The increased rate in world steel production which is driven largely by construction growth in China and Middle East including India has resulted in demand for high grade iron ore. The escalating economic growth within these regions has resulted in the depletion of the more economic mineral ore deposits. Newer ore bodies, therefore require more processing which is accompanied by issues such as fines generation.

The conventional method for processing hematite iron ore is by crushing the run of mine (ROM) material to <40 mm size fraction followed by scrubbing and/or wet screening at 10 mm to generate -40+10 mm fraction (Mohanty *et al.*, 2010). The -10+0.15 mm and -0.15 mm size fractions are usually classified as fines and slimes respectively. The slimes generated have been traditionally regarded as waste and usually dumped into slime ponds. The rejection of these slimes is considered a loss and additionally harmful to the environment. In many instances, the iron ore slimes are found to have high aluminium content with valuable Fe grade in ranges >50% (Mohanty *et al.*, 2010). In addition, in coal mining and processing a huge accumulation of coal fines (<1 mm) are generated from mechanised mining and washing operations, with over 12% of the South African (SA) annual ROM material reporting to tailing dumps (England *et al.*, 2000). Therefore, given the unused value in these materials it was paramount to exploit alternative beneficiation techniques to further increase the yields and quality of the fine fractions of both iron ore and coal in South Africa.

Numerous magnetic separation techniques (dry or wet) have been developed over the years to meet the requirement of the mineral processing industry for the concentration of different ores based on such parameters as the magnetic susceptibility differences in particles, the generation of higher magnetic field and the design of the separator (Dahe *et al.*, 1998; Svoboda, 2001; Augusto *et al.*, 2002; Hoffmann and Franzreb, 2002; Zheng and Dahe, 2003; Liu, 2007; and Dobbins and Sherrell, 2009). For example, the difference in the magnetic properties of minerals and the separation of gangue from a low grade iron ore using wet high

intensity magnetic separation (WHIMS) was demonstrated by Angadi *et al.* (2012), while the removal of gangue from ore to enhance the quality of the low grade ores was obtained by Das *et al.*, (1991); Song *et al.*, (2002); Arol, (2004); Dobbins *et al.*, (2007); Jamieson, *et al.*, (2006) and Padmanabhan and Sreenivas, (2011). Grade concentrates suitable for blast furnace application were also obtained from a low grade ore by Al-Wakeel and El-Rahman, (2006). Fine and super fine bauxite were treated under magnetic separation with a potential aluminium recovery of about 90% (Kahn *et al.*, 2003) while magnetic separation was also used for water treatment and metal removal (Augusto *et al.*, 2005; and Yavuz *et al.*, 2006a) as well was integrated in the heavy mineral process flow-sheet and for biotechnological applications (Yavus *et al.*, 2009 and Joseph *et al.*, 2010).

In this research study, a new magnetic separation technique as reported in The ASIA Miner report (2010) and developed in China, was used for the beneficiation of hematite-rich ore and coal. The equipment relies on its high intensity magnetic capability designed to attract materials with weakly magnetic attributes (The ASIA Miner report, 2010). It is composed of a corrosion resistant stainless steel rod matrixes constituting of 12% to 18% chromium content. The higher the chromium content, the more resistant the matrixes are to corrosion. The equipment was designed based on magnetic jigging principles similar to a SLon, a vertical ring and pulsating high gradient magnetic separator (VPHGMS), where the pulsation mechanisms assist in improving separation efficiency. This is achieved by agitating the slurry and keeping the particles loose in order to minimise particle entrapment thus creating more surfaces for collection of particles. Theoretically, this principle allows the separation of mixtures with small difference in density and small difference in magnetic susceptibility. Through the application of this new technique the extraction of valuable particles from previously discarded fines and slimes dumps which previously were found not to be cost-effectively viable for beneficiation, could become a feasible option. In addition, the fines generated during the mining of iron ore could be beneficiated further to generate direct reduced iron (DRI) feed material (Hearn and Dobbins, 2007) whilst coal, manganese and chromite found with gangue minerals containing iron phases could also be separated using this approach.

With all the aforementioned positive attributes of this WHIMS technique, the two ores investigated in this research study were subjected to magnetic separation by varying

operating parameters, with the aim of determining the optimum process conditions for maximum grade and recovery achievable for each type of ore.

1.1. Justification of the investigation

In 2013, an estimated 180 Mt of iron ore slimes were generated from Sishen mine and in general such slimes may still contain valuable minerals which could be added revenue to the economy (www.bdlive.co.za, excessed November 28, 2014). It was noted that, in most cases the dumped fines and slimes were not stored in lined or covered dams and were a source of extensive dust, soil and water pollution. For this reason, it was proposed that the new magnetic separator be used in this investigation as means (i) to curb the existing problems of such materials by treating the slimes and (ii) in order to beneficiate and extract the valuable products stored in them. In addition, since limited work has been reported using this magnetic separation technique in South Africa or on South African materials, it was believed that an in depth investigation was worth conducting.

1.2. Problem Statement

The magnetic separation technique employed in this research study on iron ore and on coal was dependent on their magnetic susceptibility and size distribution.

A potential problem with traditional WHIMS occurs when gangue particles are entrapped and clog at the collection point (matrix). Magnetic separation becomes ineffective when particles agglomerate on the matrix and some shutdown time is necessary in order to aggressively clean the matrix. Introducing wash water was proven to reduce the clogging of the matrix by washing off all diamagnetic particles (Hearn and Dobbins, 2007).

Another proposed solution to overcome particle entrapment, more so in fine size fractions, is to use the pulsating mechanism of the Longi LGS 500 to keep the particle loose and keep the matrix clean to create enough surface area for particles to attach to it.

Taking into account the previous experience of others, additional operating parameters such as the percentage pulp solids were investigated to improve the grade and recovery in the current study. The physical properties of the minerals, chemical composition, and mineralogical content were used in understanding their response to magnetic separation. This

research therefore focused on beneficiating the different minerals with the Longi LGS 500 by determining the optimum parameters based on the particle size fractions, percentage pulp solids, magnetic field intensity and pulsating frequency.

1.3. Hypothesis

The newly developed WHIMS (Longi LGS 500) uses the fundamental principle of magnetic separation along with an additional operation, namely a pulsation mechanism for effective particle beneficiation. The individual variables of pulp solids, magnetic field intensity and pulsation frequency were investigated in this research study, together with their effect on the mass yield of the concentrate and iron grade. The null hypothesis is therefore: that the addition of a pulsating mechanism does not improve the WHIMS performance in terms of mass yield of concentrate, Fe grade and Fe recovery.

1.4. Objectives of the research

The objective was to characterise the performance of the Longi LGS 500 by determining grade and recovery curves of the two materials by considering the following:

- Mineralogical investigations to determine mineral constituents, and particle size to effect mineral liberation.
- Magnetic separation tests using the Longi LGS 500 by varying the equipment's parameters and determine the responses of these minerals under different conditions.
- Determination of the optimum operating conditions/parameters from the results obtained.
- Establishing the grade and recovery under these conditions.
- Under these conditions, establishing whether quality (grades and recovery) products from the materials tested could be achieved by using narrow or wide ranges of size distribution in the Longi LGS 500.

1.5. Layout of the thesis

- Chapter one provides an introduction and motivation for this research with a summary of its objectives.

- Chapter two comprises of the literature review. In this section the principles of magnetic separation will be discussed, including the different types of wet high intensity magnetic separators (WHIMS) available, the history thereof and previous work conducted on the different WHIMS technologies.

- Chapter three discusses in detail the experimental methodologies. This outlines sample preparation methods, from grinding of the coarse material to fine size fractions of -1.18 mm and treatment batch wise in the Longi LGS 500 and Eriez laboratory magnetic separator which is representative of a single set of matrix from the Jones pilot separator. From the hematite-rich ore results, the optimum conditions were then used for treating the coal material in the -212 μm size fraction.

- Chapter four reports and discusses the results obtained from the mineralogy of the iron ore and the magnetic separator investigations on the two materials. The iron ore data obtained under the variable test conditions was then verified statistically using the analysis of variance (ANOVA).

- Chapter five outlines the conclusions drawn based on the overall results obtained.

- Chapter six contains the recommendations.

Chapter 2

2. Literature Survey

2.1 Principles of magnetic separation

Magnetic separation is based on the difference in the magnetic susceptibility of materials. To some degree, all materials respond to an external applied magnetic field, which is the basis for achieving separation between particles. The separation may be aimed at purifying feed materials like kaolin from iron impurities, or beneficiating materials such as iron ore from quartz (Dobbins *et al.*, 2007; Linkun and Yun, 2010, Chen *et al.*, 2012). A separation is achieved when the magnetic force attained is greater than other competing forces, for example, the force of gravity largely acts upon coarse particles, while frictional force, attractive or repulsive force, surface and hydrodynamic drag force predominantly act upon fine particles. These forces are shown in Figure 2-1. The magnitude of these forces, their nature or the characteristic of the material to be treated together with the design of the equipment determines the efficiency in separation. The nature of the material includes its particle size and magnetic susceptibility, while the equipment's variable parameters include the magnitude of the magnetic field and its capacity, matrix material and type, and rotation speed of the rotor. These form part of the equipment's design. The magnetic force or field gradient used in the separation of materials can be generated through different methods. It can be achieved through the application of a permanent magnet, an electromagnet with an iron yoke, a solenoid or a superconducting magnet which differs in magnetic field geometries and magnitude. The different types of the magnetic separators are discussed in section 2.4. Based on the difference in the mechanism by which magnet magnetic fields are generated, the efficiencies of separation also differ. One way to measure the efficiency is through the determination of grade quality and the quantity equated to recovery, achieved under the different techniques (Oberteuffer, 1974; Chakravorty, 1989).

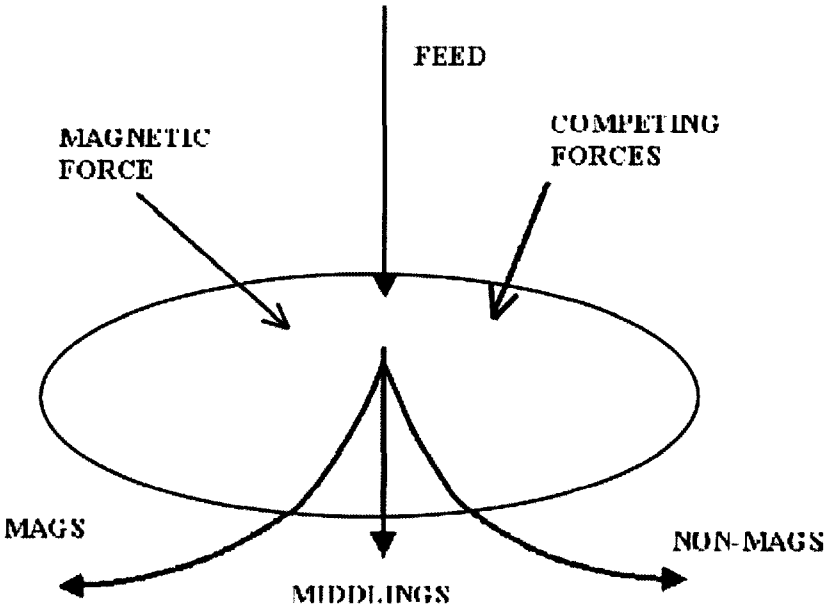

Figure 2-1: Schematic representation of forces acting upon a particle (Svoboda et al., 2003)

The principles of magnetic separation are such that when particles of different magnetic susceptibility are placed in a magnetic field, they tend to disrupt the direction or the flow of the magnetic field and at the same time lead to the particles being magnetically induced. Hence, the induced field experienced by the particles determines which direction each of the particles will be deflected, leading to a separation. For example, a paramagnetic particle in a vacuum will experience a magnetic force generally expressed as:

$$\vec{F}_m = \nabla \int_v (\vec{J} \cdot \vec{H}) dV \qquad (2.1)$$

The symbol F_m refers to a magnetic force exerted onto a particle, J is the magnetic polarisation of a particle in Telsa (T), V is the volume of the particle in (m^3), $\vec{H}$ is the magnetic field strength in Am^{-1} and ∇ is the magnetic field gradient operator with μ_o a constant at $4\pi \times 10^{-7} Hm^{-1}$. If the volume of the particle is significantly small, it can be reduced to a point dipole moment to give $\vec{\mu}_m = \vec{J}V$. Equation 2.1 can be re-written to give the force as:

$$\vec{F}_m = (\vec{\mu}_m \cdot \nabla)\vec{H} \tag{2.2}$$

For the permeability of a spherical particle which is either paramagnetic or diamagnetic the equation is given as:

$$\mu = (1+\chi)\mu_o \tag{2.3}$$

Where χ is the magnetic susceptibility and μ_o is the permeability of free space equivalent to $4\pi \cdot 10^{-7}\, Hm^{-1}$. This gives the magnetic polarisation of a particle as:

$$\vec{J} = \frac{\mu_o \chi \vec{H}}{1+\frac{\chi}{3}} \tag{2.4}$$

Rearranging equations 2.2 and 2.4, gives the force exerted on a small spherical, weakly magnetic susceptible particle in a magnetic field. The equation can be written as:

$$\vec{F}_m = \frac{\mu_o \chi V}{1+\frac{\chi}{3}}(\vec{H}\nabla)\vec{H} \tag{2.5}$$

When χ is significantly small, equation 2.5 can be simplified as:

$$\vec{F}_m = \frac{1}{2}\mu_o \chi V \nabla(\vec{H}) \tag{2.6}$$

Equation 2.6 shows that the magnetic force F_m is directly proportional to magnetic field strength H and the magnetic field gradient. An increased magnetic field strength H will cause an increase in the magnetic field in the direction of the magnetic gradient and, as a result of that, increased magnetisation of the particle. Figure 2-1 shows that there are other

forces exerted on a particle competing with F_m and that the dominance of a particular force is dependent on the particle characteristics and the type of magnetic separator used. Since the research study focused on wet high intensity magnetic separators, the theoretical equations are limited to two fundamental factors, namely the force of gravity and the hydrodynamic drag force as indicated below in equation 2.7 and 2.8, respectively. For a spherical particle with a density ρ_p the force is given by:

$$\vec{F}_g = \frac{4}{3}\pi(\rho_p - \rho_f)\vec{g} \qquad (2.7)$$

Where ρ_f is the density of the fluid medium used in separation and g is the acceleration by gravity.

$$\vec{F}_d = 6\pi\eta VS(\vec{v}(\vec{r} - \frac{d\vec{r}}{dt})) \qquad (2.8)$$

In equation 2.8, η represents the viscosity of the fluid medium, $\frac{d\vec{r}}{dt}$ is the velocity of the fluid and $\vec{v}$ is the velocity of the particle relative to the stream at position $\vec{r}$. All the forces have different dependence on the particle size S, and thus the forces will vary with particle size. The force of gravity F_g will be dominant on coarse size particles whilst F_d will be more dominant on small particles respectively (Svoboda, 1987; Alp, 2007).

2.2 Classification of materials

Materials are classified into ferromagnetic, paramagnetic and diamagnetic categories based on their strongly or weakly susceptible characteristics when experiencing the intensity of an external applied magnetic field (Svoboda, 1987; Dwari and Rao, 2009). Ferromagnetic and paramagnetic materials are known to be magnetically attracted to a magnetic field, whilst diamagnetic materials are repelled once passed through a magnetic field. The difference in the two types is that paramagnetic and ferromagnetic materials have positive susceptibilities while diamagnetic substances have negative susceptibility. Ferromagnetic materials are regarded as a special case of paramagnetism with very high susceptibility to the magnetic

forces, and may possess permanent magnetism. The direct proportionality of the magnetic field and induced field causes a strong interaction between atoms in a nucleus and results in a parallel alignment between atoms and against the force of thermal motion. Thus, ferromagnetic materials are more susceptible to a magnetic field compared to paramagnetic materials (Svoboda, 1987).

Paramagnetic response to magnetism is as a result of the competing aligning effect of the applied field and the random effect of the thermal vibrations. If, for an instant, an atom with a free electron in its outermost shell experiences an applied magnetic field, it will tend to react by moving towards the highly magnetic field regions. Particles are magnetised to some degree when they enter into the magnetic field and act as a magnetic dipole (Svoboda, 1987). In the case of diamagnetic particles, the electrical charges tend to shield the internal shell of the atom. While a particle is under the influence of the applied field, it will move in the opposite direction, thus repelled from the magnetic field. It is for this reason that diamagnetic with weak magnetic attributes are not processed magnetically (Svoboda, 1987; Chakravorty, 1989; Yves *et al.*, 2009). Coal is also classified as a weakly diamagnetic material which contains minerals associated within the organic matrix, some of which may be iron minerals. Magnetic separation may be used for coal beneficiation when the gangue minerals contain such iron phases, however their very weak magnetic susceptibilities would require strong magnetic field strength (Dwari and Rao, 2009). Previous works on the magnetic separation of pyrite from coal have shown pyrite to be a weakly paramagnetic mineral. However, with the transformation into another form called pyrrhotite through caustic microwave treatment and microwave pre-treatment (Rowson and Rice, 1989; Butcher and Rowson 1994), pyrrhotite can be converted into a strongly paramagnetic form and can easily be separated from coal in only moderate magnetic field strengths.

2.3 Background and Related Work

Magnetic separation has been used since 1955 and has proven to be one of the most effective processes for beneficiating magnetically susceptible materials (Al-Wakeel and El-Rahman, 2006; Yavuz *et al.*, 2006; Dobbins *et al.*, 2007, Dobbins *et al.*, 2009; Das *et al.*, 2010; Angadi *et al.*, 2012). Over the last three decades, the production of good quality concentrates from iron ore has been sharply increasing as a result of the high demand in the steel industry

(Svoboda and Fujita, 2003; Mohanty *et al*, 2010). This has motivated countries like India, China and South Africa with an increasing depletion in high grade iron ore reserves to improve their beneficiation techniques for run of mine (ROM), fines and slimes (Al-Wakeel and El-Rahman, 2006; Yavuz *et al.*, 2006; Das *et al.*; 2010; Kumba, 2012).

In India the demand for quality steel has been estimated to be between 56 Mt to 200 Mt in the next decade and, currently, known reserves were estimated to be able to supply steel plants with only 13 Bt to 14 Bt of iron ore concentrate in the next 35 to 40 years (Das *et al.*, 2010). In South Africa the Postmasburg mine located in the Northern Cape Province stockpiled or discarded 3.48 Mt iron ore as waste (Al-Wakeel and El-Rahman, 2006; Zogo, 2009, Li *et al.*, 2010; Angadi *et al.*, 2012; Kumba, 2012). In terms of coal, the Grootegeluk colliery was reported as contributing 18 Mtpa of reactive coal discard. This is prone to spontaneous combustion and is therefore a specific environment hazard (An independent competent person's report on the mining assets of Exxaro Resources Limited accessed 16 Jan 2013). These findings have motivated researchers to explore new beneficiation techniques for treating these high quantities of fine ores and discarded slimes as secondary resources worldwide. Treating these fines and slimes provides the potential for recycling discards, environmental pollution control and extending the resources of both ferrous and non-ferrous low grade ores (Oberteuffer, 1974; Das *et al.*, 2010; Monhaty *et al.*, 2010).

Recent studies conducted by researchers have shown that magnetic separation is a technique that could be used for pollution control, for waste water recycling and for improving beneficiation of low grade ferrous ores. Chen *et al.*, (2012) conducted an investigation using a Vibrating High Gradient Magnetic Separator (VHGMS) for the removal of ferrous minerals (hematite and limonite) from kaolin (clay). The results reported a kaolin product grade of 0.50% Fe_2O_3 with an 84.56% mass yield, and at a 42.08% iron removal rate and the results were found to be acceptable for commercial application. Jaimeson *et al.* (2006) conducted a magnetic separation investigation on Darling Range Red Sand using a combination of Low Intensity Magnetic Separator (LIMS) and Wet High Intensity Magnetic Separator (WHIMS). The results reported ~56% as Fe_2O_3 to the magnetic fraction and a relatively clean non-magnetic fraction composed of <4% Fe_2O_3. This technology was seen as having the potential to convert large volumes of hematite from stockpiles and slimes dams into commercial products.

Li *et al.*, (2011) used a magnetic separator for the recycling of red mud tailings, known as by-product in the aluminium industry. The feasibility study showed that it was possible to separate red mud tailings into high iron content and low iron content products with the former possessing a grade appropriate in iron-making and the latter with the potential for being recycled in a sintering process for alumina production for use as a construction material. Furthermore, the application of magnetic separation for the concentration of diamagnetic material such as colemanite ($CaB_3O_4(OH)_3.H_2O$) from weakly magnetic material was investigated by Alp, (2006). The results obtained showed a mass reduction of 31.47% in plant tailing disposal, and produced a colemanite concentrate with a commercially acceptable grade of 43.74% B_2O_3 at a high recovery rate of 95.06%. Economic and environmental benefits were thus attained.

2.4 The history of the development of the magnetic separator

The application of magnetic separation techniques have been largely developed and applied for specific purposes for example, in mineral beneficiation and recovery as a means of eradicating pollution and in recycling applications (Dahe, 2004). Since it is difficult and costly to treat ultra-fines and slimes by conventional methods such as gravity and flotation processes, it was necessary to continue to investigate the feasibility of new magnetic separation techniques (Arol and Aydogan, 2004). This is especially so for complex mineral compositions as the iron impurities are often locked within non-metallic ores and minerals, such as kaolin, feldspar and quartz which reduce the commercial values of these ores. Magnetic separation is also favoured due to its simple design and operation, renewability and its low cost (Newns and Pascoe, 2002; Jiao *et al.*, 2007; Chen *et al.*, 2012). It is thus to review its development history.

Numerous magnetic separation techniques have been developed over the years to meet the requirements of the mineral processing industry, with the available equipment having its own benefits and limitations. The selection of a separator is based on the susceptibility difference of particles within a material, the magnitude of the magnetic field generated within the separator, the desired product quality, material throughput and design configuration of the equipment for beneficiating different ores. The fact that materials experience different forces in the presence of magnetic field gradients, is responsible for the physical separation of the

components and mixtures under an applied external field (Svoboda and Fujita, 2003; Joseph *et al.*, 2010). For example, iron being a paramagnetic material will be separated from its associated diamagnetic gangues phases (Chakravorty, 1989; Dahe, 1998; Zheng and Dahe, 2003; Dahe, 2004; Dobbins *et al.*, 2009; Angadi *et al.*, 2012).

Magnetic separators are grouped into either low intensity or high intensity, and can be either dry or wet operational types (Svoboda, 1987; Dobbins *et al.*, 2007 and Joseph *et al.*, 2010, Chakravorty, 1989). In general, the view within industry is to reduce operational costs thus the wet process is more favourable in the early stages of the flow-sheet as a means for reducing both the drying and storage costs (Svoboda 1987; Chakravorty, 1989; Dahe, 1998; Zheng and Dahe, 2003; Svoboda 2003; Dahe, 2004; Dobbins *et al.*, 2007; Dobbins and Sherrell, 2009, Angadi *et al.*, 2012). For this research, a wet high intensity magnetic separator (WHIMS) was used. Its evolution to its current form is discussed below.

2.4.1 Dry Magnetic Separators

The dry magnetic separators are used for beneficiating coarse and highly susceptible mineral particles. They are also used for removing tramp iron and magnetic impurities, concentrating highly susceptible magnetic values and in a cleaning stage for a variety of minerals (Svoboda, 1987; Svoboda and Fujita, 2003; Dobbins *et al.*, 2009; Chen *et al.*, 2012; Angadi *et al.*, 2012). The different types of dry separators which include the high intensity roller and drum type magnetic separators will be briefly discussed in the sections below. The roller type separators are of magnitude between 5% and 10% higher in magnetic field, they offer better separation efficiencies at low costs per ton compared to their drum type counterpart (Arvidson and Henderson, 1996). The commercial drum separators can treat up to 8 mm size fraction at feed rates of over 150 t/hr (Chakravorty, 1989).

The main operational limitation experienced by the dry magnetic separators is that the feeds are commonly wet ground and have to be completely dry prior to processing which means additional operational cost. In this case, separation efficiency at fine sizes to reduced and requires high magnetic field intensity and monolayer feeding for effective separation. The magnets as the source of the magnetic field are best operated at ambient temperatures due to their sensitivity to high temperatures (Arvidson and Henderson, 1996). At elevated

temperatures of 120 °C to 150 °C, which is normally experienced the dry approach, the magnets tend to lose their magnetism and a cooling system may be required in order to prevent overheating and to maintain an efficient separation. This is also an added operational cost (Arvidson and Henderson, 1996; Dobbins *et al.*, 2009). The generation of dust during dry processing is also a major setback meaning that some efforts for dust pollution control will be required. Finally there is the need for sufficiently high magnetic field to achieve separation (Dobbins *et al.*, 2009).

Cross-belt magnetic separators are used in the beneficiation of moderate magnetically susceptible ores, and they consist of two or more poles of electromagnets as the source of the magnetic field. A continuous cross-belt allows for the magnetic particles to be attached and collected in a separate container. While the conveyor pulls towards its end pulley, the non-magnetic particles are discharged and also collected in a separate container. For efficient separation, the feed needs to be sized into narrow size ranges and the height of the poles should be adjusted to 2.5 times the coarsest size particles ranging between 75 μm and 4 mm. The main benefit of this unit is that a single pass of the feed through the separator is sufficient to recover almost all the magnetic particles compared to other dry separators which require several passes (Chakravorty, 1989).

Permanent Roll Magnet (Permroll) uses a Samarium-Cobalt (Sm-Co) and Neodymium-Iron-Boron (Nb-Fe-B) permanent magnet as the source for generating a magnetic field of up to 1.6 Telsa (T), which facilitates separation of economic values from gangue minerals. The separator has a thin belt covering the roll magnets to prevent clogging by the magnetic particles, and the products obtained from the separator are collected separately below the belt. The benefit of this equipment is their capability to treat large particle sizes of material up to 25 mm. Energy consumption the by Permroll is low at 10% of the electrical energy required by Induced Roll Magnets (Svoboda 1987; Svoboda and Fujita, 2003). The limitation of these separators is their low throughputs capacity, the high cost of replacing worn magnets and belts, along with the speed of the belt determining the separation efficiency of the system. The use of a belt affects separation by reducing the magnetic field, magnetic intensity and electrostatic interactions generated by the fine particles attached to the belt (Svoboda, 1987).

Rare Earth Roller (RER) separators are low capacity units when compared to Rare Earth Drum (RED) separators. However they are high in capacity when compared to Induced Roll Magnetic (IRM) separators. They are mostly used in the beneficiation of mineral sands, in multi process stages, for example in the final cleaning and scavenging stages to improve the quality of the product and increase recovery (Dobbins *et al.*, 2007). They use thin and open designed belts with the aim of minimising the interference with the magnetic force. The open design has limitations in that, fine particles are easily blown off and build up on the belt, thus reducing the belt life and increasing the maintenance cost. In another instant, as the material travels along the belt, there is a possibility of the particles rubbing against each other, causing the particles to be magnetised and attached to the belt. Separation efficiency can be compromised and can only increase by ensuring that the feed is in a monolayer to prevent compaction which can lead to non-magnetic particles being trapped within the feed bed and fine particle reporting to the bottom of the feed bed (Dobbins and Sherrel, 2009). However, the Rare Earth Drum (RED) is used in the early stages of processes of paramagnetic materials to improve both product quality and recovery (Dobbins *et al.*, 2007).

An Induced Roll Magnet (IRM) is used in the beneficiation of various paramagnetic minerals such as ilmenite, chromite, monazite, wolframite and garnet (Dobbins *et al.*, 2007; Chakravorty, 1989). Its limitation is that it is generally of low capacity due to the narrow allowable gap size situated between the feed pole and the roll, and also limited to a particle size range of 100 μm to 2 mm (Chakravorty, 1989). Treating particles sizes >2 mm on the IRM will require a much bigger gap size thus reducing magnetic field strength. The feed material is fed at the top of the equipment in a controlled thin layer by means of a vibrating feeder. The gap between the feed pole and the roll together with the splitter are adjustable and are of great importance for an efficient separation. In order to achieve good and effective results, the material to be treated must be dry, free-flowing and within the size range of 100 μm to 2 mm. The gap size should be adjusted to approximately 2.5 times the average particle size as with the cross-belt separators (Chakravorty, 1989). With the many operational limitations of the IRM, it is increasingly replaced by rare earth rollers (RER).

2.4.1.1 Previous work conducted using dry magnetic separators

A cross-belt magnetic separator was used by Al-Wakeel and El-Rahman, 2006 in beneficiating iron ore from Egypt. The ore treated was at +53 μm size fraction and a reported head grade of 34.30% Fe. An upgrade to 49.85% Fe and a low Fe recovery were obtained. The author reported that a finer grind is required to liberate the locked iron ore mineral in order to meet the commercial grade product specification. The application of a Permroll separator was used by Alp, 2008 in beneficiating colemanite tailings at +75 μm size fraction and a head grade of 31.52% B_2O_3. An upgrade to 43.74% B_2O_3, and recovery of 95.06% with a mass reduction of 31.47% was obtained using only magnetic separation. This was compared to a previous investigation conducted on the same tailings by Özdag and Bozkurt (1987) where a better B_2O_3 recovery of 97.7% was achieved but at a lower grade using a multi stage process consisting of attrition scrubbing/washing.

Dobbins *et al.* (2007) used an Outotec RED magnetic separator to recover mineral sands and to validate previous results obtained of 70% ilmenite from aeolian tailings. The results showed that a good quality product at 66% ilmenite was produced at the acceptable commercial specification. In order to improve both grade and recovery of the low magnetic susceptible material, Bhatti *et al.* (2009) conducted investigations on a low grade chromium ore from Balochistan in Pakistan with a head grade of 28% Cr_2O_3. The investigations were carried out under different test parameters including the magnetic field intensity, particle size and feed rate. The results showed that a magnetic field intensity of 4000 Gauss was the optimum and any increase above this point resulted in a reduced product grade. It was noted that, as the particle size was reduced and the feeding rate increased the efficiency of separation was reduced. However, a product grade of 40% Cr_2O_3 and 90% Cr_2O_3 recovery was obtained.

The industrial use of dry high intensity magnetic separators such as the cross belt, Permroll, RER, RED and fluidised bed are sharply declining due to the difficulties experienced in their operations (Svoboda, 1987; Svoboda and Fujita, 2003; Dobbins *et al.*, 2007 Dobbins *et al.*, 2009; Chakravorty, 1989). Fine materials are difficult to beneficiate as the result of mechanical entrapment of non-magnetic particles, thus causing inefficient separation, high maintenance and replacement costs (Svoboda, 1987; Chen *et al.*, 2012).

Researchers have noted that better liberation of coal through grinding will improve the efficiency of separation. The difference in the coal magnetic properties has led to various research programmes being conducted in order to increase the magnetic susceptibility mainly for those rich in pyrite prior to magnetic separation. Microwave energy has been used in treating coal to facilitate the change of FeS_2 into a more magnetically susceptible FeS (Zavitsanos *et al.*, 1978; Zavitsanos *et al.*, 1982; Butcher and Rowson 1995; Cicek *et al.*, 1996). The authors used flash pyrolysis prior to the magnetic separation. The results showed that pyrite was converted into iron sulphides based on the temperature of the pyrolysis test. In addition, the result showed that after beneficiation of the -100 μm particle size, a reduction of 35% sulphur content was obtained by flash pyrolysis and magnetic separation. A study on sulphur and ash removal from low-rank lignite coal by low temperature carbonization and dry magnetic separation was investigated by Celik and Yildirim (2000). The result was successful but there was a serious concern regarding air pollution by sulphur during the low-temperature carbonization. There appears to be an improvement in the magnetic susceptibility potential of coal for High Gradient Magnetic Separator (HGMS) beneficiation technique, at least for pyrite removal, but it was found that much work still has to be done to improve this process and to evaluate the technical and economic feasibility of the whole process for coal cleaning.

2.4.2 Wet High Intensity Magnetic Separators (WHIMS)

Wet magnetic separators were introduced as a result of the many limitations faced by dry magnetic separators. The inability of the dry separators to beneficiate high magnetic susceptible minerals such as magnetite more efficiently, at high throughput rates for a very fine size particle, and to separate minerals under high magnetic field intensity, was responsible for the design of the currently available wet high intensity magnetic separators. These separators have shown capabilities of treating various ore types and fine fractions less than 1 mm, for either strong or weakly magnetic minerals. The benefits of wet separators are that they are robust with high capacity, ease of operation and in addition, they also use an electromagnet as a source for generating the magnetic field or matrixes such as groove plates or filaments for generating disturbance within the magnetic field commonly referred to as high intensity (Corrans *et al.*, 1979; Svoboda, 1987; Chakravorty, 1989; Hearn and Dobbins, 2007).

All WHIMS units operate under the same principles but, they differ in the magnitude of the magnetic field, the type of matrix and in some instances the arrangement of the rotating rotor (Chakravorty, 1989). The application of a matrix as the point for collecting magnetic particles in WHIMS made a huge impact and improved the magnetic separation process of materials that were previously considered too fine or to have too low magnetic susceptibility. These traditional types of separators came about as a result of Jones's idea for a magnetised matrix in the form of steel wool and Frantz's idea of a high magnetic field with the aim of increasing the localised magnetic force (Svoboda and Fujita, 2003). The simple design is composed of a horizontal rotor with the matrix packed in a chamber and placed between the poles of electromagnets to generate the localised magnetic field gradient. The feed in slurry form is fed onto the matrix, the magnetic particles are collected and attach onto the matrix and the non-magnetic particles pass through the matrix and into a separate container. When the current is switched off, the magnetic particles are released from the matrix and flushed with water to ensure that all particles are collected into a separate container. Based on this idea, many advanced designs came into being (Chakravorty, 1989). Although traditional WHIMS is relatively easy to operate, for effective separation it is important to use a suitable matrix for the feed under investigation, and an appropriate feed rate, particle size, magnetic field intensity, and location of the feed and wash water. The matrixes in high intensity separators generate a strong localised magnetic field as high as $10^4 \, T/m$, with the selection of the matrix based on the characteristics of the slurry being treated. There are many types of matrixes available; steel wool, groove plates or steel balls or rods to capture the weakly magnetic particles (Svoboda, 1981; Zeng and Dahe, 2003). They serve as the collecting points for magnetically susceptible material and also as a region where the highest magnetic field is experienced, while the gaps facilitate a passage for the removal of the non-magnetic particles (Hearn and Dobbins, 2007). It is also observed that effective separations are achieved at particle sizes >100 μm (Corrans *et al.*, 1979 Dobbins and Hearn, 2007).

The many limitations of the traditional WHIMS have resulted in low separation efficiency of very fine size fractions as a result of entrainment, clogging of the matrix and low throughputs, compared to the latest technology of high intensity magnetic separators (Dobbins and Hearn, 2007; Das *et al.*, 2010). Poor selectivity during separation and the clogging of the matrix has resulted in diminished industrial use. These limitations drove the

development of a vertical magnetic separator (VMS) which was designed in the Czech Republic and later became the foundation for developing the SLon VPHGMS (Zeng and Dahe, 2003; Hearn and Dobbins, 2007). The improvements on the VMS included a vertical rotor instead of the horizontal one, reverse water flush to keep the matrix clean and a bottom feeder with a mechanism for controlling the velocity of the slurry. This design configuration made it possible to treat finer particles which were considered untreatable or too fine for processing under gravity techniques (Dobbins, 2007). China made further improvements on the VMS to achieve better separation efficiencies by introducing the SLon VPHGMS. It has a similar design to the VMS but it has an additional feature, a pulsating mechanism that agitates the slurry and keeps particles in suspension to assist in improving the product quality and recovery (Dahe *et al.*, 1998; Zeng and Dahe, 2003; Dahe, 2004). Another set of separators are the superconducting magnetic separators. These are considered to be of highly advanced technologies which are able to generate high magnetic field strengths of up to 2T. With the initiatives put forward by both Jones and Frantz, many high intensity magnetic separators have been designed and commercialised (Svoboda, 1987, 2003).

2.4.2.1 Previous work conducted using WHIMS

Extensive work has been conducted using different wet high intensity magnetic separators. This section aims to review the different materials treated in those processes, having various head grades and of different size fractions. The early successful application of the WHIMS separator was on kaolin purification, iron-ore and beach sand beneficiation (Svoboda and Fujita, 2003). Investigations were conducted for the removal of gangue phases from a low grade iron ore using WHIMS by many researchers. For example, Angadi *et al.* (2012); Arol, (2004); Jamieson *et al.* (2006); Dobbins *et al.* (2007); Das *et al.* (2010) and Padmanabhan and Sreenivas, (2011) concentrated different ores from their gangue minerals and attained grades suitable for commercial applications. Iron ore with suitable grades for blast furnace application was also recovered from a low grade ore by Al-Wakeel and El-Rahman, (2006).

The inferior separation efficiency experienced by the high intensity magnetic separator when processing fines was investigated by Chen *et al.* (2011). These investigations were in contrast to those reported on the influence of key variables such as magnetic field intensity, matrix type and shape and slurry velocity on the performance of the high intensity magnetic

separator (Li and Watson, 1995; Newns and Pascoe, 2002). The results showed a higher recovery for finer magnetic particles due to the smaller magnetic leakage factor, higher magnetic induction and no direct contact of feed flow on the magnetic deposits on the vertical magnetic matrix elements of the newly designed separator. With continuing research on improving the separation efficiencies of the existing high intensity separators, a new separator called the superconducting magnetic separator was used by Li *et al.* (2011) to beneficiate extremely fine red mud particles at <100 μm. The results showed that the ability to separate fine weakly magnetic minerals, and the capability to generate a very high magnitude of magnetic field makes this separator a potentially superior separator to other units.

Investigations into the optimisation of a high intensity magnetic separator to beneficiate scandium (Sc) by removing the Fe contaminant were conducted by Likun and Yun, (2010). The head grade for the material treated was reported to be 48.90 g/t Sc, 11.45% Fe. Mineralogical analysis showed that scandium was the major mineral and biotite, tremolite, ilmenite, and tantalite were the dominant gangue mineral phases present. Ilmenite was separated from the other gangue minerals by using its high specific gravity, and it was removed by a gravity technique. A -37 μm sized fraction feed was used and the results showed that a magnetic product containing 62.34% Fe and Sc grade of 8.14 g/t with a loss of 0.97% Sc was achievable, and a non-magnetic Sc product with an upgrade to 51.40% Sc was also attained. Pilot scale investigations were carried out on the same size fraction using the same material and flow-sheet, along with the same low magnetic separator followed by high intensity magnetic separators. The results showed that 315 g/t Sc at 78% recovery was achievable and that other rare earth elements which have low magnetic susceptibility could also be concentrated through high intensity magnetic separation.

Fine and super fine bauxite was treated by magnetic separation with the potential to evaluate the occurrence of iron bearing minerals and to verify the possibilities of minimising the iron content of the bauxite by Kahn *et al.* (2003). The results showed that for bauxite fine and superfine products, Fe_2O_3 grades of 8% Fe_2O_3 and 6% Fe_2O_3, with 53 to 55% of total Al_2O_3 were obtained from fine and superfine bauxite feed, with 19.50% Fe_2O_3 and 18.40% Fe_2O_3 grades, respectively. The author concluded that without further comminution, potential aluminum recoveries of about 90% by gravity concentration or magnetic separation could be

attained. The separation of gangue from a low grade iron ore using traditional WHIMS (Gaustec G-340) with a capacity of 200 t/hr was conducted by Angadi *et al.* (2012) to enhance the quality of the low grade ore. A low grade iron ore from Kolkata, India was used with a head grade of 49.27% Fe. The mineralogical report showed that the iron mineral was mainly present in the hematite and goethite phases with quartz and kaolinite as the major gangue mineral phases within the ore. The results showed that an upgrade of up to 62% Fe in the concentrate stream was achievable using WHIMS.

An iron and titanium material containing vanadium as gangue was treated in a SLon VPHGMS (Dobbins *et al.*, 2007). The objective was to remove 17% to 20% gangue in order to improve the product quality of the fine magnetite and titanium. The results reported an upgrade to 47.50% TiO_2 and doubling the recovery at the same time. By discarding the majority of the mass by magnetic separation, the SLon VPHGMS technology also showed that it could be used as a waste rejecting stage prior to the flotation process. Zheng *et al.* (2003) used the SLon VPHGMS separator in a test in a Qidashan mineral processing plant in China. The aim of the investigation was to meet metallurgical specifications of 66% Fe and reduce the high energy used in the plant. Previous tests with the WHIMS 2000 in the same plant showed that it was only capable of beneficiating up to a grade of 63% Fe, 3% short of meeting the required specifications. The material was then treated by a SLon-1500 and the results showed magnetic products with much higher Fe grades and recoveries, with low Fe losses to the tailings streams. The improved quality product was a result of the pulsating mechanism provided by the SLon VPHGMS, preventing the matrix from clogging. By keeping the matrix clean the particles have more attaching space which increases the recovery.

Mohanty *et al.* (2010) conducted a set of experiments on slimes from mines around the Barbil area, eastern India. One set of the experiments comprised of desliming prior to magnetic separation and another test was a direct magnetic separation using traditional WHIMS. The feed used was -150 μm at a head grade of 58.64% Fe, and was analysed through polished sections at size range of –150+100 μm. The result showed that the major phases are hematite with a substantial quantity of goethite. The slimes were then subjected to magnetic separation using Jones WHIMS at various intensities. The investigation showed that by increasing the magnetic field intensity of the WHIMS, low magnetic susceptible iron minerals were

attracted thus reducing the product grade. However, the authors concluded that beneficiation by WHIMS was capable of beneficiating Fe to >61% Fe grade with a high mass yield of ~80%. Another investigation was conducted by Srivastava and Kawatra (2009) on a low grade hematite ore from Minnesota in a USA stockpile. Mineralogical investigations on the ore showed that hematite (Fe_2O_3), silica (SiO_2), and manganite (MnO.OH) were present as major phases. The magnetic separation results reported a beneficiation of the feed from 27.30% Fe to 45.24% Fe with a 42.06% Fe recovery for the -25 μm size fraction. However major Fe losses to the tailings stream were reported, indicating that WHIMS was not entirely efficient in beneficiating this particular ore at this fine size.

2.5 Modelling of high intensity magnetic separation

The upgrade and development leading to high performance of magnetic separators has been intensely researched with the main focus on understanding the fundamentals of particle capture, enhanced separation efficiency and favourable parameters that would lead to the design of new separators. The enhancement in the quantity of particles captured within a magnetic separator is a function of different variables such as particulate constituents and properties, feed properties, and matrix design. Svoboda *et al.* (1989) proposed and developed a mathematical model to determine the collision efficiency of particles with the matrix of a high intensity magnetic separator. He found that the capability and efficiency of the separator for particle capturing was based on the interaction of the static dipolar magnetic contact between the matrix and the coarse particles, and also between each fines particle, in addition to the hydrodynamic shear stress and surface forces.

Another mathematical model was proposed by Tucker *et al.* (1994). The model was used in predicting particle recovery in a WHIMS unit, against the model developed by Svoboda *et al.* (1989) for particle recovery. The method predicts the capability of the separator for particle recovery as a function of particle size and magnetic susceptibility. Furthermore, for effective magnetic separation and particle capture in the matrix, the assumption made was that the magnetic force must be higher than the force of gravity and hydrodynamic drag force. Under this model, the separation efficiency of the separator is defined based on the transfer coefficients known as (L_{ijk}), where (i), is the transferring particle size, (j) magnetic susceptibility or specific gravity, and (k) is the output flow stream of the separator. The

proposed model by Tucker *et al.* (1994) for the threshold field H_O needed for particle capture in the separator is given in Equation (2.9),

$$H_o = a + \frac{P1}{\chi_j^b} + \frac{c}{S_i^2} \tag{2.9}$$

Where χ_j, represents the magnetic susceptibility, S_i is the particle size, a is the constant related to the type of matrix used, $P1$ stands for the model parameter and C is the scaling coefficient.

2.5.1 Analysis Of Variance

Analysis of variance (ANOVA) is a mathematical method which incorporates statistics for analysing experimental data (Angadi *et al.*, 2012). The model uses a number of discrete independent variables at n levels i.e. the tests runs are conducted at different set parameter levels. An example is given by variables ($X_i Y_j Z_k$) where the performance test result is R_{ij}, thus all the R_{ij}'s are independent of each other and follow the normal distribution. This method has been widely used within mineral processing and other industries. It is considered a powerful tool for analysing and comparing experimental results (Stahle and Wold, 1989; Marin-Galiano and Kunert, 2006; Kherad-Pajouh and Olivier Renaud, 2010). Its popularity is as a result of the fact that it is robust to non-normal data and is not easily affected by violations of the model assumptions relative to other models available (Marin-Galiano and Kunert, 2006). The model aims to evaluate the effects of various factors or parameters, either in random effects or fixed effects. With the random effect method, parameters investigated are not analysed in isolation but in a random manner to the researcher's interest. Under the fixed factor effect, the model assumes that the user is in control of the properties of the factors, in the sense that a factor will always have the same effect on an analysis and that it will always be different in the same way under the same conditions. These factor effects can be analysed in various combinations (Stahle and Wold, 1989). Through the results obtained by ANOVA, one is able to determine whether to accept or reject the null hypothesis (Driscoll, 1996). The model uses a mathematical relationship between varying factors such as grade or mass yield. The relationship can be constructed using a first order polynomial principle as expressed below:

$$Y = a_o + a_1X_1 + a_2X_2 + a_3X_3 + a_4X_1X_2 + a_5X_1X_3 + a_6X_2X_3 + a_7X_1X_2X_3 \qquad (2.10)$$

From equation 2.10 above, Y represents the grade or mass yield of concentrate and X is the varying factor set parameters. In regard to this research study, the varying factors are pulp solids as X_1 in (%), magnetic field intensity as X_2 in Gauss (G) and pulsation frequency as X_3 in (Hz). The model determines the grade/mass yield values and compares them to values determined from the experimental data. For the Longi LGS 500 WHIMS investigations, the statistical method was also used in studying the importance of particle size to the mass yield of concentrate or grade attained. Ultimately, the model with the best correlation coefficient is reported (Nakhaei *et al.*, 2012).

2.6 Longi LGS 500

The magnetic separator used in this research study is a newly (2008) designed wet high intensity magnetic separator called Longi LGS 500 and is shown in Figure 2-2. A few studies conducted on Chinese iron ores have shown tremendous improvement in the beneficiation of minerals such as hematite, martite, vanadic titanomagnetite, manganese and other weakly magnetic minerals at very fine particle sizes (The ASIA Miner report, 2010 and Longi Magnet Co. LTD, 2010). The separator has a high intensity magnetic capability, also designed to attract materials with weakly magnetic attributes (The ASIA Miner report, 2010). The equipment has corrosion resistant stainless steel rod matrixes with of 12% to 18% chromium content. The higher the chromium content, the more resistant the matrixes are to corrosion. A cooling system allows water to pass through which means little or no heat generation occurs during the runs and keep the material cool. The equipment was designed based on magnetic jigging principles similar to the SLon VPHGMS, where the pulsation mechanism improves separation efficiency by agitating the slurry and keeping the particles loose, in order to minimise particle entrapment thus creating more surface area on the matrix for collection of the particles. Theoretically, this principle allows the separation of mixtures with a small difference in density and in magnetic susceptibility, and also the separation of non-magnetic and magnetic fine mixtures with a component density ratio of less than 2.

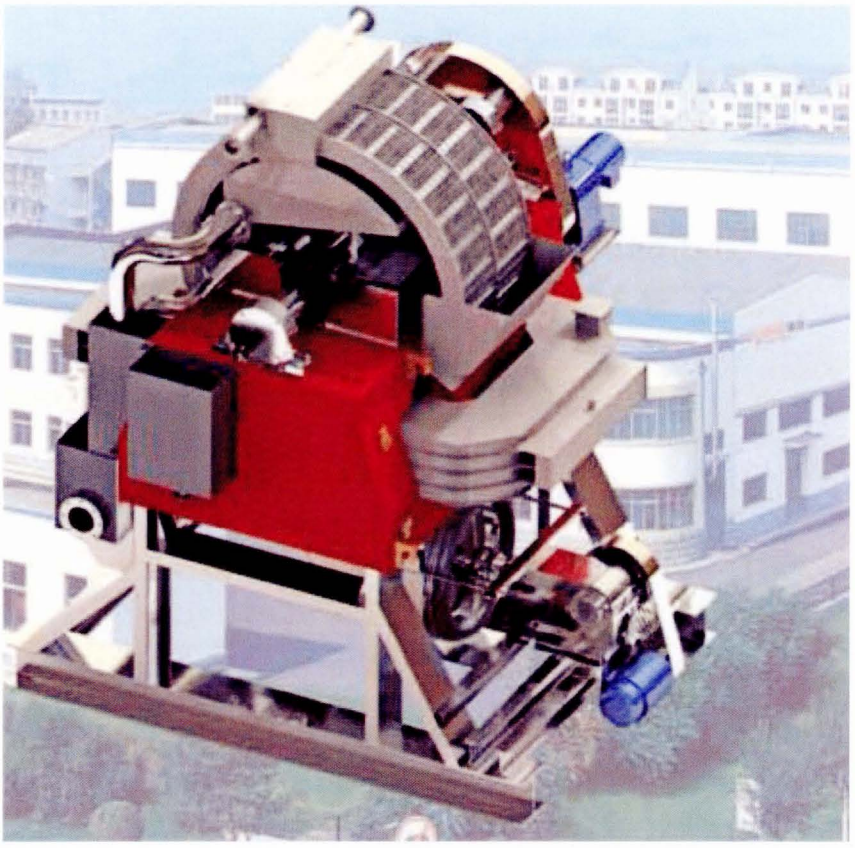

Figure 2-2: Longi LGS 500 (Longi Magnet Co. LTD, 2010)

Other benefits of the Longi WHIMS series technology is that tailings recovery rates are increased by up to 3% as a result of the design of its magnetic field which is directly exposed to the slurry as it passes through the separator. This magnetic separator also has the capability of saving up to 40% in power and water (The ASIA Miner report, 2010). Both the Longi LGS 500 and the SLon VPHGMS have capabilities to effectively separate fine particle sizes, even as they approach a 10 μm particle size (Hearn and Dobbins, 2007; The ASIA Miner report, 2010). The magnetic separation of minerals within the Longi LGS 500 separator uses the natural differences within the minerals in a magnetic field, their magnetic bulk property, the vertically rotating rotor of the separator, the backwashing water system and various adjustable pulsation mechanisms within the separator for improving the efficiency in separation (The ASIA Miner report, 2010).

Based upon the research and development as reviewed above, this research study focused on the capabilities of the Longi LGS 500 magnetic separator for the beneficiation of a low grade

South African hematite-rich ore and a weakly diamagnetic coal. The operating parameters were used i.e. pulp solids, magnetic field intensity and pulsating frequency at different particle sizes were used with the aim of determining the optimum process conditions to achieve maximum recovery and grade.

2.7 Summary

It is evident that the continued increase in demand for a better quality product prompted researchers to investigate and develop different magnetic separation techniques, in order to improve the efficiency of separation and ease of application for beneficiation of different minerals. The performance of each technique has also been researched to further understand the fundamentals of magnetic susceptibility and particle capture under magnetic fields, in order to enhance separation and achieve the best operating parameters that would lead to commercially acceptable products. The enhancement in the quantity of particles captured within a magnetic separator was shown to be a function of different variables, predominantly, the feed characteristics and the design of the equipment. The widely used statistical model (ANOVA) which was briefly discussed in section 2.5.1 is applied in Chapter 4, to verify the data obtained from the Longi LGS 500 investigations.

Chapter 3

3 Material and Methodology

3.1. Material

This section describes the main sample preparation and analytical techniques that were used and briefly provide the working principles of the equipment along with the international standard methods that were employed in conducting the investigations. A low grade material, predominantly Fe oxide in the form of hematite with silicates as the main gangue mineral, was acquired from the Sishen mine, Northern Cape of South Africa and a high ash content coal material was obtained from Witbank in the Mpumalanga region. The materials were supplied by Anglo Research and Anglo Coal for the entire research program. Prior to beneficiation with the Longi LGS 500, the hematite-rich coarse size fraction (>8 mm) material was subjected to particle size reduction to generate a <1 mm size fraction. This was achieved by the application of a High Pressure Grinding Roll (HPGR). The coal material at 50 mm size fraction was subjected to particle size reduction using a primary jaw crusher followed by a laboratory size cone crusher to achieve 100% -212 μm. For ease of illustration, the sample preparation for the hematite and coal are summarised in Figure 3-1 and Figure 3-2 respectively.

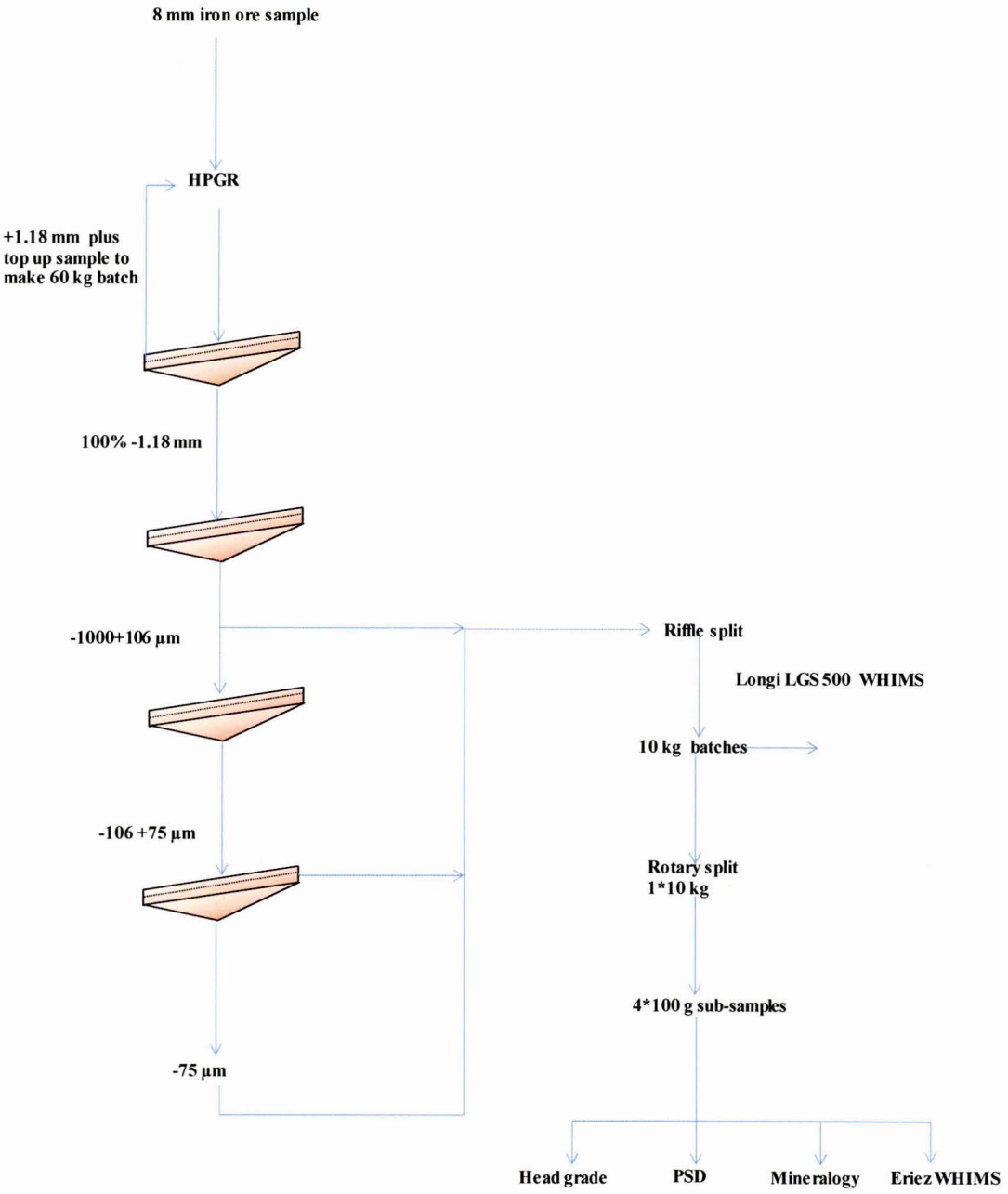

Figure 3-1: Sample preparation for the hematite material

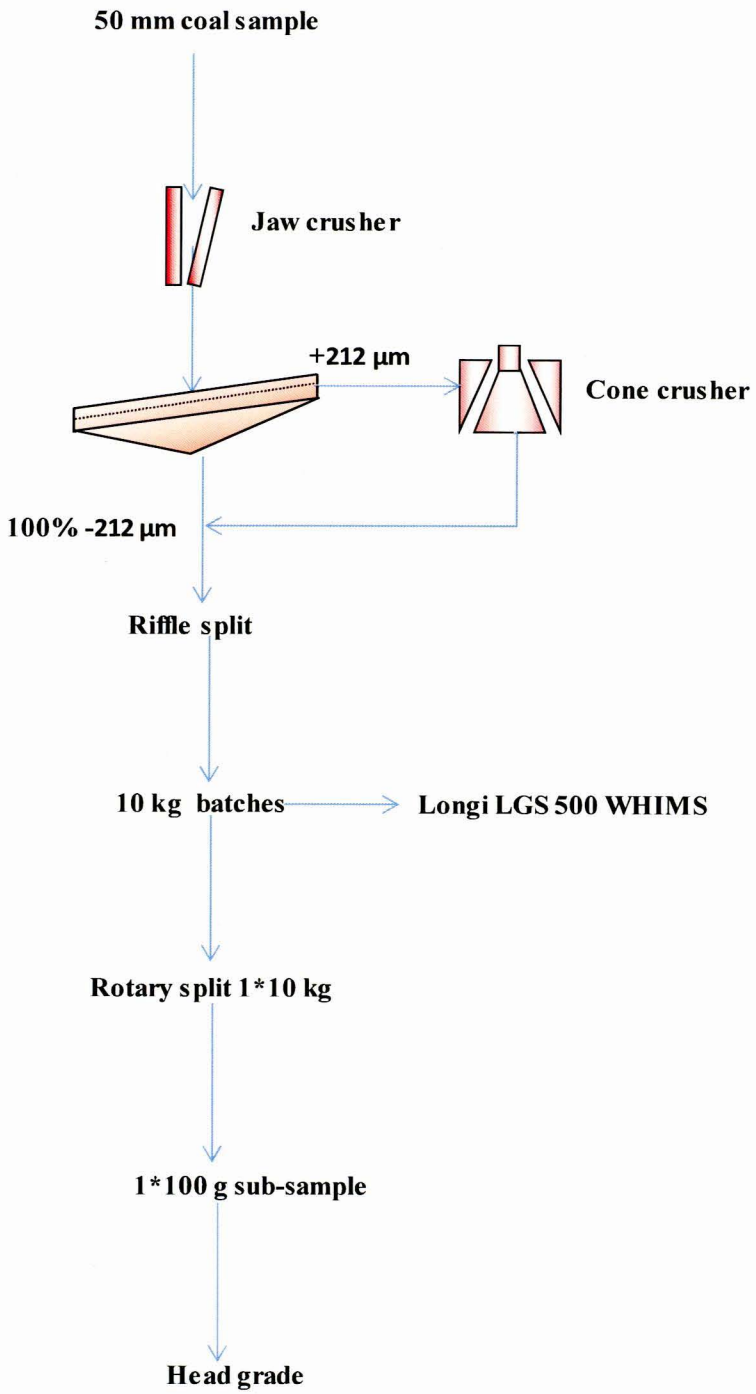

Figure 3-2: Sample preparation for the coal material

3.1.1 Sample Preparation (ISO 3082:2009)

3.1.1.1 Iron ore sample preparation

The 'as received' coarse size fraction of iron ore was subjected to a Polysius Labwall High Pressure Grinding Roll (HPGR) for particle size reduction to <1.18 mm. The objective was to generate enough material for magnetic separation investigations at -1000+106 µm, -106+75 µm and -75 µm size fractions. Each of the individual size fractions was blended and sub-sampled using a Jones chute and spinning riffle splitters to generate a homogeneous sample. The screened, dry sub-samples were taken as described in section 3.1.1.3 for particle size distribution analyses to determine the Fe, SiO_2 and Al_2O_3 distribution. Mineral Liberation analysis (MLA) equipped with Scanning Electron Microscope (SEM) and X-ray Diffraction (XRD) was used for the particle size distribution and grade determinations. The remaining material was kept aside for subsequent magnetic separation investigations on both the Longi LGS 500 and Eriez WHIMS, respectively. X-ray Fluorescence (XRF) and Induced Coupled Plasma Optical Emission Spectroscopy (ICP-OES) were used to determine the elemental and chemical compositions of the feed and magnetic separation products.

3.1.1.2 Coal ore sample preparation

The 'as received' coarse size fraction of coal material was fed to a jaw crusher for particle size reduction to -1.7 mm. The -1.7 mm generated from the jaw crusher was screened by a Sweco vibrating screen at 212 µm, generating -1700+212 µm and -212 µm size fractions. The -212 µm was kept aside and the -1700+212 µm was further crushed to -212 µm using a cone crusher. The objective was to generate material at the fine size of -212 µm size fractions for magnetic separation tests. All the -212 µm was then composited, blended and sub-sampled using the same methods described in section 3.1.2. The sub-samples were then taken for particle size distribution analyses using the Mastersizer 2000. The remaining material was kept aside in 10 kg batches for magnetic separation investigation using the Longi LGS 500 while Thermogravimetric Analysis (TGA) was used to determine the moisture and ash contents.

3.1.1.3 The operation of the HPGR and the Jones's splitter

The 'as received' 8 mm iron ore feed was introduced by a conveyer belt into the HPGR equipment which had a 0.250 m diameter and 0.100 m width. From a hopper, the material then passed through a gap and into the compression zone of the equipment. The compression zone is where the two grind rollers are situated and where inter particle breakage is facilitated at a pressure which is set at 60 bars. The ground material was transported by a conveyer belt from the grinder onto a Sweco vibrating screen equipped with a -1.18 mm aperture sieve. The undersize was kept aside to prevent over grinding and the oversize processed further by topping up with fresh coarse feed material to make up the next 60 kg batch, simulating a closed circuit. The process was repeated several times until all the material was ground to 100% -1.18 mm size fraction. Subsequent to particle size reduction, all the fine (-1.18 mm) material was screened over 106 μm and 75 μm aperture sieves to generate fractions of -1000+106 μm, -106+75 μm and -75 μm. These size fractions were kept aside for blending with a Jones chute splitter prior to sub-sampling. The Jones splitter is preferable as sampling errors are minimal compared to sample scooping and cone and quartering methods (Gerlach *et al.*, 2002). This equipment consists of a V-shaped box with apertures of equal dimensional area at right angles along the box's axis to perform the splitting action. The two rectangular trays were placed on either side of the main box and used as sub-sample collectors. The feed materials were individually introduced into the box and split into two equal halves. One half was kept aside and the other half subjected to the same process ultimately achieving 10 kg batches to be sub-sampled for particle size distribution, mineralogy, magnetic separation by means of the Longi LGS 500 and Eriez wet high magnetic separator.

From one randomly selected 10 kg sample from each of the size fractions, smaller sub-samples were taken using the spinning riffle splitter. The splitter consists of a cone shaped hopper which holds a maximum of a 10 kg batch at a time with an aperture at the bottom for the material to pass through and onto the vibrating feeder. The rotating splitter with 10 x 1 kg capacity containers produces equivalent and homogeneous sub-samples. Again two containers opposite each other were randomly selected. The first 1 kg sample was used for particle size distribution while the second 1 kg was re-introduced into the splitter to generate smaller 100 g sub-samples for head grade determination and mineralogical investigations.

3.2. Iron ore analyses

A number of techniques with the respective standard were used to determine the physical properties and chemical composition of the material. The techniques used were X-ray Diffractometer (XRD), Mineral Liberation Analyser (MLA), X-ray Fluorescent spectrometry (XRF), laboratory scale sieves and the Mastersizer 2000 instrument.

3.2.1 X-Ray Diffraction (XRD, ISO 17025)

A representative 5-10 g sub-sample from individual iron ore size fractions was pulverised into fine powder (<10 μm) using a steel pulverising bowl in preparation for analysis by XRD. The diffractometer used was a Siemens D500 with a step size of 0.02° 2θ, and a counting time of 1 s per step, applied over a range of 5 to 80°, 2θ with Ni filtered Cu-Kα radiation (40 Kv, 30 mA). The Fe oxide and silicate phases were identified using Bruker Eva software and the peaks were matched with the historical information from the database in order to correctly identify all the peaks in relation to an element in the diffractogram.

3.2.2 Mineral Liberation Analyser (MLA, ISO 17025)

An automated Mineral Liberation Analyser (MLA) model Zeiss Evo MA 15 SEM with a Bruker Energy Dispersive X ray Spectroscopy (EDS) detector system and Back Scattered Electron (BSE) was used to analyse the minerals of interest in the iron ore mainly Fe and SiO_2 and to determine their association. In addition the equipment was used to measure particle size, the particle density and to estimate grades for the individual fractions without physical analysis. For simplicity in this research study only data pertaining to particle size distribution and elemental composition were used. MLA is a quantitative analyser that uses a Scanning Electron Microscope (SEM) with extended Back Scattered Electron liberation analysis (XBSE) mode. This is an advanced method where each BSE determines the atomic mass of an element. Over a thousand particles in polished sections for each of the sized fractions were analysed and processed to generate a statistically representative data set of the overall material. This data was then classified into particle size, density, weight percent of the particle population, area of particle and shape factor, circularity and perimeter of each particle during offline processing. The SEM data output for each table product was then arranged into 14 specific density classes ranging from 2.65 to 5.25 g/cm^3 and into 10 size classes ranging from 1000 μm to 10 μm. An Equivalent Circle Diameter (ECD) was determined from the shape factors and circularity equations, as shown in equations 3.1 and

3.2. The size of each particle was calculated as the diameter of a circle with an equivalent cross-sectional area of the particle (Bergmann, 2010). For this investigation, data output using the DataView software provided numerical data which was further translated into excel spreadsheets to determine the elemental composition using offline processing. Again, it should be noted that the estimated particle size distribution and grades were of specific importance for this research.

$$\text{Shape factor} = \frac{Perimeter}{2\pi\left(\sqrt{area/\pi}\right)} \tag{3.1}$$

$$\text{Circularity} = \frac{4\pi area}{(Perimeter)^2} \tag{3.2}$$

3.2.3 Particle Size Distribution on the -1.18 m iron material (PSD, ISO 2395-1990)

The representative 1 kg of iron ore taken during the blending and sub-sampling process was taken for particle size distribution analyses using the 200 mm diameter laboratory hand sieves. All 11 sieves (1.7 mm, 1.18 mm, 800 µm 600 µm, 425 µm, 300 µm, 212 µm, 106 µm, 75 µm, 53 µm and 25 µm were stacked on top of each other, from the one with the largest aperture to the smallest. Once the sieves were stacked, the feed material was fed over the top sieve and placed in a Pascal shaker to provide a vibrating effect that assists in keeping particles loose, and thereby preventing the apertures from clogging. This effect also permits smaller particles to efficiently pass through the sieve and coarse particles to be retained within the top wide sieve. All size fractions retained within the 11 stacked sieves were collected and weighed, with each mass recorded to determine the particle size distribution and assayed to determine the mineral distribution.

3.2.4 Particle Size Distribution on the coal material (PSD, ISO 2395-1990)

Particle size distributions were determined on the coal feed and the Longi LGS 500 products using a Malvern Mastersizer 2000. The equipment is a laser particle size analyser, measuring particles within the range of 0.01 to 1000 µm. It adopts both the Mie and Fraunhofer approximation theories. It consists of multiple lasers, an optical filter, lens and photo detector that is connected to a computer using a Microsoft version 5.60 software. The software allows

for computation of the particle size distribution and the data output is then stored as cumulative value percentages against the particle diameter.

3.2.5 X-ray Fluorescence (XRF, ISO 9001 & ISO 14001)

Representative 5-10 g sub-samples from the individual iron ore size fractions (-1000+106 µm, -106 + 75 µm and -75 µm) were pulverised into fine powder (<10 µm) and analysed using a MXF-2400 multi-channel X-ray Fluorescence spectrometer. Test samples were prepared by mixing with flux and then fused with beads using the Katanax instrument at 1100 °C. The analyses were conducted for 3 minutes per sample under vacuum at 50 kV and 75 mA. The results obtained were then qualitatively identified by comparing to standards with known composition from other techniques. Subsequent to assaying the test feed material reported an overall head grade of 44.15 % Fe, 13.74 % SiO_2 and 14.02 % Al_2O_3.

3.2.6 Induced Coupled Plasma Emission Spectroscopy (ICP-OES, ASD-MET-OES-SP005)

A 1g sample was taken from the individual iron ore size fractions (-1000+106 µm, -106+75 µm and -75 µm) which were pulverised into fine powder. Once the samples were prepared, about ~0.2 g of sample was weighed and mixed, fused with a strong oxidising agent (sodium peroxide). The molten mix was then leached in hydrochloric acid, diluted to a known volume and assayed by Induced Coupled Plasma Emission Spectroscopy (ICP-OES). The equipment is a multi-element analytical technique that can analyse more than ten elements simultaneously, with long dynamic range, meaning that they can be used to analyse high concentrations without the need for further intermediate dilutions. It is calibrated with multi-element calibration standards which are prepared and assayed with the samples whenever possible to ensure that the matrix matched.

3.3. Coal analysis

3.3.1 Thermogravimetric Analysis (TGA, ASTM D-5142)

A representative 1 g sub-sample of coal was taken from the feed and the Longi LGS 500 WHIMS products for proximate analyses and tested in accordance with the ASTM D-5142 standard. This was to determine the inherent moisture and the ash content present within the coal. The thermogravimetric equipment was operated under a nitrogen (N_2) atmosphere for moisture and volatile matter analysis at temperatures of 107° C and 950° C respectively, with

the ash analysis carried out under low oxygen atmosphere and at an end temperature of 750°C.

3.4. Experimental Methods

3.4.1 Beneficiation Studies using the Longi LSG 500 Wet High Intensity Magnetic Separator

Each of the iron ore and coal samples were individually prepared under a range of conditions. The pulp was agitated for 5 minutes to maintain homogeneity, and then the valve was opened to feed directly onto the rotating rotor through two feeding inlets. As the rotor rotates at a standard speed of 4 revolutions per minute (rpm), the magnetic particles attached to the magnetically-induced 2 mm thick stainless steel matrixes and the non-magnetic particles pass through the matrix gaps, with each stream collecting in separate containers. The pulp flows into the active volume where it experiences agitation supplied by the pulsator. The rubber drum head of the pulsator moves back and forth as a result of the frequency converter. This is to assist in keeping particles loose and prevents the clogging of the matrix. As the ring rotates, the attached magnetic particles are collected from the pulp and vigorously washed off the matrix into the concentrate holding plate and collected in the concentrate container. The non-magnetic particles are thrown off through the non-magnetic outlets and collected into a separate collector. In addition to varying the pulp solids, the magnetic field intensity and pulsation frequency were varied to determine the effects of each factor. The resulting three products, the magnetic, middlings and non-magnetic products, were individually collected, filtered and dried at 105° C. Once dry, the products were blended and then sub-sampled in preparation for elemental and chemical analyses. Grade recovery determination was obtained from equation 3.3 shown below.

$$\text{Recovery} = \frac{Measured\ grade * Mass\ percentage}{Calculated\ grade} \tag{3.3}$$

3.4.2 A representation of Longi LGS 500 WHIMS

Photographs of the Longi LGS 500 used during the research study are shown in Figure 3-3 to Figure 3-7. The operational features are:

a) Rotor wash water system to clean the matrix and prevent clogging
b) Matrix made up of 2 mm thick steel rods bolted into the rotor as the collecting point
c) 500 mm diameter steel rotor kept at standard rotating speed of 4rpm
d) Feed inlet
e) Cooling water system to prevent the magnet from overheating
f) An excitation electromagnetic coil allowing variation of the magnetic field intensity
g) Active volume
h) Pulsator for agitating the pulp in the active volume
i) Launder for collecting the magnetic particles
j) Outlet collector for the non-magnetic particles

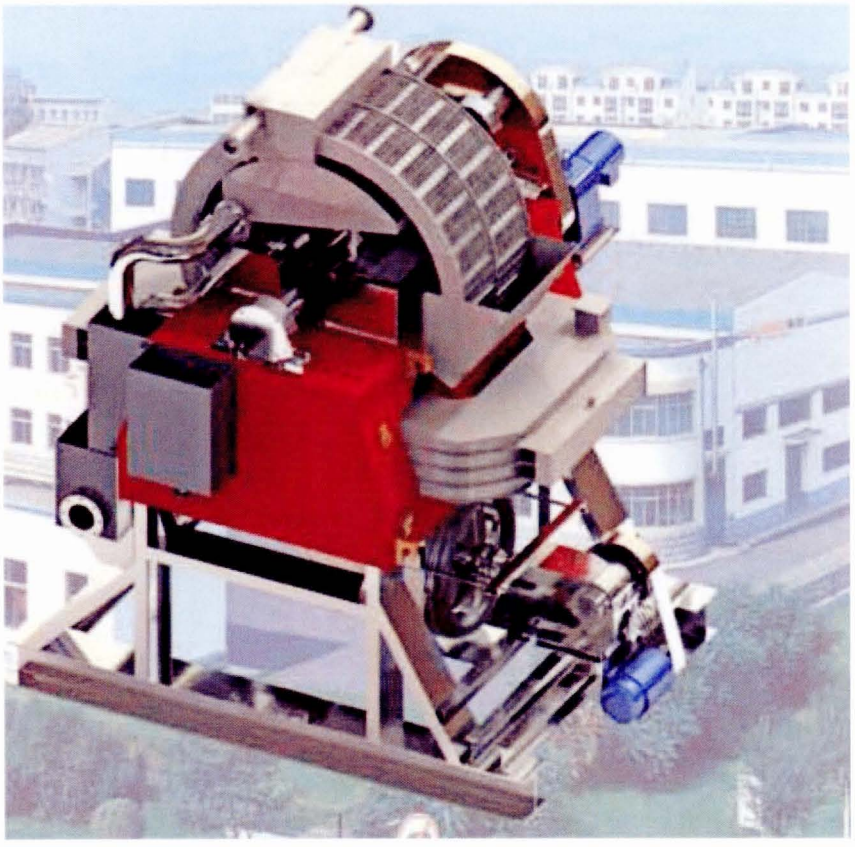

Figure 3-3: Longi LGS 500 (Longi Magnet Co. LTD, 2010)

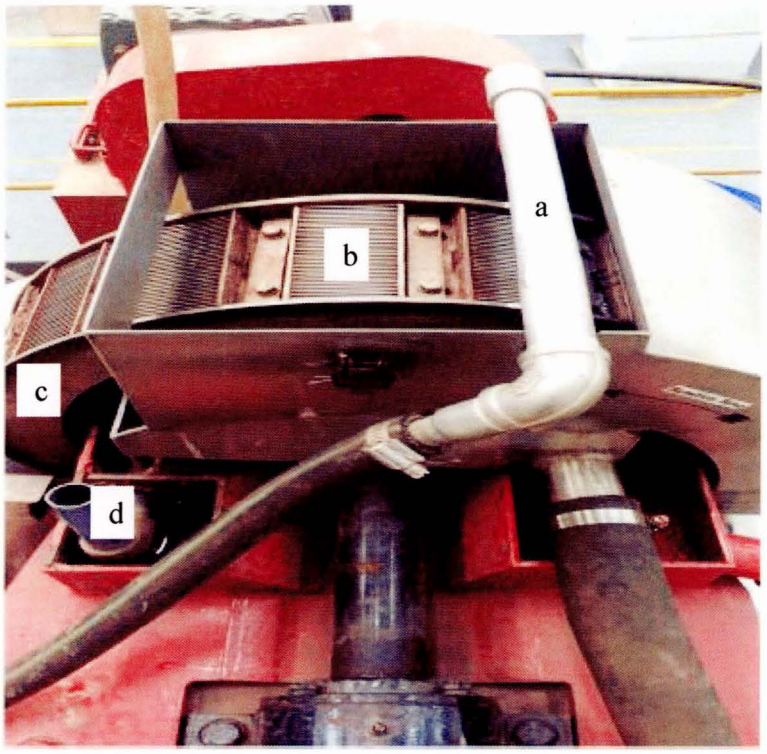

Figure 3-4: Top view of the Longi LGS 500 (Mintek, 2014)

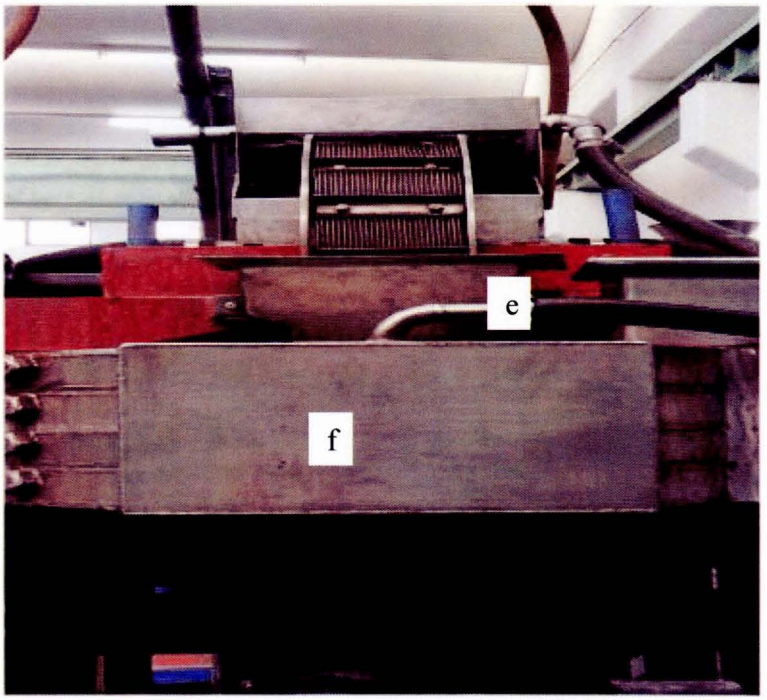

Figure 3-5: Front view of the Longi LGS 500 (Mintek, 2014)



Figure 3-6: Side view of the Longi LGS 500 (Mintek, 2014)

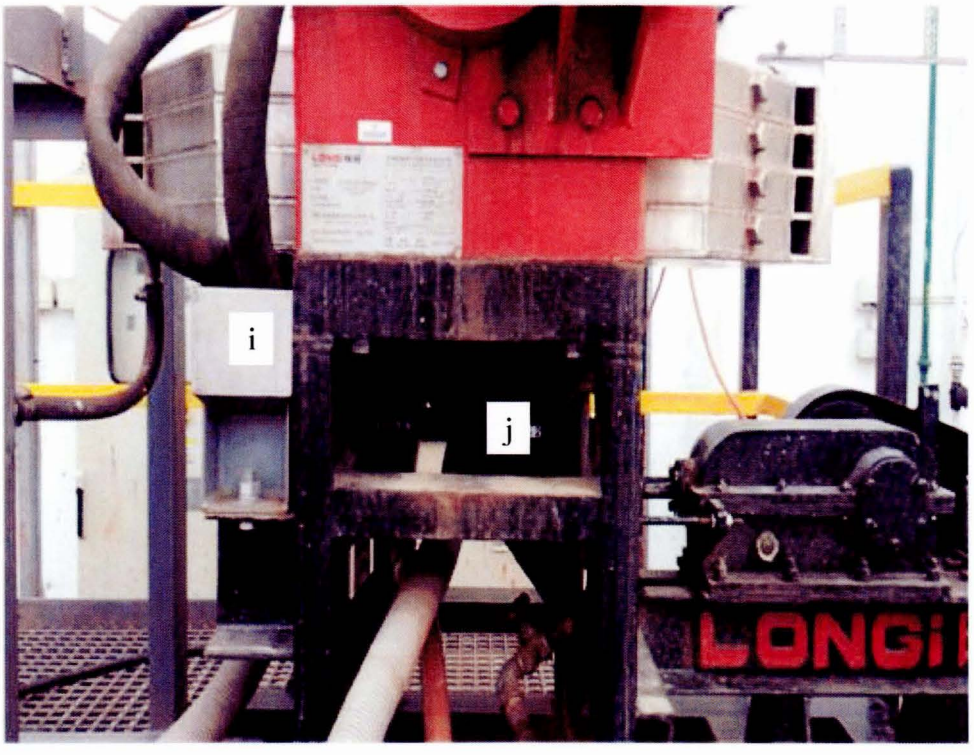

Figure 3-7: Side view of the Longi LGS 500 (Mintek, 2014)

3.5. Comparison testwork with Eriez Wet High Intensity Magnetic Separator (WHIMS)

The iron ore material was also tested in the Eriez WHIMS separator to compare the results with the Longi LGS 500 tests. The investigations were conducted using a stainless steel matrix at the same magnetic intensity as the Longi LGS 500 at 2800 Gauss, 5500 Gauss and 10000 Gauss, respectively. The products, i.e. the magnetic and non-magnetic fractions, were individually analysed by XRF and ICP-OES. The results were used to evaluate the performance of the Longi LGS 500 and its separation efficiency when compared with the performance of the Eriez unit.

Chapter 4

4. RESULTS AND DISCUSSION

In this chapter, the results obtained from the mineralogical investigation of the iron ore at different size fractions are reported and discussed along with the Longi LGS 500 WHIMS performance that is compared with that of the Eriez laboratory WHIMS. The optimum operating conditions at which the tests were conducted and their effects are presented, including the responses of the ore to different conditions. These findings are validated statistically by using the Analysis of Variance method (ANOVA). In addition, the results obtained from the treatment of the coal material by the Longi LGS 500 at optimum test conditions, are also reported and discussed.

4.1. Characterisation: Particle Size Distribution for Iron Ore

The results in Table 4-1 and

Table 4-2 show the particle size distribution and elemental composition on the -1.18 mm feed material as determined by SEM and sieve stacking methods. Both results showed Fe and SiO_2 as the major elements, reporting feed grades of 53.51% Fe, 13.30% SiO_2 and 8.32% Al_2O_3, and 43.45% Fe, 14.49% SiO_2, and 13.66% Al_2O_3 respectively.

Some differences were observed between the two methods used in that the SEM method reported a slight finer size distribution and higher Fe grades when compared to the sieve stacking and chemical analysis methods. The head grade showed Fe grades ranging from 47.38% Fe to 65.46% Fe within the 32 μm and 1010 μm size fractions respectively within the Fe concentrated in the large size factions. On the other hand, the chemically determined head grade from the sieve stacking results reported a relatively similar Fe grade throughout the size fractions and this at the lower ranges of 40.30% Fe to 44.63% Fe. Furthermore, the closeness of the sizing and elemental composition determination techniques is shown in Figure 4-1, indicating acceptable correlation in mass and Fe distributions between the two techniques that were used.

Table 4-1: PSD determined from SEM analysis for the -1.18 mm

Average size (µm)	Mass (%)	Cumulative Mass (%)	% Passing	Grade (%)			Fe grade Distribution (%)	Cum. Fe grade Distribution (%)
				Total Fe	SiO_2	Al_2O_3		
1010	2.68	2.68	100	65.46	3.65	2.71	3.28	3.28
714	14.52	17.20	97.32	55.84	11.50	6.83	15.15	18.43
505	22.81	40.00	82.80	56.76	10.32	7.25	24.19	42.62
357	23.13	63.13	60.00	52.65	14.19	8.89	22.76	65.38
245	19.13	82.26	36.87	50.49	16.32	9.57	18.05	83.43
141	14.47	96.73	17.74	50.56	16.19	9.45	13.67	97.10
71	2.77	99.50	3.27	47.38	19.37	10.59	2.45	99.55
32	0.50	100.0	0.50	47.67	18.73	10.71	0.44	100
Calculated grade	100	-	-	**53.51**	**13.50**	**8.32**	100	-

Table 4-2: PSD determined from sieve stacking analysis for the -1.18 mm

Average size (µm)	Mass (%)	Cumulative Mass (%)	% Passing	Grade (%)			Fe grade Distribution (%)	Cum. Fe grade Distribution (%)
				Total Fe	SiO_2	Al_2O_3		
1416	0.06	0.06	100	43.81	15.10	15.20	0.06	0.06
1001	4.72	4.78	99.94	43.75	14.45	14.50	4.74	4.80
714	19.99	24.77	95.22	44.63	13.80	13.10	20.50	25.30
505	16.40	41.18	75.23	44.18	13.60	13.90	16.64	41.94
357	14.19	55.37	58.82	44.15	13.40	13.80	14.39	56.33
252	10.76	66.13	44.63	44.16	13.70	13.90	10.92	67.25
178	14.65	80.78	33.87	43.62	14.40	13.60	14.68	81.93
126	3.01	83.80	19.22	41.51	15.70	13.70	2.87	84.80
89	6.33	90.12	16.20	41.51	17.10	13.40	6.03	90.84
63	3.14	93.26	9.88	40.30	18.60	13.60	2.90	93.74
45	6.74	100	6.74	40.43	17.60	13.90	6.26	100
Calculated grade	100	-	-	**43.54**	**14.49**	**13.66**	100	-

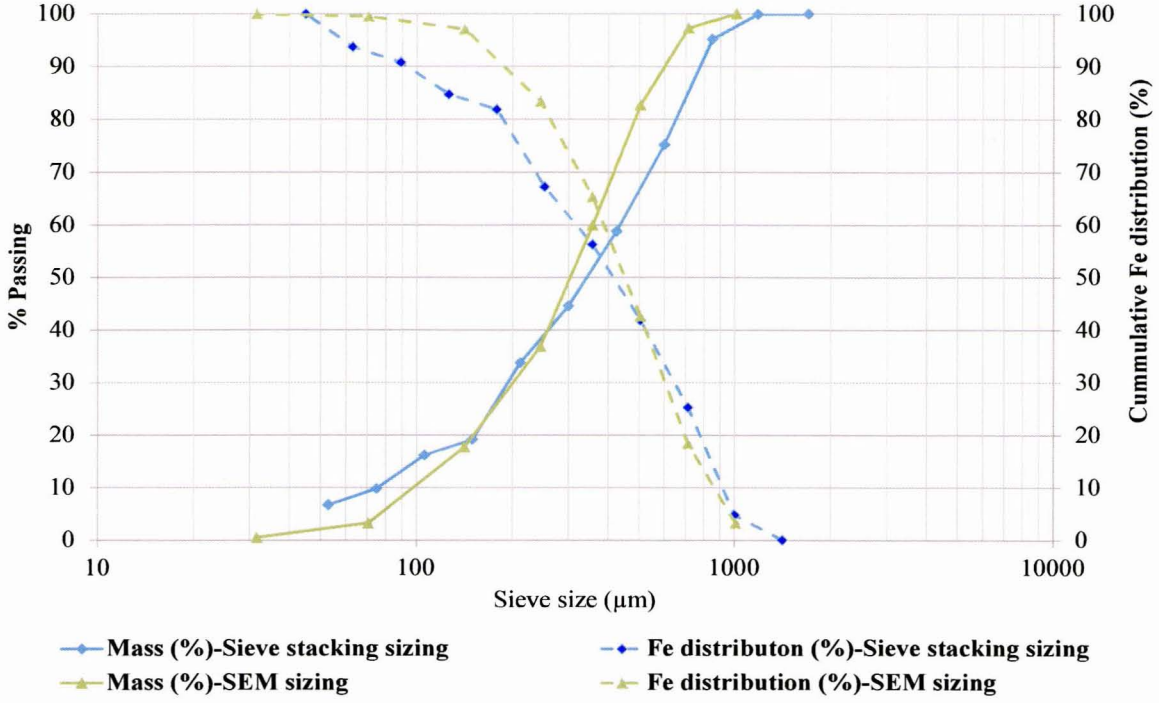

Figure 4-1: SEM and Sieve stacking particle size distribution results

The three size classes namely -1000+106 µm, -106+75 µm and -75 µm size fractions were also analysed using the SEM method. Table 4-3 to Table 4-5 show the particle size distributions and the grades as determined by SEM analysis. The results from the -1000+106 µm size fraction in Table 4-3 showed that the majority of the mass was distributed within a wide size range of 714 µm and 141 µm with masses of 14.35% to 13.08% with corresponding Fe grades >50% Fe. At the size fraction of -106+75 µm in Table 4-4, the bulk of the material at 77.59% was reported in the 71 µm size fraction with Fe grade of 49.00% Fe. Lastly, the -75 µm fraction in Table 4-5 reported a mass of 46.07% at the much finer size fraction of 32 µm and a corresponding Fe grade of 36.66% Fe. The calculated head grades were observed to decrease as the material size became finer and were reported to be 53.63% Fe, 15.24% SiO_2 and 9.11% Al_2O_3 for -1000+106 µm fraction, 49.10% Fe, 18.13% SiO_2 and 9.47% Al_2O_3 for 106+75 µm, and 36.65% Fe, 28.71% SiO_2 and 15.17% Al_2O_3 for the -75 µm fraction respectively.

Table 4-3: PSD determined from SEM analysis for the -1000+106 μm size fraction

Average size (μm)	Mass (%)	Cumulative Mass (%)	% Passing	Grade (%)			Fe grade Distribution (%)	Cum. Fe grade Distribution (%)
				Total Fe	SiO_2	Al_2O_3		
1010	1.35	1.35	100	66.71	2.19	1.81	1.74	1.74
714	14.35	15.70	98.65	54.25	12.96	8.22	15.08	16.82
505	23.30	39.00	84.30	52.24	14.75	8.63	23.57	40.39
357	24.67	63.67	61.00	50.39	16.07	9.94	24.08	64.47
245	18.13	81.80	36.33	51.38	15.43	9.25	18.04	82.52
141	13.08	94.88	18.20	51.08	15.77	9.22	12.95	95.46
71	3.47	98.35	5.12	47.03	19.95	10.54	3.16	98.62
32	1.64	100	1.65	43.13	24.03	11.49	1.37	100
Calculated grade	100	-	-	**51.63**	**15.24**	**9.11**	100	-

Table 4-4: PSD determined form SEM analysis for the -106+75 μm size fraction

Average size (μm)	Mass (%)	Cumulative Mass (%)	% Passing	Grade (%)			Fe grade Distribution (%)	Cum. Fe grade Distribution (%)
				Total Fe	SiO_2	Al_2O_3		
245	0.23	0.23	100	38.67	24.87	16.56	0.18	0.18
141	10.35	10.57	99.77	53.17	14.48	7.83	11.21	11.38
71	77.59	88.17	89.43	49.00	18.37	9.40	77.43	88.81
32	10.19	98.35	11.83	47.69	18.69	10.53	9.89	98.70
14	1.63	99.98	1.65	38.64	25.53	15.62	1.28	99.98
3	0.02	100	0.02	40.16	24.13	16.52	0.02	100
Calculated grade	100	-	-	**49.10**	**18.13**	**9.47**	100	-

Table 4-5: PSD determined form SEM analysis for the -75 μm size fraction

Average size (μm)	Mass (%)	Cumulative Mass (%)	% Passing	Grade (%)			Fe grade Distribution (%)	Cum. Fe grade Distribution (%)
				Total Fe	SiO_2	Al_2O_3		
141	1.96	1.96	100	43.03	25.17	12.92	2.30	2.30
71	17.50	19.46	98.04	39.34	27.10	12.91	18.79	21.09
32	46.07	65.53	80.54	36.66	29.19	14.77	46.09	67.18
14	34.34	99.88	34.47	34.86	29.12	16.99	32.67	99.85
3	0.12	100	0.12	45.32	20.55	13.40	0.15	100
Calculated grade	100	-	-	**36.65**	**28.71**	**15.17**	100	-

4.2. Scanning Electron Microscope on Iron ore

The morphology and surface element distributions of the iron ore feed material at different size fractions are presented in Figure 4-2 to Figure 4-5. These are SEM-Back Scatter Electron (BSE) images. The BSE images show Fe oxide (white) and silicates gangue (grey) as the main components. At these size fractions (-1000+106 μm, -106+75 μm and -75 μm) both coarse and fine silicates were depicted as either free, fine inclusions, disseminated and attached gangue to the Fe oxide mineral. These images, particularly in Figure 4-4 and Figure 4-5 clearly show that much finer grind sizes at <75 μm will be required to achieve full liberation of the Fe mineral. Without the intergrowth of the different elements present, the beneficiation of this ore using magnetic separation should be achievable.

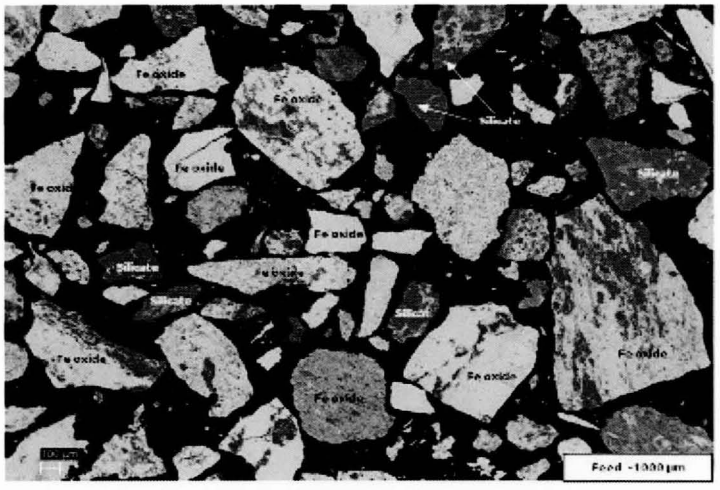

Figure 4-2: BSE image from the -1000 μm feed

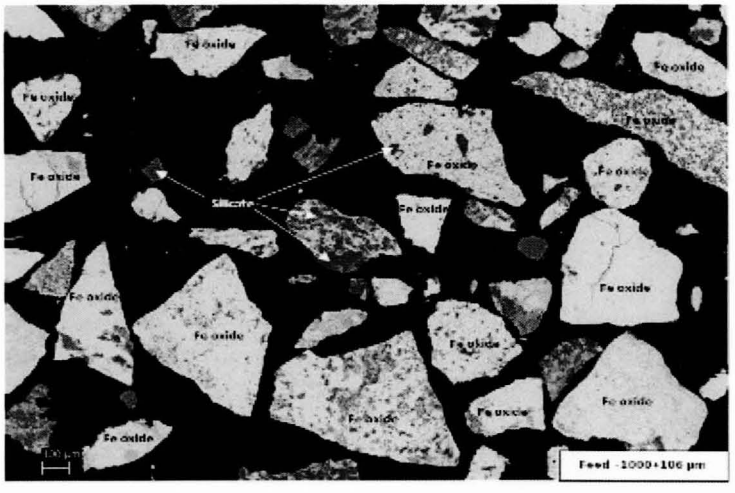

Figure 4-3: BSE image from the -1000 +106 μm feed

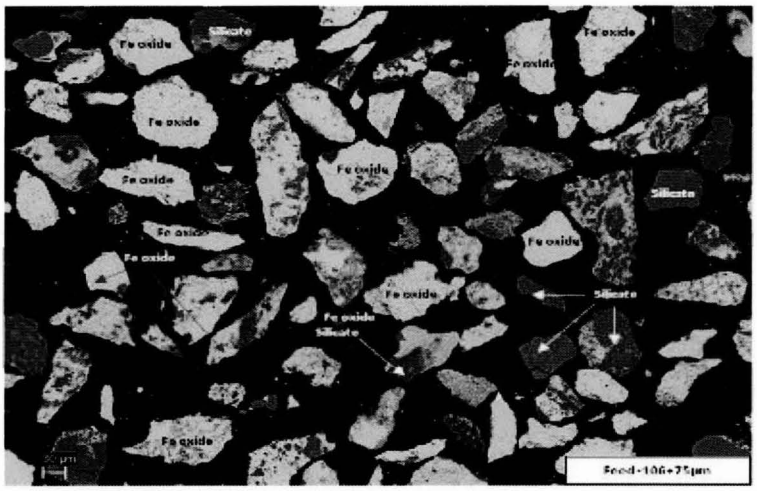

Figure 4-4: BSE image from the -106 +75 µm feed

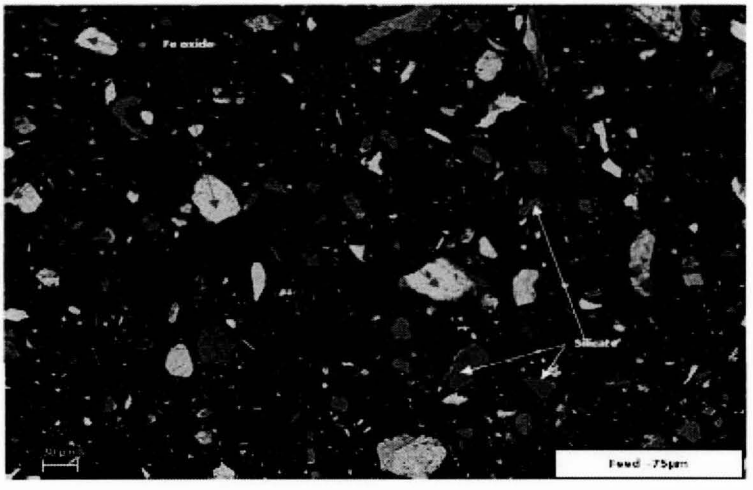

Figure 4-5: BSE images from the -75 µm feed

4.3. Head Grade Determination of iron ore feed

The elemental composition of the sample as chemically determined from the different size fractions is shown in Table 4-6.

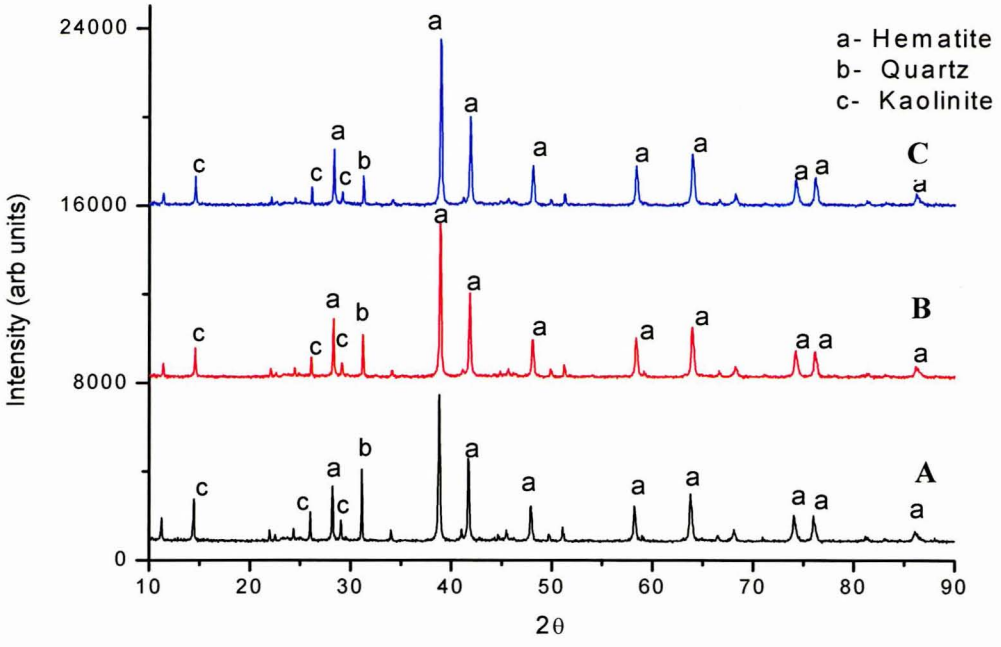

Figure 4-6: XRD patterns for the -1000+106μm feed and the different Longi magnetic separation products.

- **A** is the feed,
- **B** is magnetic concentrates for 30% pulp solids, 1000 Gauss and 12 Hz and
- **C** is the magnetic concentrate for the 20% pulp solids, 2800 Gauss and 12 Hz.

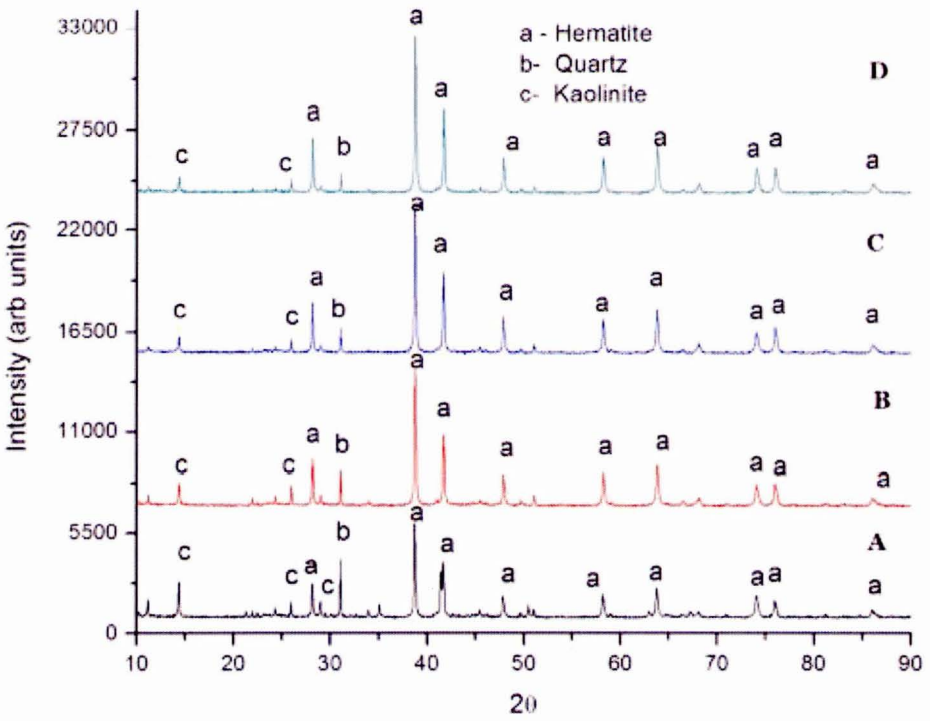

Figure 4-7: XRD patterns for the -106+75µm feed and the different Longi magnetic separation products.

- **A** is the feed,
- **B** is the magnetic concentrate for 30% pulp solids, 1000 Gauss 12 Hz ,
- **C** is the magnetic concentrates for 20% pulp solids, 2800 Gauss and 12 Hz and
- **D** is the magnetic concentrate for 30% pup solids, 2800 Gauss and 25.2 Hz

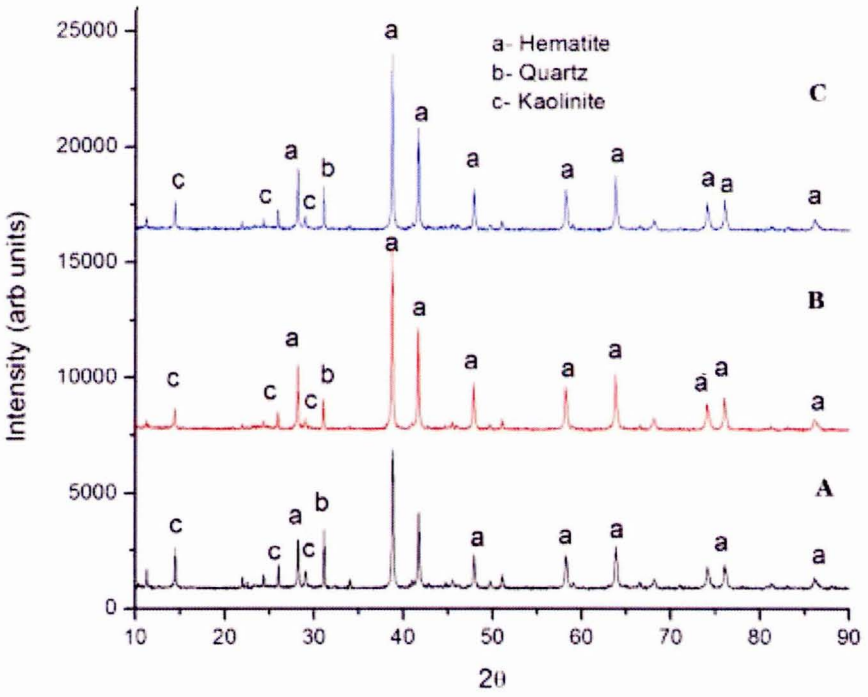

Figure 4-8: XRD patterns for the -75μm feed and the Longi magnetic separation products

- **A** is the feed,
- **B** is the magnetic concentrate for 20% pulp solids, 2800 Gauss and 12 Hz product and
- **C** is magnetic concentrate for 30% pulp solids, 2800 Gauss and 25.2 Hz product.

For the -1000+106 μm size fraction in Figure 4-6, the results showed that the concentrate from the test conducted at 30% pulp solids, 1000 Gauss and 12 Hz had the lowest peak intensities for quartz and kaolinite compared to results obtained from the feed and 20% pulp solids, 2800 Gauss and 12 Hz concentrate. The results obtained from the -106+75 μm size fraction in Figure 4-7, showed a decrease in peak intensity for quartz and kaolinite from a magnetic field intensity concentrate of 1000 Gauss to 2800 Gauss and an increase in hematite peak intensity. The same trend was also observed for the -75 μm size fraction in Figure 4-8, with an increase in hematite peak intensity as the feed was subjected to variable pulp solids and pulsation frequencies.

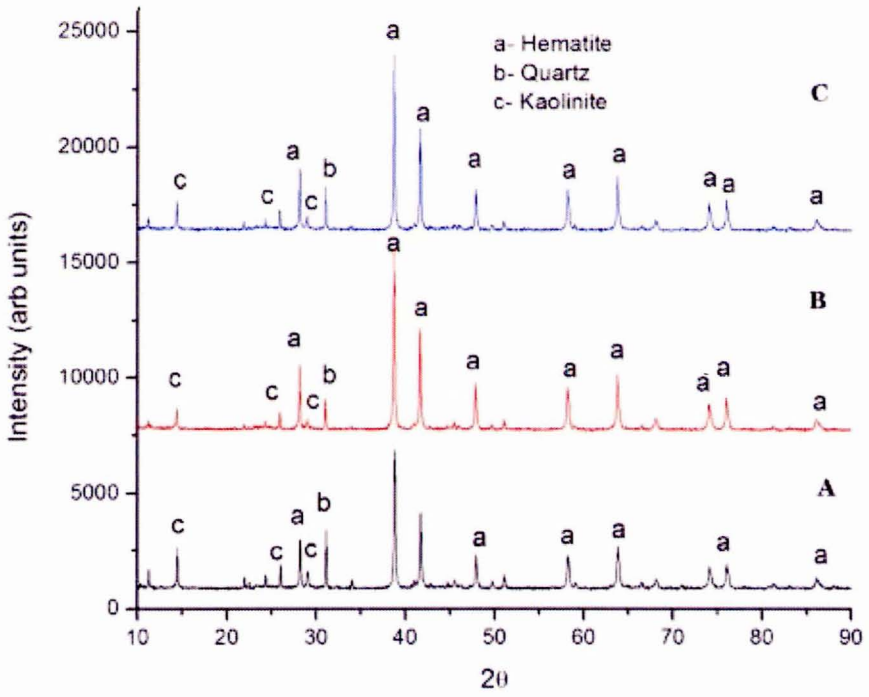

Figure 4-8: XRD patterns for the -75μm feed and the Longi magnetic separation products

- **A** is the feed,
- **B** is the magnetic concentrate for 20% pulp solids, 2800 Gauss and 12 Hz product and
- **C** is magnetic concentrate for 30% pulp solids, 2800 Gauss and 25.2 Hz product.

For the -1000+106 μm size fraction in Figure 4-6, the results showed that the concentrate from the test conducted at 30% pulp solids, 1000 Gauss and 12 Hz had the lowest peak intensities for quartz and kaolinite compared to results obtained from the feed and 20% pulp solids, 2800 Gauss and 12 Hz concentrate. The results obtained from the -106+75 μm size fraction in Figure 4-7, showed a decrease in peak intensity for quartz and kaolinite from a magnetic field intensity concentrate of 1000 Gauss to 2800 Gauss and an increase in hematite peak intensity. The same trend was also observed for the -75 μm size fraction in Figure 4-8, with an increase in hematite peak intensity as the feed was subjected to variable pulp solids and pulsation frequencies.

4.5. Wet High Intensity Magnetic Separation (Longi LGS 500): Iron ore material

The separation efficiency of WHIMS is dependent upon and is influenced by the mineral properties, such as particle size, magnetic susceptibility and the equipment's operating parameters. In addition, investigations conducted by Joseph *et a*l, (2010) supported the fact that the fine particle sizes tend to experience lower separation efficiencies when compared to coarser size particles. In this research study, the separation efficiency of the Longi unit for three different size fractions with the variables of pulp solids, magnetic field intensity and pulsation frequency was determined. The results were validated by using the Analysis of Variance (ANOVA) as outlined in section 4.8. The effects of each of the set of variables were reported and are discussed in detail in the sections below.

4.5.1 Effects of pulp solids

As stated by Joseph *et al*, (2010), any variation in pulp solids will alter the velocity at which particles are introduced to the magnetic separator and therefore it may be expected to alter the process efficiency during separation. As pulp solids decrease below a threshold value, the pulp velocity increases, causing a rapid flow through the rotating rotor, thus reducing particle capture and recovery capabilities of the magnetically induced particles. For example, an increase in pulp solids above a known threshold value tends to form non-selective agglomerated particles and overloads the matrix. This reduces the recovery capability of the matrix (Joseph *et al*, 2010). In this study, the effect of varying pulp solids was investigated while the magnetic field and pulsation frequency were kept constant at 2800 Gauss and 12 Hz. The results obtained are discussed below.

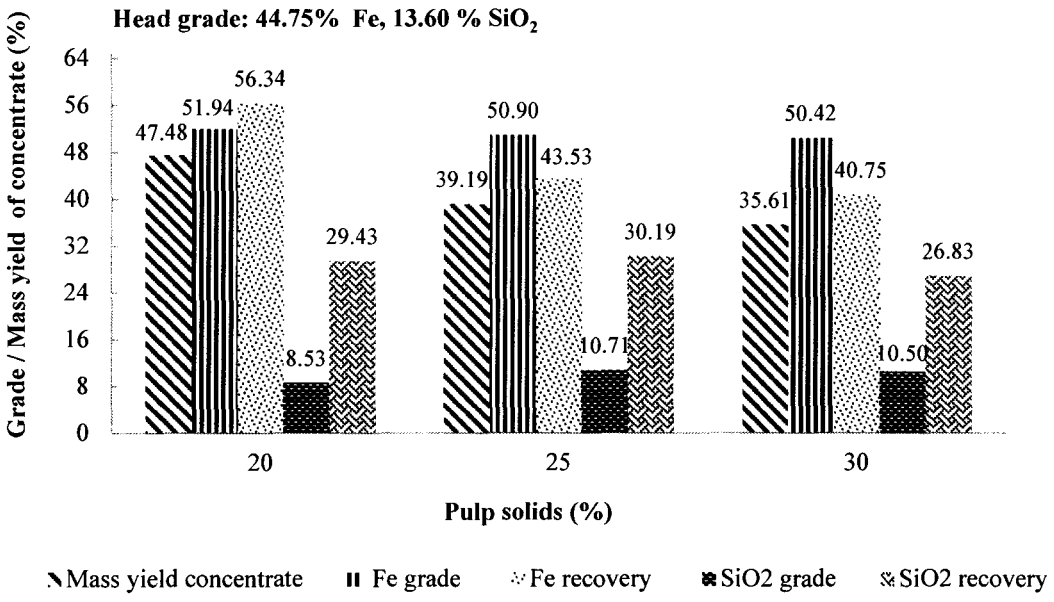

Figure 4-9: Effects of changes in pulp solids for the -1000+106 µm size fraction

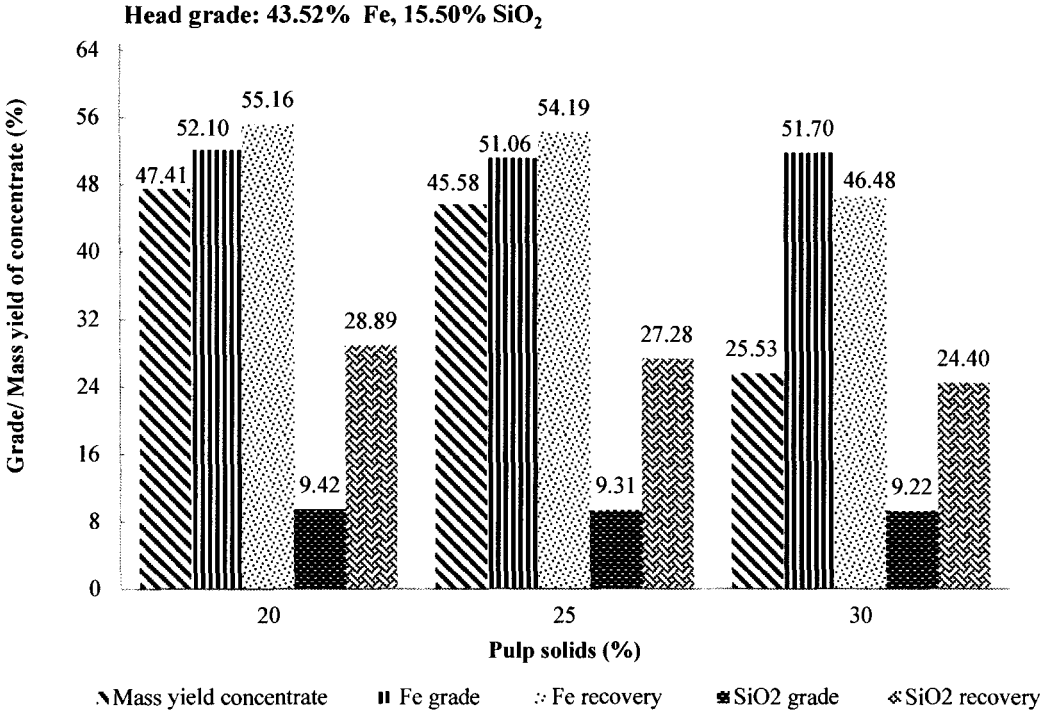

Figure 4-10: Effects of changes in pulp solids for the -106+75 µm size fraction

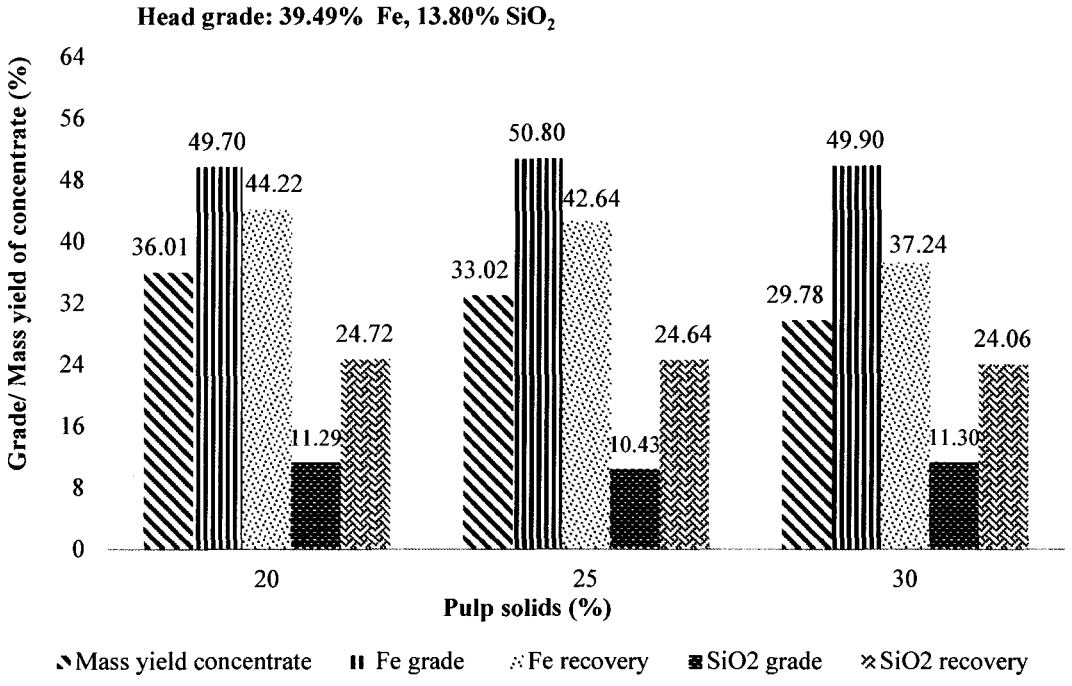

Figure 4-11: Effects of changes in pulp solids for the -75 μm size fraction

The results of the beneficiation of iron ore were promising where comparing the mass yield of concentrate and the Fe grade. The results for the -1000+106 μm size fraction in Figure 4-9 showed that as the pulp solids increased from 20% to 25% and then 30%, there was a decrease in the mass yield of concentrate from 47.48% to 35.61% and an marginal increase in the SiO_2 content from 8.53% SiO_2 to 10.50% SiO_2. The Fe grades were observed to remain within the same range, between 50.42% Fe and 51.92% Fe. The results for the -106+75 μm size fraction in Figure 4-10, showed a decrease in mass yield of concentrate from 47.41% to 25.53%, but the Fe grade remained within the same range of between 51.06% Fe and 52.10% Fe with the SiO_2 content remaining within the same range of 9.22% SiO_2 to 9.42% SiO_2. A similar trend was also observed for the -75 μm size fraction in Figure 4-11, where an increase in pulp solids resulted in the mass yield of concentrate decreasing from 36.01% to 29.78%, and the silica content along with the Fe grades remaining within the range of 10.43% to 11.30% for SiO_2 and 49.70% Fe to 50.80% respectively.

The results obtained in this study were supported by the results that were reported by Arbiter (1980), where the author conducted tests on the effect of varying pulp solids on a tin oxide feed material using the wet high intensity magnetic separation technique. The results provided by the author showed that an increase in pulp solids was not effective in upgrading the tin grade and that the grade was significantly higher at lower pulp solids at ≤25%.

It is thought therefore that the decrease in separation efficiency of the iron ore as the pulp solids increased from 20% to 25% and 30%, could be as a result of rapid agglomeration of particles on the matrix. This could have caused some particles to be prevented from attaching to the matrix due to unavailable surface area, hence the decrease in both the mass yields to concentrate and Fe recoveries.

4.5.2. Effects of magnetic field intensity

The principle of magnetism states that, the higher the magnetic field intensity, the higher the probability of a particle being captured (Angadi *et al*, 2012). In other words, the efficiency of a magnetic separator for effective removal of non-magnetic particles from magnetic particles depends on the intensity and density of the magnetic flux generated, along with the matrix type that is used. Investigations on the effect of varying the current to generate the magnetic field strength from 1000 Gauss to 5500 Gauss and 10000 Gauss were conducted. The pulp solid was kept constant at 30% and the pulsation frequency was kept constant at 12 Hz. The results are discussed below.

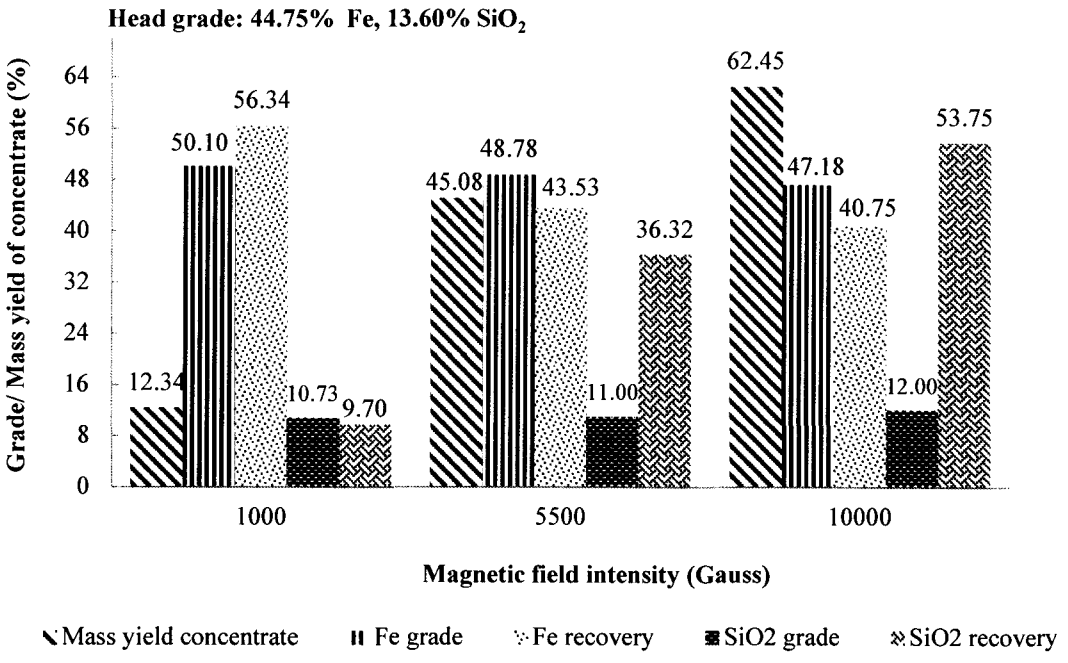

Figure 4-12: Effects of changes in magnetic field intensity for the -1000+106 μm size fraction

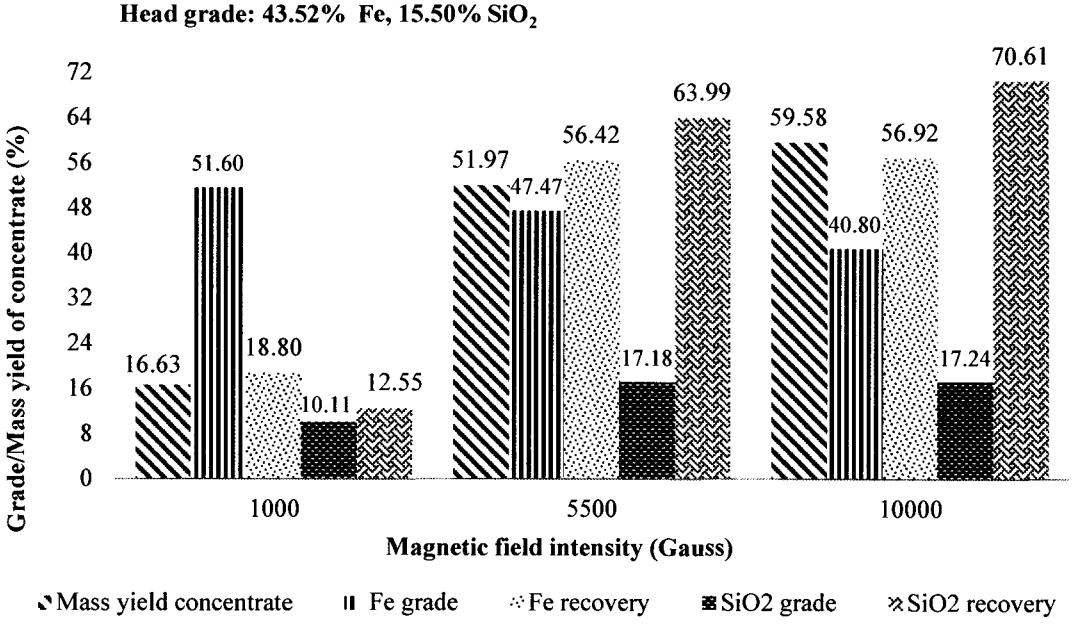

Figure 4-13: Effects of changes in magnetic field intensity for the -106+75 μm size fraction

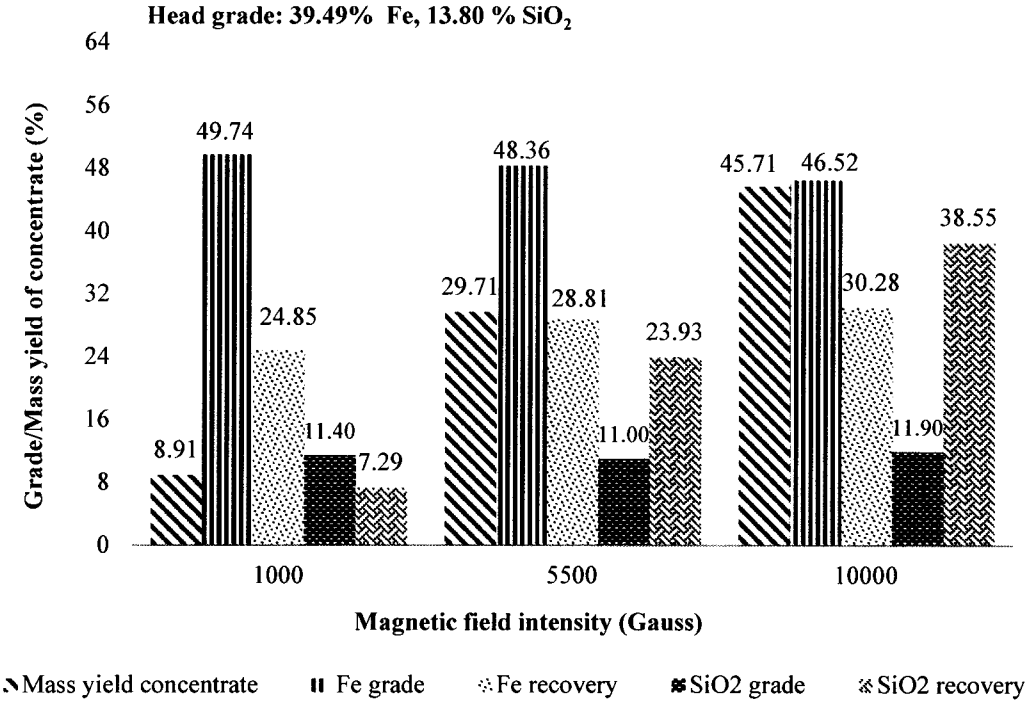

Figure 4-14: Effects of changes in magnetic field intensity for the -75 μm size fraction

The variation of the magnetic field intensity was shown to have a major effect on the magnetic separation results. From a separation efficiency point of view, an increase in magnetic field intensity had a positive effect on the mass yield of concentrate as more particles were attached to the matrix. However, it had a negative effect on the quality. For the -1000+106 μm size fraction in Figure 4-12, the increase in magnetic field intensity produced an increase in mass yield of concentrate from 12.34% to 62.45%. The SiO_2 content increased from 10.73% SiO_2 to 12.00% SiO_2 and it diluted the Fe grade from 50.10% Fe to 47.18% Fe. At the size fraction of -106+75 μm in Figure 4-13, the results followed the same trend, with an increase in mass yield of concentrate and a decrease in the Fe grade as the magnetic field intensity increased. The results were 16.63% to 59.58% for the mass yield of concentrate and the Fe grade reduced from 51.60% Fe to 40.80% Fe. The SiO_2 content in the same size fraction increased from 10.11% SiO_2 to 17.24% SiO_2. At the finer size fraction of -75 μm in Figure 4-14 the results followed a similar trend to the first two size fractions, where the mass yield of concentrate increased with an increase in magnetic field intensity from 8.91% to 45.71%. The SiO_2 content remained within the same range of 11.40% SiO_2 to 11.90% SiO_2 but the Fe grade decreased from 49.74% to 46.52% respectively. These results are in

agreement with those reported by Angadi *et al.* (2012), where magnetic separation at variable magnetic field strength from 9000 Gauss to 14000 Gauss using WHIMS were conducted. Those results showed an increase in the mass yield of concentrate from 10.90% to 20.10% and a decrease in Fe grade from 61.51% Fe to 55.75% Fe. This was considered to be due to the increase in particles attaching to the matrix as the magnetic field strength increased and the non-magnetic particles being entrapped within those agglomerated magnetic particles. The current results in terms of the size fractions are also reflected by Natarajan *et al.* (1992) where the recovery of uranium particles was found to reduce by 20% as the size fraction decreased from 10 μm to <5 μm, mainly as a result of low or non-availability of an adequate magnetic force to overcome the hydrodynamic drag force offered by the slurry such that the uranium mineral particle is pinned onto the matrix.

In summary, an increase in the magnetic field intensity from 1000 Gauss to 5500 Gauss and 10000 Gauss showed that the Longi LGS 500 WHIMS has matrix capabilities to generate enough force to facilitate particle capture. Particle capture was observed to increase in all size ranges particularly for the coarse size fraction of -1000+106 μm at a high magnetic field of 10000 Gauss. The response to a varying magnetic field was supported by findings by Chen *et al.* (2012), where the same effect was investigated on the SLon VPHGMS equipment. The author indicated that at the low magnetic field intensity, mainly the coarse sized and highly susceptible particles are easily captured compared to the fine particles. As the magnetic field intensity increased even more, the fine sized and weakly susceptible particles can also be recovered. At the same time, this increase causes the magnetic particles to form fine agglomerates to overload on the matrix thereby mechanically entrapping the non-magnetic particles. The mechanically entrapped non-magnetic particles are then released from the agglomerates when the rotating rotor moved away from the highly magnetised separating zone to where the magnetic field was lowest and released into the magnetic product launder, thus increasing the mass yield of concentrate and diluting the product grade at the same time.

Based on the results from this testwork, it would appear that to achieve high Fe recoveries, a high magnetic field intensity of >1000 Gauss needs to be applied. However this would compromise the product Fe grade as a result of accumulated diluting gangue minerals. At such a high magnetic field intensity, this process could be used as a primary rejection stage prior to downstream cleaning stages. Alternatively, to achieve a reasonable Fe grade of ~50%

Fe with <10% SiO_2, 1000 Gauss needs to be applied but this would compromise the overall product recovery with Fe recoveries of <20%.

4.5.3 Effects of pulsation frequency

In order to reduce the non-magnetic particle entrainment, clogging of the matrix and to improve product quality, the pulsation mechanism of the Longi LGS 500 magnetic separator was used. Its effect is such that, as the pulsating frequency increases it increases the competing forces (hydrodynamic and drag forces) acting upon the non-magnetic particles, preventing the trapping of non-magnetic particles on the matrix, thereby increasing the product yield and grade (Dahe *et al*, 1998). The current testwork was conducted by varying the pulsation frequency from 6.5 Hz to 19.5 Hz and 25.2 Hz, while the magnetic field intensity and pulp solids were kept constant at 2800 Gauss and 30% pulp solids. The results are discussed below.

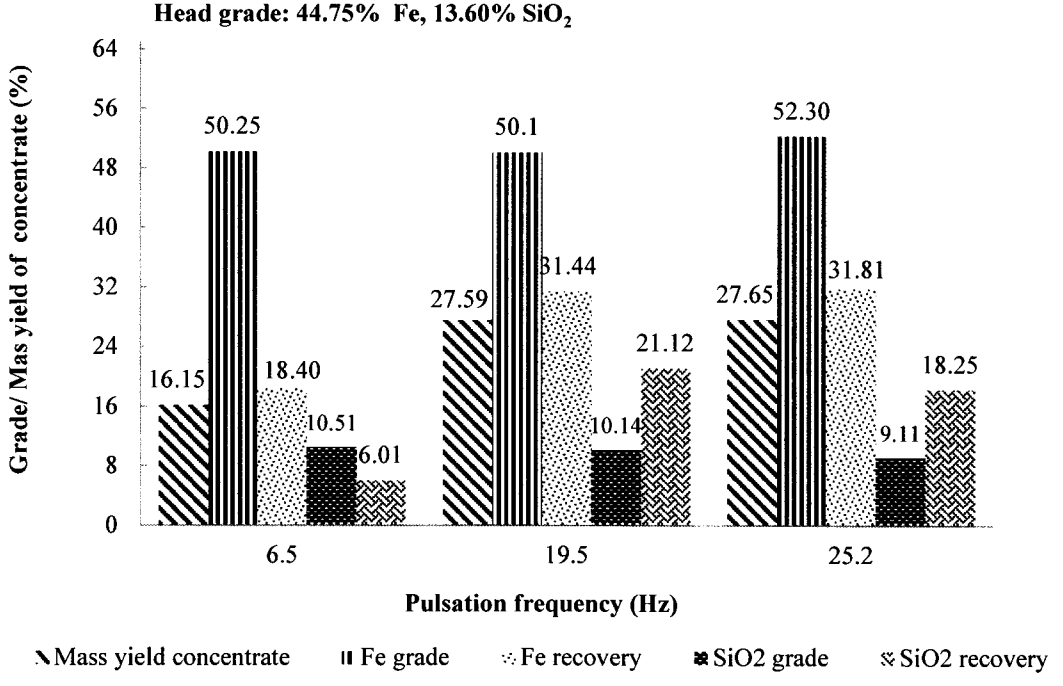

Figure 4-15: Effects of changes in pulsation frequency for the -1000+106 μm size fraction

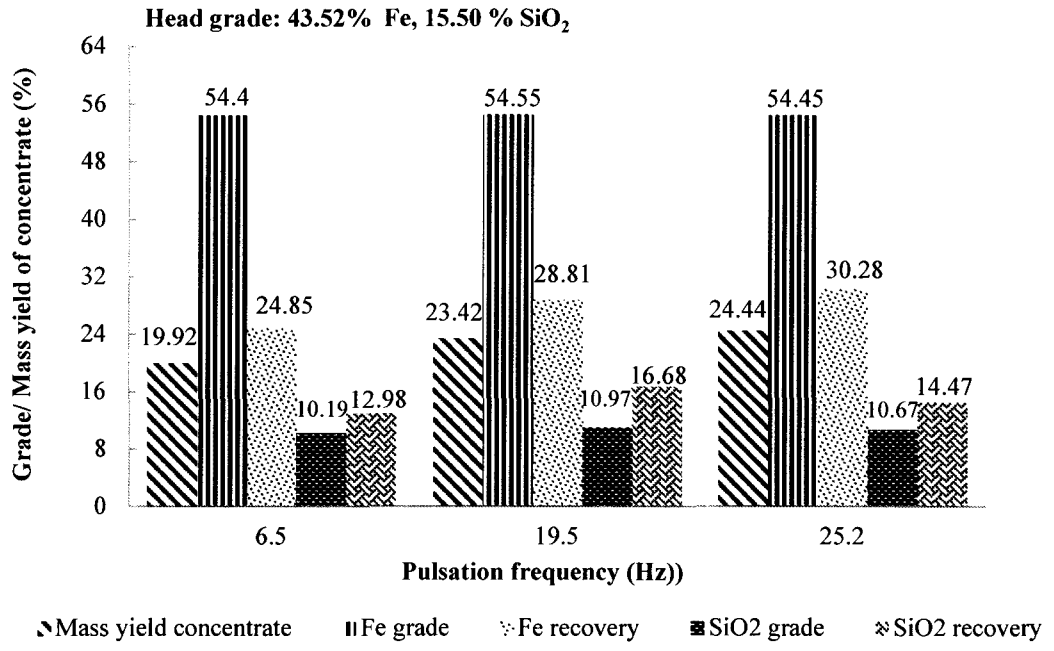

Figure 4-16: Effects of changes in pulsation frequency for the -106+75 μm size fraction

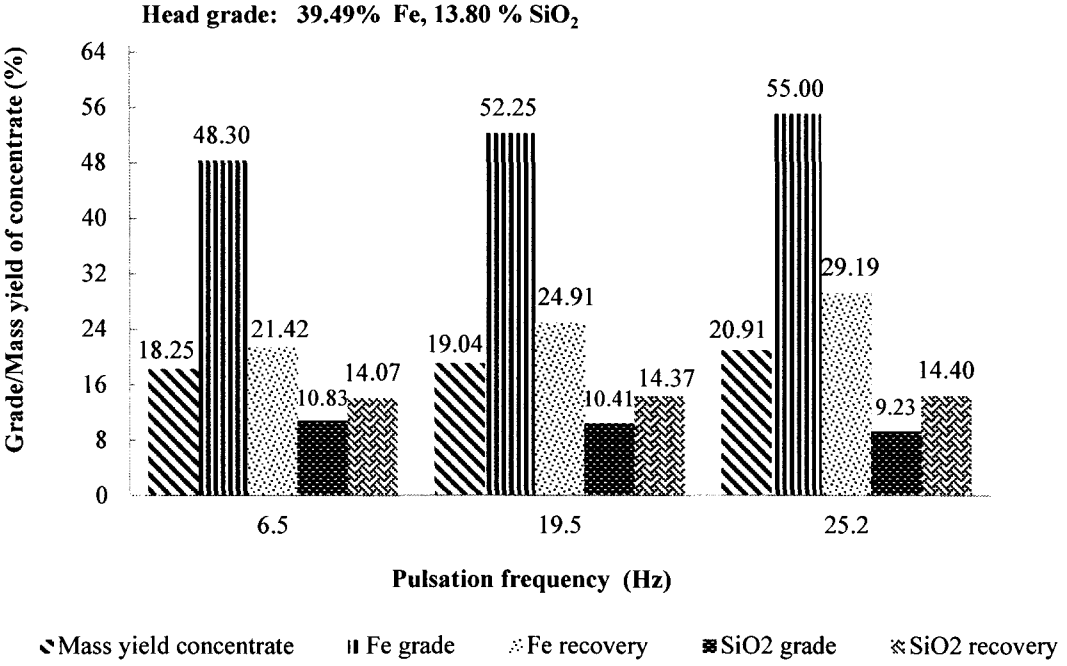

Figure 4-17: Effects of changes in pulsation frequency for the -75 μm size fraction

The results for this testwork showed that an increase in pulsation frequency had a positive effect mainly on the mass yield of concentrate and marginally so on the Fe grade for the -1000+106 and-106+75 μm fractions. The investigations on the -1000+106 μm size fraction in Figure 4-15 showed that as the pulsating frequency increased from 6.5 Hz to 19.5 Hz and 25.2 Hz, the mass yield of concentrate and the Fe grade increased from 16.15% to 27.65% and the Fe grade remained within the same range, between 50.25% Fe to 52.30% Fe respectively. The SiO_2 content marginally decreased from 10.51% SiO_2 to 9.11%. A similar trend was observed for the -106+75 μm size fraction in Figure 4-16; the mass yield of concentrate increased from 19.92% to 24.44% and the Fe grade remained within the same range between 54.40% Fe and 54.55% Fe. The SiO_2 content ranged between 10.19% and 10.67%. The -75 μm size fraction in Figure 4-18 reported better Fe concentration. The increase in the pulsation frequency caused an increase in the mass yield of concentrate from 18.25% to 20.91%, while the Fe grade increased from 48.30% to 55.00% Fe. The SiO_2 content decreased from 10.83% SiO_2 to 9.23% SiO_2.

These results are in agreement with those reported by Zeng and Dahe (2003) where the pulsation mechanism of the SLon VPHGMS was investigated using iron ore material. They reported an improved Fe grade from 15.78% Fe to 30.06% Fe which was attributed to the increasing pulsation frequency that kept the matrix clean and prevented it from clogging. Dahe *et al.* (1998) illustrated the effects of pulsation frequency using equation 4.1.

$$G_m = {G_{\max}}\Big/{1 + A_{nm}}\; K' F_i \Big/ F_c \qquad (4.1)$$

Where G_m represented the grade and $G_{\max}$ is the maximum grade achievable on the magnetic product, A_{nm} is the mass ratio of non-magnetic to magnetic particles in the feed, K' is a constant, F_i is the interaction force between magnetic and non-magnetic particles and F_c is the competing force. The equation showed that an increase in pulsation frequency caused an increase in the competing force (F_c) acting upon non-magnetic particles, thereby reducing the overall denominator and resulting in an increasing product grade G_m.

Findings by Dahe and Chen, (1998) also supported the abovementioned results. An investigation into the influence of the pulsating mechanism was conducted and the authors concluded that the pulsating mechanism produced two effects. Firstly, it causes the particles to collide and attach to the matrix which increased particle capture thus increasing product recovery. Secondly, it increased the competing forces acting on the non-magnetic particles which were favorable for preventing the mechanical entrapment of non-magnetic particles by agglomeration, thereby resulting in a better quality final product.

Observations of the three size fractions that were treated in the current research study showed that the pulsation frequency had a major effect on the quality of the product with the maximum achievable Fe grades of 52% Fe for the -1000+ 106 μm and 55% Fe for the -106+75 μm and -75 μm size fractions. Thus a high pulsation frequency was necessary to release the non-magnetic particles from the matrix thereby keeping the matrix clean and producing a good quality product.

The optimum operating conditions in the testwork to produce the best Fe grade and product recovery were a pulsation frequency of 25.2 Hz, pulp solids of 20% and magnetic field intensity of 1000 Gauss

4.6. Laboratory scale Eriez WHIMS: Iron ore material

The Eriez WHIMS was used to compare its performance to thatof the newly developed Longi LGS 500. The magnetic field intensity was varied from a current of 3 A to 7 A and 20 A which is equivalent to 2800 Gauss to 5500 Gauss and 10000 Gauss. The pulp solids were varied at 20%, 25% and 30%. However at these levels the matrix blocked and separation was not achievable. Thus to solve the clogging problem, the pulp solids was reduced and kept constant at 5% pulp solids.

Table 4-7: Eriez WHIMS results on the -1000+106 μm

Stream	Intensity (A)	Intensity (G)	Mass (%)	Grade (%)			Recovery (%)		
				Total Fe	SiO_2	Al_2O_3	Total Fe	SiO_2	Al_2O_3
Mags			14.77	54.67	7.94	9.65	18.19	8.44	10.41
Non Mags	3	2800	85.23	42.60	14.91	14.39	81.81	91.56	89.59
Total			100	**44.38**	**13.88**	**13.69**	**100**	**100**	**100**
Mags			75.16	44.98	11.40	11.39	75.78	63.99	63.91
Non Mags	6.6	5500	24.84	43.52	19.42	19.47	24.22	36.01	36.09
Total			100	**44.62**	**13.39**	**13.40**	100	100	100
Mags			81.03	44.10	11.50	12.55	80.71	66.70	73.01
Non Mags	20	10000	18.97	45.00	24.52	19.81	19.29	33.30	26.99
Calculated grade	-	-	100	**44.27**	**13.97**	**13.93**	100	100	100
Measured grade	-	-	-	**44.75**	**13.60**	**13.65**	-	-	-

Table 4-8: Eriez WHIMS results on the -106 +75 μm

Stream	Intensity (A)	Intensity (G)	Mass (%)	Grade (%)			Recovery (%)		
				Total Fe	SiO_2	Al_2O_3	Total Fe	SiO_2	Al_2O_3
Mags			17.93	52.05	11.56	12.17	21.27	15.08	15.65
Non Mags	3	2800	82.07	42.10	14.21	14.33	78.73	84.92	84.35
Total			100	**43.88**	**13.74**	**13.94**	100	100	100
Mags			40.80	45.80	12.90	12.38	42.33	34.42	41.86
Non Mags	6.6	5500	59.20	43.00	16.93	11.85	57.67	65.58	58.14
Total			100	**44.14**	**15.29**	**12.07**	100	100	100
Mags			45.03	44.07	16.27	12.65	44.70	48.33	45.13
Non Mags	20	10000	54.97	44.65	14.25	12.60	55.30	51.67	54.87
Calculated grade	-	-	100	**44.39**	**15.16**	**12.62**	100	100	100
Measured grade	-	-	-	**43.52**	**15.50**	**12.60**	-	-	-

Table 4-9: Eriez WHIMS results on the -75 μm

Stream	Intensity (A)	Intensity (G)	Mass (%)	Grade (%)			Recovery (%)		
				Total Fe	SiO_2	Al_2O_3	Total Fe	SiO_2	Al_2O_3
Mags			14.03	53.95	9.83	10.34	19.02	10.31	8.16
Non Mags	3	2800	85.97	37.50	13.96	18.99	80.98	89.69	91.84
Total			100	**39.81**	**13.38**	**17.78**	100	100	100
Mags			22.07	51.40	12.40	12.72	28.73	20.07	15.07
Non Mags	6.6	5500	77.93	36.10	13.98	20.29	71.27	79.93	84.93
Total			100	**39.48**	**13.63**	**18.62**	100	100	100
Mags			27.40	50.30	13.05	12.59	34.74	25.80	18.88
Non Mags	20	10000	72.60	35.65	14.16	20.41	65.26	74.20	81.12
Calculated grade	-	-	100	**39.66**	**13.86**	**18.27**	100	100	100
Measured grade	-	-	-	**39.49**	**13.80**	**18.10**	-	-	-

The results from the Eriez testwork for the -1000+106 μm size fraction in Table 4-7 show that with an increase in magnetic field intensity and at a pulp density of 5%, there was an increase in the mass yield of concentrate from 14.77% to 81.03%, with a decrease in the Fe grade from 54.67% Fe to 44.10% Fe. The Fe recovery for the magnetic product showed an increase from 18.19% to 80.71%. The results for the -106+75 μm size fraction in Figure 4-8 reported a similar trend, with the mass yield of concentrate increasing from 17.93% to 45.03% but with a decreasing Fe grade from 52.05% to 44.07% Fe. The Fe recoveries were much lower, at 21.27% to 44.70% when compared to the coarser size fraction. Much lower

mass yields of concentrate were reported for the -75 μm size fraction in Figure 4-9, which were reported at 14.03% to 27.40%. The results overall showed good potential for upgrading the Fe grade. At high pulp densities of 20%, 25% and 30% there were matrix blockages which reduced the separation efficiency. The opposite was reported on the Longi LGS 500 tests at the same pulp density of 20%, 25% and 30%

4.7. Wet High Intensity Magnetic Separation (Longi LGS 500): Coal material

A coal material at -212 μm sizing was subjected to the Longi LGS 500 WHIMS to determine if it was possible to use the magnetic separation technique as a cleaning process on such a material and to compare two extremes, one being magnetically susceptible (iron ore sample) and the other not (coal sample). The tests were conducted at the parameters suitable for the low susceptible material at 20% pulp density, 10000 Gauss and 25.2 Hz. The results are discussed below.

Table 4-10: Magnetic separation 1st test over 30 seconds retention time

Size fraction (μm)	Mass (%)	Moisture (%)	Ash Grade(%)	Recovery (%)
Mags	0.34	2.47	16.19	0.36
Midds	8.88	2.26	13.57	8.01
Non mags	90.78	3.42	15.19	91.63
Measured grade	100	**3.31**	**15.05**	100

Table 4-11: Magnetic separation 2nd test over 1 minute retention time

Size fraction (μm)	Mass (%)	Moisture (%)	Ash Grade(%)	Recovery (%)
Mags	4.02	3.30	16.60	4.72
Midds	10.77	2.45	13.84	10.55
Non mags	85.22	5.28	14.04	84.72
Measured grade	**100**	**4.90**	**14.12**	100

The results obtained from this testwork were not promising, with the bulk of the feed sample mass (85.22% to 90.78%) reporting to the non-magnetic stream as product, 0.34% to 4.02% reported to the magnetic fraction and 8.88% to 10.77% to the middlings. The ash content results were similar for both tests with minor variations to the moisture content. Also it was observed that the separation to the middling stream was lower at 9% when the pulp was retained in the active volume for a short period of time (30 seconds) compared to 11% when it was kept for 1 minute. This is considered to be as a result of the pulsating effect with its

cleaning capabilities and allowing for the free surface of the magnetic particle to attach to the matrix. This jigging motion keeps particles in suspension giving opportunity to those magnetic particles in the active volume to attach to the matrix. The results show that retention time has an effect on separation. The particle size distribution was included to support the results which are reported in section 4.7.1 below.

4.7.1. Particle Size Distribution Analysis

Table 4-12 and Table 4-13 shows the particle size distribution results of the coal feed and products obtained from the Longi LGS 500 magnetic separation tests.

Table 4-12: Particle size distribution from the 1st test

Stream	Particle Size Distribution (µm)		
	D_{90}	D_{50}	D_{10}
Feed	209.00	85.00	12.00
Mags	190.55	83.00	20.89
Midds	144.54	47.86	7.59
Non-mags	208.00	91.20	14.45

Table 4-13: Particle size distribution from the 2nd test

Stream	Particle Size Distribution (µm)		
	D_{90}	D_{50}	D_{10}
Feed	209.00	85.00	12.00
Mags	190.55	75.86	14.45
Midds	144.54	51.99	7.59
Non-mags	208.93	83.18	15.85

The results in Table 4-12 and Table 4-13 show that the coarse sized particles are distributed in the non-magnetic stream with 90% of the particles reported as <208 µm. This proportion of particle sizes can be attributed to the coarse magnetically susceptible particles. It was noted that the ± 9 to 11% in the middlings (midds) stream reported a distribution of finer size particle, with 90% of the particles as <145 µm. This could be as a result of the slow settling rate of the fine non-magnetic coal particles which could have washed off and been collected as the middlings fractions.

4.8. Analysis of Variance (ANOVA): Statistical analysis

The method of analysing data using the analysis of variance (ANOVA) is widely used in mineral processing for evaluating the significance of the variables that are used during investigations (Angadi *et al*, 2012, Murty *et al*, 2013). The ANOVA outputs were obtained from a Microsoft office, Excel 2010 spreadsheet, using data from twenty-seven (27) test runs on the iron ore material at three size fractions. The test runs were based on the full factorial design 3^3 following the equation shown below.

$$N = 2^z \tag{4.2}$$

Where N is the number of investigation and z is the number of variables.

The effects of the three variables were investigated at three levels namely: X_1-pulp solids (%), X_2-magnetic field intensity (Gauss) and X_3-pulsation frequency (Hz). The estimated coefficients from the mathematical model together with the ANOVA outputs are discussed in the section 4.8.1 and 4.8.2 below.

Table 4-14: Longi LGS 500 unit parameters

Variable	Level		
X_1 (%)	20	25	30
X_2 (Gauss)	1000	5500	10000
X_3 (Hz)	6.50	19.50	25.20

Table 4-15: Full factorial design (3^3) investigation matrix on the Longi LGS 500 unit

Input	X_1 (pulp density)	X_2 (magnetic field intensity)	X_3 (pulsation frequency)
1	0.20	2800	12.00
2	0.25	2800	12.00
3	0.30	2800	12.00
Input	**X_1 (pulp density)**	**X_2 (magnetic field intensity)**	**X_3 (pulsation frequency)**
1	0.30	1000	12.00
2	0.30	5500	12.00
3	0.30	10000	12.00
Input	**X_1 (pulp density)**	**X_2 (magnetic field intensity)**	**X_3 (pulsation frequency)**
1	0.30	2800	6.50
2	0.30	2800	19.50
3	0.30	2800	25.20

4.8.1. Interaction effects

Table 4-16 and Table 4-17 show the ANOVA outputs and the discussion was based on the null hypothesis, which makes comparison of the mean between groups and mean within a group. The hypothesis suggests that there is no difference between the two means i.e. effects of the variables are the same and the decisions on whether to accept or reject the hypothesis were based on the ratio between the F value and F critical. If F value <F critical then the null hypothesis will be accepted, and the opposite is true. If F value >F critical, the null hypothesis will be rejected. The results show that of the three variables, X_2 has the largest positive sum of all square value, followed by X_3 which has a more significant effect while X_1 reported a negative sum of square value, suggesting the least effect. Thus as the parameters X_2 and X_3 were increased, the mass yield of concentrate and Fe grade were also increased. The opposite was true for X_1, whereby an increase in parameters had a negative impact on the mass yield of concentrate with the Fe grade remaining within the same range. The order of significant effect was $X_2 > X_3 > X_1$ and $X_2X_3 > X_1X_2 > X_1X_3 > X_1X_2X_3$.

To achieve a good product quality (grade and recovery) using the Longi LGS 500 for treatment of a low grade hematite material at three size fractions, a balance between the main parameters X_2 and X_3 would be required. X_2X_3 was shown to have the most effect compared to X_1X_2 and the more complex $X_1X_2X_3$, further supporting the fact that the two variables were the main parameters for achieving optimum separation. Thus a balance could be achieved at a low magnetic field intensity thus allowing for recovery of the highly susceptible particles free of gangue and at a high pulsation frequency ensuring that all the non-magnetic particles are not attached to the matrix or even entrapped within the non-selective agglomerates.

Table 4-16: ANOVA output for mass yield of concentrate

Groups	Count	SOS	Average	Variance
Column 1: X_1	27	1807.06	66.93	133.61
Column 2: X_2	27	508.63	18.84	167.33
Column 3: X_3	27	86.59	3.21	4.55
Column 4: X_1X_2	27	81.23	3.01	40.83
Column 5: X_1X_3	27	46.24	1.71	1.86
Column 6: X_2X_3	27	151.71	5.62	78.89
Column 7: $X_1X_2X_3$	27	144.69	5.36	78.16

Table 4-17: ANOVA output for Fe grade

Groups	Count	SOS	Average	Varience
Column 1: X_1	27	26.59	0.98	21.80
Column 2: X_2	27	74.97	2.78	9.78
Column 3: X_3	27	87.23	3.23	4.32
Column 4: X_1X_2	27	263.34	9.75	51.09
Column 5: X_1X_3	27	79.27	2.94	1.32
Column 6: X_2X_3	27	407.59	15.10	95.81
Column 7: $X_1X_2X_3$	27	391.92	14.52	102.82

Table 4-18 and Table 4-19 summarises the ANOVA outputs for the iron ore, from which the sum of all squares (SOS), degree of freedom (df), mean square (MS), F value, probability (p) value and Fcritical were determined and conclusions drawn. The p value gives an indication of the significance of variables in predicting the responses to individual and interaction effects. (Murty *et al*, 2013 and Statsoft, 2013).

Table 4-18: ANOVA summary output data for mass yield

Source of Variation	SOS	df	MS	F value	P-value	F crit
Between Groups	126612.45	6.00	21102.07	292.37	0.00	2.15
Within Groups	13136.10	182.00	72.18			
Total	139748.54	188.00				

Table 4-19: ANOVA summary output data for Fe grade

Source of Variation	SOS	df	MS	F value	P-value	F crit
Between Groups	14533.46	6.00	2422.24	59.09	0.00	2.15
Within Groups	7460.39	182.00	40.99			
Total	21993.85	188.00				

The results in Table 4-18 and Table 4-19 reported a low p value at <0.05 indicating that the model is significant at the 95% confidence level. Based on these results, the variables were considered significant for the magnetic separation process.

4.8.2. The mathematical model

The regression equation as shown in 4.3 is the mathematical model that is use to determine how well the model fits to the actual data. A Microsoft 2010 excel spreadsheet was used to determine this relationship, principally for mass yield of concentrate and Fe grades. In general, the smaller the difference between the model and the actual values, the higher the regression coefficient (R^2) and the better the fit and closer to 100%.

$$Y = a_o + a_1X_1 + a_2X_2 + a_3X_3 + a_4X_1X_2 + a_5X_1X_3 + a_6X_2X_3 + a_7X_1X_2X_3 \qquad (4.3)$$

Where Y is the Fe grade or mass yield of concentrate and X is the independent variable.

Figure 4-18 to Figure 4-20 show correlations between the modelled outputs and the actual values.

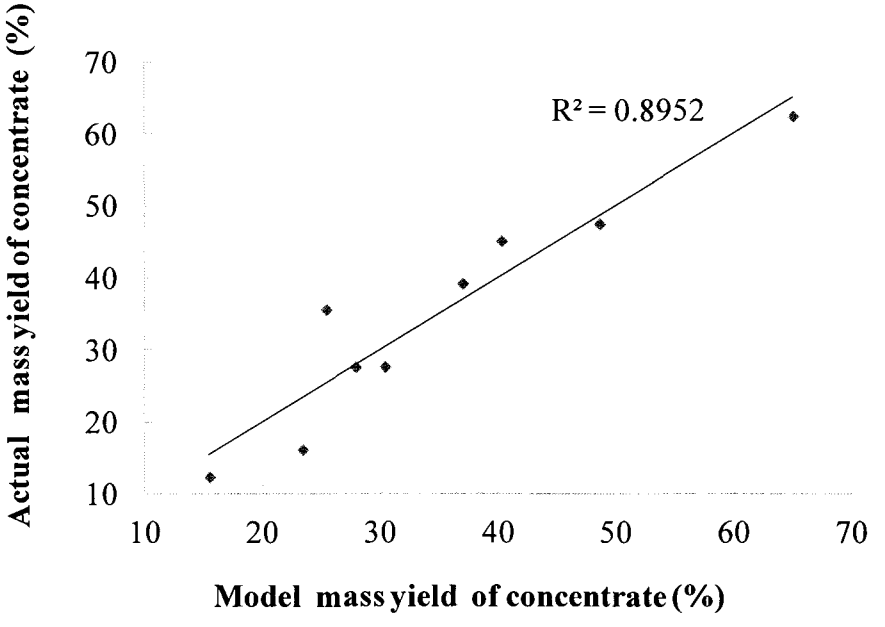

Figure 4-18: Mass yield relationship between the model and actual data for the treatment of the -1000+106μm fraction

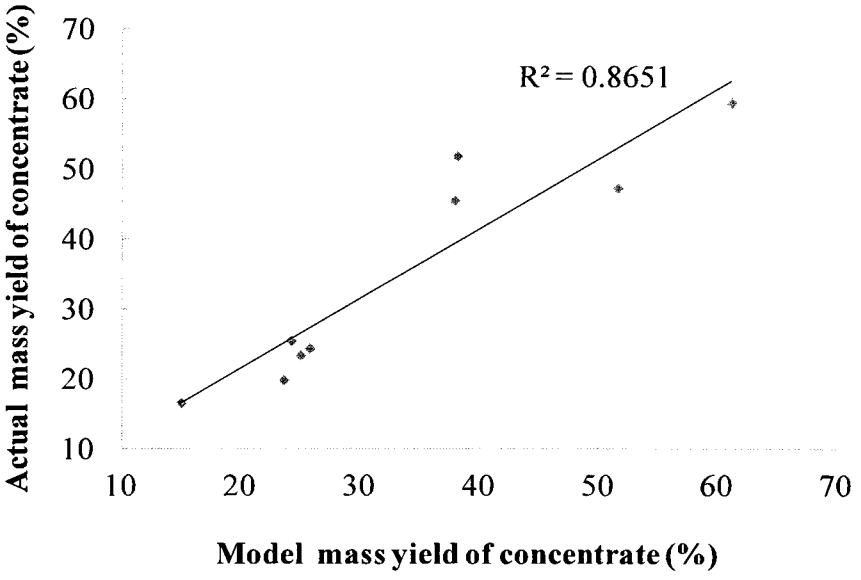

Figure 4-19: Mass yield relationship between the model and actual data for the treatment of the 106+75μm fraction

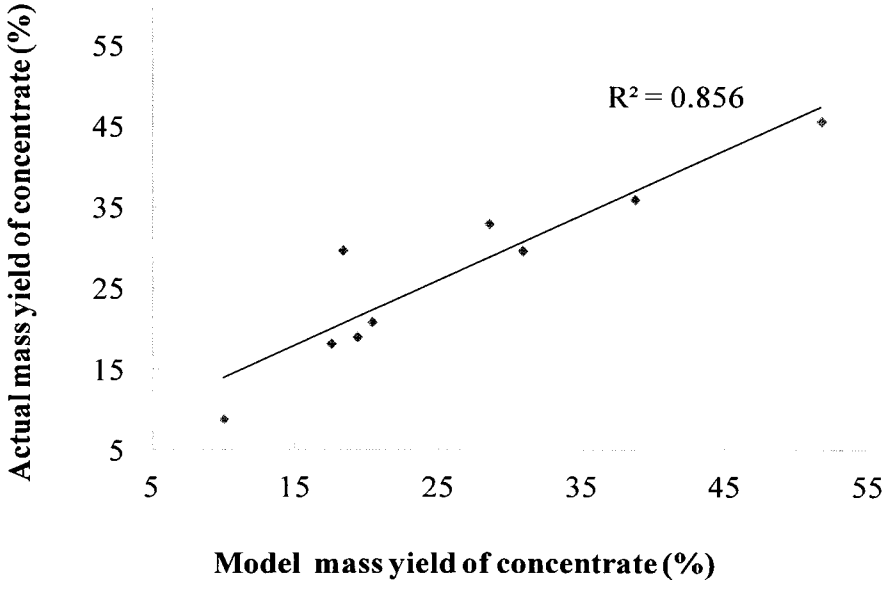

Figure 4-20: Mass yield relationship between the model and actual data for the treatment of the -75 μm fraction

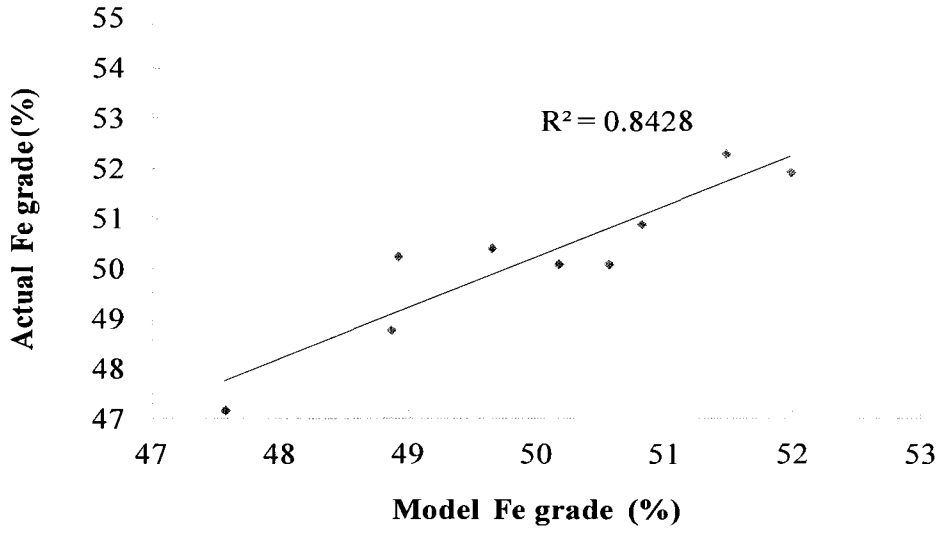

Figure 4-21: Fe grade relationship between the model and actual data for the treatment of the -1000+106 μm fraction

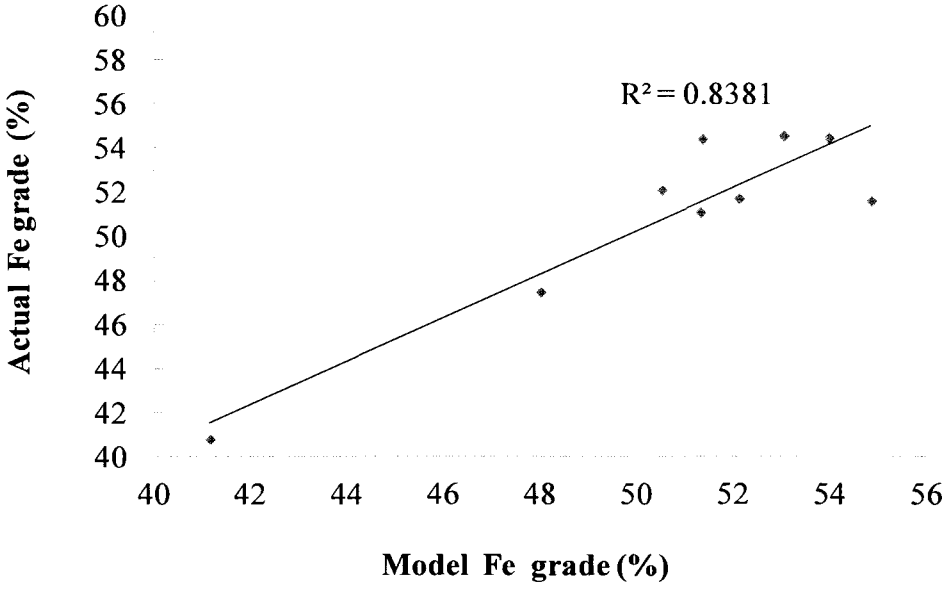

Figure 4-22: Fe grade relationship between the model and actual data for the treatment of the -106+75μm fraction

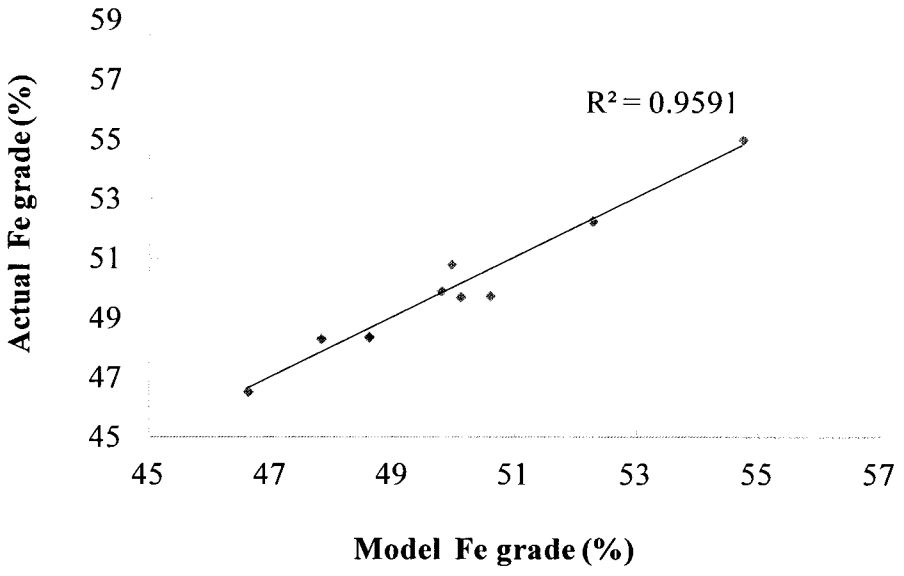

Figure 4-23: Fe grade relationship between the model and actual data for the treatment of the -75 μm fraction

The results further confirmed that X_2 reported the highest positive values, indicating that it has the most significant effect. X_2X_3 interaction was shown to have contributed the most positive value to the modelled value. The responses reported R^2 coefficients of 0.90, 0.87, 0.86 for mass yield of concentrates and 0.84, 0.85, 0.96 for Fe grade -1000 +106 μm, -106+75 μm and -75 μm size fractions respectively, further suggesting the significance of the model. The authors Joglekar and May (1987) suggested that a good R^2 fit should be at least 0.80. The results could be further supported by results attained by Aziz *et al.* (2012), who reported R^2 values of 0.93 for manganese recovery and 0.94 for iron recovery. Again the results by Tripathy *et al.* (2010), reported R^2 values of 0.94 for chromite grade and 0.93 for chromite recovery.

4.9. Summary

The WHIMS investigations were conducted on three size fractions consisting of slightly different mineral Fe and SiO_2 values. The results showed that the Longi LGS 500 possesses good capabilities for beneficiating the material even at wide size ranges. For example the -75

μm size fraction reported up to ~55% Fe. The analysis of variance together with the regression model was applied to validate the effects of the three operating variables that were investigated. From the model outputs, the null hypothesis qualified to be rejected indicating that the effects of the parameters were significant to the mass yield of concentrate and the Fe grade responses, particularly the magnetic field intensity and pulsation frequency. In addition, the R^2 regression coefficients from the modelled and actual values were in good correlation and were reported to be in the range of 0.84 to 0.96.

CHAPTER 5

5. CONCLUSION

This research study investigated the beneficiation capabilities of the newly developed Longi LGS 500 WHIMS. The investigations were conducted on a low grade iron ore material prepared to three size fractions and a coal material prepared at a single size fraction. Three operating parameters were investigated for the iron ore material. These were the effects of varying the pulp solids, magnetic field intensity and pulsation frequency. The results obtained were validated using ANOVA and a mathematical regression model. The coal material on the other hand was treated at a set of optimum parameters that were determined from the iron ore investigations and deemed to be suitable for a material with a low magnetic susceptibility. From the research investigations, the following conclusions can be drawn:

- The Longi LGS 500 shows good potential for beneficiating low grade iron ore fines.
- The SEM determined sizing distribution on the -1.18 mm feed material was reported to be slightly finer compared to the sieve stacking method. However there was a good correlation in terms of the mass and Fe distribution between the two methods.
- The automated SEM analysis could be a technique that could be combined with other processes for fines characterisation.
- The MLA back scatter images showed complex mineral associations in all three size fractions. This indicated that a much finer grind at <75 μm would be required to fully liberate the Fe oxide grains from the silicate gangue to achieve an improved recovery of the product.
- The increase in pulp solids from 20% to 25% and 30% had a negative effect on the mass yield of concentrate. At pulp solids >20%, the mass yield of concentrates and Fe recoveries were shown to decrease with no significant effect on the Fe grade. This could be as the result of the rapid agglomeration of particles on the matrix and caused some paramagnetic particles to be prevented from attaching to the matrix due to unavailable surface area.
- The changes in magnetic intensity from 1000 Gauss, 5500 Gauss and 10000 Gauss increased the mass yield of concentrates. The matrix was possibly overloaded by the agglomated particles, mechanically entrapping weakly diamagnetic gangue. As a result, the SiO_2 was increased which diluted the Fe grade.

- The pulsation mechanism on the other hand, positively affected the overall quality of the product, particularly the -75μm size fraction. An increase from 6.5 Hz to 19.5 Hz and 25.5 Hz showed an increase in the mass yield of concentrates and the Fe grade. This is because the matrix was kept clean to allow free, highly susceptible particles to attach to the matrix.

The magnetic separation results for the iron ore were verified using the statistical model and the following was observed:

- X_2 (magnetic field intensity) had the most positive effect on the mass yields of concentrate while it had a negative effect on the Fe grades.
- The X_3 (pulsation frequency) had a positive effect on both the mass yield of concentrates and Fe grades.
- The X_1 (pulp solids) had a negative effect on the mass yield of concentrates but the Fe grades were not affected by the changes.
- The interactions between parameters were shown to be essential, the most notable was that between X_2X_3 which had the most effect, followed by X_1X_3 then $X_1X_2X_3$. These results supported the fact that of the three variables investigated, X_2 and X_3 had the most impact on this particular sample of iron ore fines.
- The probability (p) values from the mass yield of concentrates and Fe grades were reported to be <0.05, qualifying for the null hypothesis to be rejected. This was supported by the fact that the effects of X_1, X_2 and X_3 on the material were indeed different.
- The results were validated by comparing the modelled and actual values. The correlations were satisfactory, reporting R^2 regression coefficients ranging from 0.84 to 0.96.
- The optimum conditions for the treatment of the iron ore were achieved at 20% pulp solids, 1000 Gauss and a pulsation frequency of 25.2 Hz.

CHAPTER 6

6. RECOMMENDATIONS

The following recommendations are made and are based on the observations and results of research work to date.

- The complex mineral associations suggested that a much finer grind of <75 μm should be undertaken to fully liberate the Fe oxide grains from the silicate gangue to achieve a better quality and yield of product.
- It was observed that the magnetic field intensity and the pulsation frequency played a major role during separation. More investigations should be conducted to further optimise the operating parameters for the individual size fractions.
- An electron microprobe analysis should be conducted on the iron ore material to better define the Fe form present to better understand the difference between the chemical and SEM determined head grades.
- A two stage operation should be undertaken to produce a primary concentrates for second stage cleaning.
- A microscopic/mineralogical investigation of the iron ore agglomeration should be undertaken to ascertain the phases of gangue material in the concentrate.
- A separate detailed investigation should be conducted on the coal to gain a better understanding of its response to magnetic separation. This would include both Fe and S analyses on the feed and magnetic separation products.

7. REFERENCES

Kumba Iron ore integrated annual report: Strong Fundamentals in an uncertain economic environment. (2011). Available at http://www.kumba.co.za/reports/kumbaar2011/integrated /bus/bus_rev_marke-t.php. Accessed, July 18, 2012.

Monhanty, S. Nayak, B and Bhattacharyya, K.K. (2010). High Intensity Magnetic Separation of Iron Ore slimes and its limitations. National Metallurgical Laboratory, pages 173-178.

England, T. (2000). The economic agglomeration of fine coal for industrial and commercial use: A review of the past and present work both locally and internationally. Coaltech 2020 report (unpublished).

Dahe, X. Liu, S and Chen, J. (1998). New technology of pulsating high gradient magnetic separation. International Journal of Mineral Processing, Volume 54, pages 111–127.

Svoboda, J. (2001). A realistic description of the process of high gradient magnetic separation, Minerals Engineering, No. 11, Volume 14, pages 1493-1503.

Augusto, P.A, Augusto, P and Castelo-Grande, T. (2002). Magnetic classification, Minerals Engineering, No 2, Volume 15, Pages 35-43.

Hoffmann, C; Franzreb, M. and Holl, W.H. (2002). A novel high-gradient magnetic separator (HGMS) design for biotech applications, IEEE Transactions on Applied Superconductivity, No. 1. Volume 12, pages. 963-966.

Zeng, W and Dahe, X. (2003). The latest application of SLon vertical ring and pulsating high-gradient magnetic separator. Minerals Engineering, Volume 16, pages 563–565.

Dobbins, M.N, Dunn, P, and Sherrell. I. (2009). Recent advances in magnetic separator designs and applications. Proceedings of the 7th International Heavy Minerals Conference. South African Institute of Mining and Metallurgy, pages 197-203.

Angadi, S. I, Ho-Seok Jeon, Mohanthy.S, Prakash. S and Das, S. (2012). Analysis of Wet High-Intensity Magnetic Separation of Low-Grade Indian Iron Ore using Statistical Technique, Separation Science and Technology, volume 47:8, Pages 1129-1138.

Das, B, Prakash, S, Bhoumik, S.K, Mohapatra, B.K and. Narasimhan, K.S. (1991). Magnetic Separation of Iron Ore Slimes by Wet High Intensity Magnetic Separator, Transactions Indian Institute Metals. No. 5, Volume 44 page 355.

Song, S, Lu, S and Lopez-Valdivieso, A. (2002). Magnetic separation of hematite and limonite fines as hydrophobic flocs from iron ores. Minerals Engineering, No.6, Volume 15, 2002.

Arol, A.I and Aydogan, A. (2004). Recovery enhancement of magnetite fines in magnetic separation. Physicochemical and Engineering Aspects, No.2, Volume 232, pages 151-154.

Dobbins, M.N, Domenico, J, and Dunn, P. (2007). A discussion of magnetic separation techniques for concentrating ilmenite and chromite ores. Proceedings of the 6th International Heavy Minerals Conference, South African Institute of Mining and Metallurgy, pages 63-70

www.bdlive.co.za, excessed November 28, 2014

Jamieson, E. Jones, A. Cooling, D and Stockton, N. (2006). Magnetic separation of Red Sand to produce value. Minerals Engineering, Volume19, pages 1603–1605.

Padmanabhan, N.P.H and Sreenivas, T. (2011). Process parametric study for the recovery of very-fine size uranium values on super-conducting high gradient magnetic separator. Advanced Powder Technology, Volume 22, pages 131-137.

Al-Wakeel, M. I and Abd El-Rahman, M. K. (2006). Beneficiation of low grade Ghorabi iron ore. Trans Institute of Materials, Mineral and Mining, No. 4, volume 115, pages 177-182.

Kahn, H. Tassinari, M.M.L and Ratti, G. (2003). Characterization of bauxite fines aiming to minimize their iron content. Minerals Engineering, Volume 16, pages 1313–1315.

Yavuz,C.T, Mayo, J. T, Yu. W. W, Prakash, A, Falkner,J.C, Yean, S, Cong, L, Shipley, H.J, Kan, A, Tomson, M, Natelson, D and Colvin, V.L. (2006). Low-Field Magnetic Separation of Monodisperse Fe_3O_4 Nanocrystals, Science, Volume 314, page 964.

Yavuz, C. T. Prakash, B.A. Mayoa, J.T and Colvin, V.L. (2009). Magnetic separations: From steel plants to biotechnology. Chemical Engineering Science, Volume 64, pages 2510-2521.

Joseph, P.F. Prasad, V.G.K. Janarthanan, A. J and Viswanath, R.V. (2010). Wet High Magnetic Separation: Efforts taken to adapt the machine to the mineral separation plant of Irel, Chavara. Proceedings of the XI International Seminar, Mineral Processing Technology, pages 166 -172.

The ASIA Miner report (LONGI): LGS WHIMS improves concentrate efficiency, (2010). First quarter January-March, page 33.

Hearn, S.B and Dobbins, M.N. (2007). SLon magnetic separator: A new approach for recovering and concentrating iron ore fines. Montreal Energy and Mines, April 29- May 2.

Das, B. Mishra, B.K. Prakash, S. Das, S.K. Reddy, P.S.R and Angadi, S.I. (2010). Magnetic and flotation studies of banded hematite quartzite (BHQ) ore for the production of pellet grade concentrate. International Journal of Minerals Metallurgy and Materials, No. 6, Volume 17, pages 675-682.

Zogo, B. (2009). Beneficiation potential of low grade iron ore from a discard lumpy stockpile and fines tailings dam at Beeshoek nine, April 2009.

An independent competent person's report on the mining assets of Exxaro Resources Limited accessed January 16, 2013.

Oberteuffer, J.A. (1974). Magnetic separation: A review of principles, devices and applications, Transactions on magnetic, Volume 2, pages 223-238.

Chen, L, Lia, G, Qian Z and Chen J. (2012). Vibrating high gradient magnetic separation for purification of iron impurities under dry condition, International Journal of Mineral Processing, Volume 102-103, pages 136–140.

Li, Y, Wang, J, Wang, X, Wang, B, Luan, Z. (2011). Feasibility study of iron mineral separation from red mud by high gradient superconducting magnetic separation, Science Direct, Volume 471, Pages 91-96.

Alp, I. (2007). Application of magnetic separation technology for the recovery of colemanite from plant tailings, Department of Mining Engineering, pages 431-438.

Dahe, X. (2004). SLon Magnetic separation applied in the ilmenite processing industry. Physical Separation in Science and Engineering, No. 3-4, Volume 13, pages 119–126.

Li, C, Sun. H, Bai. J and Li, L. (2010), Innovative methodology for comprehensive utilization of iron ore tailings Part 1. The recovery of iron from iron ore tailings using magnetic separation after magnetizing roasting. Journal of Hazardous Materials, Volume 174. Pages 71–77.

Newns, A, Pascoe, R.D. (2002). Influence of path length and slurry velocity on the removal of iron from kaolin using a high gradient magnetic separator, Minerals Engineering, No. 6, Volume 15.

Jiao, H and Shi, C. (2007). Research on Dry Permanent Magnetic Separator of Fine Coal, School of material science and engineering, pages 2464 -2468.

Svoboda, J. (1987). Magnetic Methods for the Treatment of Minerals, Developments in Mineral Processing, Volume 8, pages 590-605.

Dwari R. K. and Rao K. H. (1997). DRY BENEFICIATION OF COAL, Mineral Processing & Extractive Metall, Review 28, pages 177–234.

Chakravorty, N. (1989). Magnetic Separation in Third Short Term Refresher Course on Classification and Concentration, Dec. 10th - 17th December Institute for Miners and Metal Workers Education.

Likun, G and Yun, C. (2010). A study on the rare earth ore containing scandium by high gradient magnetic separation, Journal of Rare Earths, No. 4, Volume 28, pages 622.

Rayner, J.G, Napier-Munn, T.J. (2000). The mechanism of magnetic capture in the wet drum magnetic separator, Minerals Engineering, No.3, Volume.13, Pages 277–285

Tucker, P. (1994). Modelling wet high magnetic separation: A case study. Minerals Engineering, No. 10, Volume 7, pages 1281-1300.

Shao, Y.; Veasey, T.J.; Rowson, N.A. (1996) Magnetic flocculation of hematite minerals. Magnetic and Electrical Separation, Volume 7: page 227.

Rezlescu, N, Murarui, V, Rotariu, O and Badescu, V. (1995). Capture modelling for an axial high gradient magnetic separation filter with a bounded flow field, Powder technology, Volume 83, page 259-264.

Stahle, L and Wold, S. (1989), Analysis of Variance (ANOVA). Chemomerrics and Intelligent Laboratory Systems, Volume 6, pages 259-272.

Marin-Galiano, M and Kunert.J. (2006). Comparison of ANOVA with the Tobit model for analysing sensory data, Food Quality and Preference, Volume 17, pages 209–218.

Kherad-Pajouh, S, Renaud, O. (2010). An exact permutation method for testing any effect in balanced and unbalanced fixed effect ANOVA, Computational Statistics and Data Analysis, Volume 54, page 1881-1893.

Driscoll C, W (2007). Robustness of the ANOVA and Tukey-Kramer Statistical Test, Computers Engineering, No. 1/2, Volume 31, pages 265-268.

Nakhaei, F, Mosavi M.R., Sam, A, Vaghei Y. (2012). Recovery and grade accurate prediction of pilot plant flotation column concentrate: Neural network and statistical techniques, International Journal of Mineral Processing, Volume 110–111, pages 140–154.

Svoboda, J and Fujita, T. (2003). 'Recent developments in magnetic methods of material separation'. Minerals Engineering, Volume16, pages 785–792.

Corrans I, J and Levin, J. (1979). Wet magnetic separation for the concentration of Witwatersrand gold-uranium ores and residue, Journal of the South African Institute of mining and metallurgy, page 210-228.

Svoboda, J. (1981). A theoretical approach to the magnetic flocculation of weakly magnetic minerals. International Journal for Mineral Processing, No. 4, Volume 8, pages 377-390.

Chen, L. (2011). Effect of magnetic field orientation on high gradient magnetic separation performance, Minerals Engineering, Volume 24, pages 88-90.

Bergmann, P. (2010). Modelling of Fines Gravity Separation, The Southern African Institute of Mining and Metallurgy, Proceedings of the fines beneficiation and dewatering and agglomeration.

Gerlach, R.W and Nocerino, J.M. (2003). Guidance for Obtaining Representative Laboratory Analytical Subsamples from Particulate Laboratory Samples, U.S. Environmental Protection Agency report.

Tripathy, S.K, Ramamurthy, Y, Sahu1, G.P. and Tathavadkar V. (2010). Ultra fine chromite concentration using spiral concentrator, Proceedings of the XI International Seminar on Mineral Processing Technology, pages. 144–150.

Natarajan, R, Sreenivas, T, Rao, N. K. (1992). Pre-concentration of low-grade uranium ores by gravity and magnetic methods: a case study with copper tailings from Singhbhum, Bihar, India. Exploration and Research for Atomic Minerals, Volume 5, page 93.

Zeng W. and Dahe, X. (2003). The latest application of SLon vertical ring and pulsating high-gradient magnetic separator. Minerals Engineering, Volume 16, pages 563-565

Murty, V.G.K, Murthy, V.R, JaiSankar, N, Bhavya Manjeera, P and Kumar, P. (2013). Operation and optimization of silliminite beneficiation from beach sands, International Journal of Advanced Research, Volume 1, pages 347-355.

Statsoft electronic statistics textbook, accessed Nov 01, 2013

Joglekar, A. M and May, A.T. (1987). Product excellence through design of experiments. Cereal Foods World, Volume 32, pages 857-868.

Aziz, D, Shafaei, S.Z, Noaparast, M, Abodollahi, H. (2012). Modelling and optimization of low-grade Mn bearing ore leaching using response surface methodology and central composite rotatable design, Transactions of Nonferrous Metals Society of China, Volume 22, pages 2295-2305.

8. APPENDICES

8.1. Appendix A: Effects of changing the pulp solids

Table 8-20: -1000+106 µm at 20% pulp solids

Size Fraction (µm)	Mass (%)	Grade (%)			Recovery (%)		
		Total Fe	SiO_2	Al_2O_3	Total Fe	SiO_2	Al_2O_3
Mags	47.48	51.94	8.53	10.20	56.34	29.43	35.27
Midds	9.63	36.26	17.10	17.90	7.98	11.96	12.55
Non mags	42.89	36.40	18.80	16.70	35.68	58.60	52.18
Calculated head grade	**100**	43.76	13.76	13.73	100	100	100
Measured head grade		44.75	13.60	13.65			

Table 8-21: -1000+106 µm at 25% pulp solids

Size Fraction (µm)	Mass (%)	Grade (%)			Recovery (%)		
		Total Fe	SiO_2	Al_2O_3	Total Fe	SiO_3	Al_2O_3
Mags	39.19	50.90	10.71	12.95	43.53	30.19	35.17
Midds	4.47	40.00	16.93	18.56	3.90	5.44	5.75
Non mags	56.35	42.75	15.88	15.13	52.57	64.37	59.09
Calculated head grade	**100**	45.82	13.90	14.43	100	100	100
Measured head grade		44.75	13.60	13.65			

Table 8-22: -1000+106 µm at 30% pulp solids

Size Fraction (µm)	Mass (%)	Grade (%)			Recovery (%)		
		Total Fe	SiO_2	Al_2O_3	Total Fe	SiO_2	Al_2O_3
Mags	35.61	50.42	10.50	11.50	40.75	26.83	28.31
Midds	2.52	42.43	15.50	16.10	2.43	2.80	2.80
Non mags	61.87	40.47	15.85	16.10	56.83	70.37	68.88
Calculated head grade	**100**	44.06	13.94	14.46	100	100	100
Measured head grade		44.75	13.60	13.65			

Table 8-23: -106+75 µm at 20% pulp solids

Size Fraction (µm)	Mass (%)	Grade (%)			Recovery (%)		
		Total Fe	SiO_2	Al_2O_3	Total Fe	SiO_2	Al_2O_3
Mags	47.41	52.10	9.42	10.51	55.16	28.89	39.15
Midds	4.49	40.00	19.91	14.22	4.01	5.79	5.02
Non mags	48.10	38.0	20.98	14.77	40.83	65.32	55.83
Calculated head grade	**100**	44.77	15.45	12.73	100	100	100
Measured head grade		43.52	15.50	12.60			

Table 8-24: -106+75 µm at 25% pulp solids

Size Fraction (µm)	Mass (%)	Grade (%)			Recovery (%)		
		Total Fe	SiO_2	Al_2O_3	Total Fe	SiO_2	Al_2O_3
Mags	45.58	51.06	9.31	9.62	54.19	27.28	34.35
Midds	15.57	36.65	20.50	15.40	13.28	20.52	18.78
Non mags	38.85	35.95	20.90	15.40	32.52	52.20	46.87
Calculated head grade	**100**	42.95	15.55	12.77	100	100	100
Measured head grade		43.52	15.50	12.60			

Table 8-25: -106+75 µm at 30% pulp solids

Size Fraction (µm)	Mass (%)	Grade (%)			Recovery (%)		
		Total Fe	SiO_2	Al_2O_3	Total Fe	SiO_2	Al_2O_3
Mags	40.11	51.70	9.22	10.00	46.48	24.40	32.06
Midds	9.64	39.20	19.04	14.58	8.47	12.11	11.24
Non mags	50.25	40.00	19.16	14.12	45.05	63.49	56.71
Calculated head grade	**100**	44.62	15.16	12.51	100	100	100
Measured head grade		43.52	15.50	12.60			

Table 8-26: -75 µm at 20% pulp solids

Size Fraction (µm)	Mass (%)	Grade (%)			Recovery (%)		
		Total Fe	SiO_2	Al_2O_3	Total Fe	SiO_2	Al_2O_3
Mags	36.01	49.70	11.29	10.99	44.22	28.93	22.37
Midds	16.03	32.79	15.20	23.00	12.99	17.34	20.84
Non mags	47.96	36.12	15.75	20.95	42.79	53.74	56.79
Calculated head grade	**100**	40.48	14.06	17.69	100	100	100
Measured head grade		39.49	13.80	18.10			

Table 8-27: -75 µm at 25% pulp solids

Size Fraction (µm)	Mass (%)	Grade (%)			Recovery (%)		
		Total Fe	SiO_2	Al_2O_3	Total Fe	SiO_2	Al_2O_3
Mags	33.02	50.80	10.43	10.92	42.64	24.64	20.46
Midds	18.79	35.50	15.84	20.29	16.95	21.29	21.63
Non mags	48.18	33.00	15.69	21.19	40.41	54.07	57.92
Calculated head grade	**100**	39.35	13.98	17.63	100	100	100
Measured head grade		39.49	13.80	18.10			

Table 8-28: -75 µm at 30% pulp solids

Size Fraction (µm)	Mass (%)	Grade (%)			Recovery (%)		
		Total Fe	SiO_2	Al_2O_3	Total Fe	SiO_2	Al_2O_3
Mags	29.78	49.90	11.30	10.83	37.24	24.06	18.02
Midds	10.70	37.40	15.80	20.33	10.03	12.09	12.15
Non mags	59.52	35.35	15.00	21.00	52.73	63.85	69.83
Calculated head grade	**100**	39.90	13.98	17.90	100	100	100
Measured head grade		39.49	13.80	18.10			

8.2.Appendix B: Effects of changing the magnetic field intensity

Table 8-29: -1000+106 μm at 1000 Gauss

Size Fraction (μm)	Mass (%)	Grade (%)			Recovery (%)		
		Total Fe	SiO_2	Al_2O_3	Total Fe	SiO_3	Al_2O_3
Mags	12.34	50.10	10.73	14.01	13.80	9.70	11.02
Midds	2.90	40.2	16.00	16.03	2.60	3.40	2.96
Non mags	84.75	44.2	14.00	15.93	83.59	86.90	86.02
Calculated head grade	**100**	44.81	13.65	15.70	100.00	100	100
Measured head grade		44.75	13.60	13.65			

Table 8-30: -1000+106 μm at 5500 Gauss

Size Fraction (μm)	Mass (%)	Grade (%)			Recovery (%)		
		Total Fe	SiO_2	Al_2O_3	Total Fe	SiO_2	Al_2O_3
Mags	45.08	48.78	11.00	12.60	49.95	36.32	40.85
Midds	8.26	40.51	17.70	16.50	7.60	10.70	9.80
Non mags	46.67	40.04	15.50	14.70	42.45	52.98	49.35
Calculated head grade	**100**	44.02	13.65	13.90	100	100	100
Measured head grade		44.75	13.60	13.65			

Table 8-31: -1000+106 μm at 10000 Gauss

Size Fraction (μm)	Mass (%)	Grade (%)			Recovery (%)		
		Total Fe	SiO_2	Al_2O_3	Total Fe	SiO_2	Al_2O_3
Mags	62.45	47.18	12.00	13.70	66.26	53.75	60.30
Midds	11.51	45.31	14.40	14.10	11.73	11.89	11.44
Non mags	26.04	37.58	18.40	15.40	22.00	34.36	28.26
Calculated head grade	**100**	44.47	13.94	14.19	100	100	100
Measured head grade		44.75	13.60	13.65			

Table 8-32: -106+75 μm at 1000 Gauss

Size Fraction (μm)	Mass (%)	Grade (%)			Recovery (%)		
		Total Fe	SiO_2	Al_2O_3	Total Fe	SiO_2	Al_2O_3
Mags	16.63	51.60	10.11	20.94	18.80	12.55	21.68
Midds	3.56	43.40	16.48	15.27	3.38	4.38	3.38
Non mags	79.81	44.50	13.94	15.08	77.82	83.07	74.94
Calculated head grade	**100**	45.64	13.39	16.06	100	100	100
Measured head grade		44.75	13.60	13.65			

Table 8-33: -106+75 μm at 5500 Gauss

Size Fraction (μm)	Mass (%)	Grade (%)			Recovery (%)		
		Total Fe	SiO_2	Al_2O_3	Total Fe	SiO_2	Al_2O_3
Mags	51.94	47.47	17.18	17.44	56.42	63.99	60.79
Midds	5.28	39.00	14.08	16.97	4.72	5.34	6.02
Non mags	42.78	39.70	10.00	11.57	38.86	30.68	33.20
Calculated head grade	**100**	43.70	13.94	14.91	100	100	100
Measured head grade		44.75	13.60	13.65			

Table 8-34: -106+75 µm at 10000 Gauss

Size Fraction (µm)	Mass (%)	Grade (%)			Recovery (%)		
		Total Fe	SiO_2	Al_2O_3	Total Fe	SiO_2	Al_2O_3
Mags	59.58	41.80	17.24	15.84	56.92	70.61	61.22
Midds	10.94	40.50	11.79	13.59	10.13	8.87	9.64
Non mags	29.48	48.90	10.13	15.23	32.95	20.53	29.13
Calculated head grade	**100**	43.75	14.55	15.41	100	100	100
Measured head grade		44.75	13.60	13.65			

Table 8-35:-75 µm at 1000 Gauss

Size Fraction (µm)	Mass (%)	Grade (%)			Recovery (%)		
		Total Fe	SiO_2	Al_2O_3	Total Fe	SiO_2	Al_2O_3
Mags	8.91	49.74	11.40	9.20	11.15	7.29	4.44
Midds	18.34	38.19	14.30	19.90	17.62	18.82	19.79
Non mags	72.75	38.93	14.15	19.20	71.24	73.89	75.76
Calculated head grade	**100**	39.76	13.93	18.44	100	100	100
Measured head grade		39.49	13.80	18.10			

Table 8-36: -75 µm at 5500 Gauss

Size Fraction (µm)	Mass (%)	Grade (%)			Recovery (%)		
		Total Fe	SiO_2	Al_2O_3	Total Fe	SiO_2	Al_2O_3
Mags	29.71	48.36	11.00	11.90	35.91	23.93	19.98
Midds	42.99	36.89	14.00	19.60	39.63	44.08	47.62
Non mags	27.30	35.84	16.00	21.00	24.46	31.99	32.40
Calculated head grade	**100**	40.01	13.65	17.69	100	100	100
Measured head grade		39.49	13.80	18.10			

Table 8-37: -75 µm at 10000 Gauss

Size Fraction (µm)	Mass (%)	Grade (%)			Recovery (%)		
		Total Fe	SiO_2	Al_2O_3	Total Fe	SiO_2	Al_2O_3
Mags	45.71	46.52	11.90	13.10	52.47	38.55	33.53
Midds	29.01	37.01	15.50	20.60	26.49	31.87	33.46
Non mags	25.29	33.71	16.50	23.30	21.04	29.58	33.00
Calculated head grade	**100**	40.52	14.11	17.85	100	100	100
Measured head grade		39.49	13.80	18.10			

8.3.Appendix C: Effects of changing pulsation frequency

Table 8-38: -1000+106 μm at 6.5 Hz

Size Fraction (μm)	Mass (%)	Grade (%)			Recovery (%)		
		Total Fe	SiO_3	Al_2O_3	Total Fe	SiO_3	Al_2O_3
Mags	16.15	50.25	10.51	12.58	18.40	6.01	6.93
Midds	2.30	39.30	15.63	13.24	14.39	5.76	4.71
Non mags	81.55	43.0	13.90	13.41	15.75	87.26	81.17
Calculated head grade	**100**	44.09	13.39	13.27	48.55	99.03	92.81
Measured head grade		44.75	13.60	13.65			

Table 8-39: -1000+106 μm at 19.5 Hz

Size Fraction (μm)	Mass (%)	Grade (%)			Recovery (%)		
		Total Fe	SiO_2	Al_2O_3	Total Fe	SiO_3	Al_2O_3
Mags	27.59	50.10	10.14	12.00	31.44	21.12	24.53
Midds	1.83	41.57	15.60	14.840	1.73	2.15	2.01
Non mags	70.58	41.63	14.400	14.050	66.8	76.7	73.5
Calculated head grade	**100**	43.97	13.25	13.50	100	100	100
Measured head grade		44.75	13.60	13.65			

Table 8-40: -1000+106 μm at 25.2 Hz

Size Fraction (μm)	Mass (%)	Grade (%)			Recovery (%)		
		Total Fe	SiO_3	Al_2O_3	Total Fe	SiO_3	Al_2O_3
Mags	27.65	52.30	9.11	12.13	31.81	18.25	24.03
Midds	1.54	40.20	15.75	15.16	1.37	1.76	1.68
Non mags	70.80	42.90	15.59	14.65	66.82	79.98	74.29
Calculated head grade	**100**	45.46	13.80	13.96	100	100	100
Measured head grade		44.75	13.60	13.65			

Table 8-41: -106+75 μm at 6.5 Hz

Size Fraction (μm)	Mass (%)	Grade (%)			Recovery (%)		
		Total Fe	SiO_3	Al_2O_3	Total Fe	SiO_3	Al_2O_3
Mags	19.92	54.40	10.19	10.9809	24.85	12.98	16.51
Midds	4.61	39.80	16.2426	13.61	4.21	4.79	4.74
Non mags	75.47	41.00	17.04	13.82	70.94	82.23	78.74
Calculated head grade	**100**	43.61	15.64	13.24	100	100	100
Measured head grade		43.52	15.50	12.60			

Table 8-42: -106+75 μm at 19.5 Hz

Size Fraction (μm)	Mass (%)	Grade (%)			Recovery (%)		
		Total Fe	SiO_2	Al_2O_3	Total Fe	SiO_2	Al_2O_3
Mags	23.42	54.55	10.97	9.56	28.81	16.68	18.03
Midds	6.08	39.30	15.80	13.41	5.39	6.24	6.57
Non mags	70.49	41.40	16.85	13.29	65.80	77.09	75.40
Calculated head grade	**100**	44.35	15.41	12.42	100	100	100
Measured head grade		43.52	15.50	12.60			

Table 8-43: -106+75 µm at 25.2 Hz

Size Fraction (µm)	Mass (%)	Grade (%)			Recovery (%)		
		Total Fe	SiO_2	Al_2O_3	Total Fe	SiO_2	Al_2O_3
Mags	24.44	54.45	7.67	9.24	30.28	14.47	15.69
Midds	4.52	39.70	16.59	17.05	4.09	5.79	5.35
Non mags	71.04	40.60	14.55	16.01	65.63	79.75	78.96
Calculated head grade	**100**	43.94	12.96	14.40	100	100	100
Measured head grade		43.52	15.50	12.60			

Table 8-44: -75 µm at 6.5 Hz

Size Fraction (µm)	Mass (%)	Grade (%)			Recovery (%)		
		Total Fe	SiO_2	Al_2O_3	Total Fe	SiO_2	Al_2O_3
Mags	18.25	48.30	10.83	11.40	21.42	14.07	11.32
Midds	14.86	38.9	14.17	19.75	14.05	15.00	15.98
Non mags	66.89	39.7	14.89	19.97	64.53	70.93	72.71
Calculated head grade	**100**	41.15	14.04	18.37	100	100	100
Measured head grade		39.49	13.80	18.10			

Table 8-45: -75 µm at 19.5 Hz

Size Fraction (µm)	Mass (%)	Grade (%)			Recovery (%)		
		Total Fe	SiO_2	Al_2O_3	Total Fe	SiO_2	Al_2O_3
Mags	19.04	52.25	10.41	10.57	24.91	14.37	11.20
Midds	10.76	35.40	15.26	19.24	9.53	11.90	11.51
Non mags	70.20	37.30	14.49	19.80	65.56	73.73	77.29
Calculated head grade	**100**	39.94	13.80	17.98	100	100	100
Measured head grade		39.49	13.80	18.10			

Table 8-46: -75 µm at 25.2 Hz

Size Fraction (µm)	Mass (%)	Grade (%)			Recovery (%)		
		Total Fe	SiO_2	Al_2O_3	Total Fe	SiO_2	Al_2O_3
Mags	20.91	55.00	9.23	11.18	29.19	14.40	13.54
Midds	17.42	34.10	15.58	15.08	15.08	20.25	15.21
Non mags	61.67	35.60	14.20	19.95	55.73	65.35	71.25
Calculated head grade	**100**	39.39	13.40	17.27	100	100	100
Measured head grade		39.49	13.80	18.10			

8.4. Appendix D: Regression coefficient data

Table 8-28: Model output for mass yields of concentrate

-1000+106 µm		A	B	C	D	E	F	G	H	SOS
Actual (%)	Model (%)	74.50	-231.62	0.01	0.05	0.00	0.01	0.00	0.00	
		Constant	AX_1	AX_2	AX_3	AX_1X_2	AX_1X_3	AX_2X_3	$AX_1X_2X_3$	
47.48	48.58	74.50	-46.32	15.41	4.99	0.00	0.18	0.27	-0.18	1.20
39.19	36.99	74.50	-57.91	15.41	4.99	0.00	0.23	0.27	-0.23	4.81
35.61	25.41	74.50	-69.49	15.41	4.99	0.00	0.28	0.27	-0.27	103.91
12.34	15.51	74.50	-69.49	5.50	4.99	0.00	0.28	0.10	-0.10	10.00
45.08	40.27	74.50	-69.49	30.27	4.99	0.00	0.28	0.54	-0.54	23.05
62.45	65.04	74.50	-69.49	55.04	4.99	0.00	0.28	0.98	-0.98	6.71
16.15	23.42	74.50	-69.49	15.41	2.99	0.00	0.17	0.16	-0.16	52.88
27.59	27.91	74.50	-69.49	15.41	7.48	0.00	0.41	0.41	-0.41	0.10
27.65	30.40	74.50	-69.49	15.41	9.97	0.00	0.55	0.55	-0.55	7.56
										210.22
-106+75 µm		A	B	C	D	E	F	G	H	SOS
Actual (%)	Model (%)	90.30	-273.34	0.01	0.02	0.00	0.06	0.00	0.00	
		Constant	AX_1	AX_2	AX_3	AX_1X_2	AX_1X_3	AX_2X_3	$AX_1X_2X_3$	
47.41	51.56	90.30	-54.67	14.37	1.57	-0.38	1.19	1.08	-0.57	0.01
45.58	37.90	90.30	-68.33	14.37	1.57	-0.48	1.49	1.08	-0.71	0.03
25.53	24.23	90.30	-82.00	14.37	1.57	-0.57	1.79	1.08	-0.85	0.00
16.63	14.99	90.30	-82.00	5.13	1.57	-0.21	1.79	0.39	-0.30	0.01
51.97	38.08	90.30	-82.00	28.22	1.57	-1.13	1.79	2.12	-1.67	0.07
59.58	61.18	90.30	-82.00	51.32	1.57	-2.05	1.79	2.12	-3.04	0.00
19.92	23.60	90.30	-82.00	14.37	0.94	-0.57	1.07	0.65	-0.51	0.03
23.42	25.01	90.30	-82.00	14.37	2.35	-0.57	2.68	1.62	-1.27	0.00
24.44	25.79	90.30	-82.00	14.37	3.13	-0.57	3.58	2.16	-1.70	0.00
										0.16
-75 µm		A	B	C	D	E	F	G	H	SOS
Actual (%)	Model (%)	64.42	-203.69	0.00	0.02	0.01	0.09	0.00	0.00	
		Constant	AX_1	AX_2	AX_3	AX_1X_2	AX_1X_3	AX_2X_3	$AX_1X_2X_3$	
36.01	38.70	64.42	-40.74	12.99	2.02	5.14	1.83	10.46	-6.97	0.01
33.02	28.51	64.42	-50.92	12.99	2.02	6.42	2.29	10.46	-8.71	0.02
29.78	18.33	64.42	-61.11	12.99	2.02	7.70	2.75	10.46	-10.46	0.15
8.91	9.98	64.42	-61.11	4.64	2.02	2.75	2.75	3.73	-3.73	0.01
29.71	30.85	64.42	-61.11	25.51	2.02	15.13	2.75	20.54	-20.54	0.00
45.71	51.73	64.42	-61.11	46.39	2.02	27.52	2.75	37.35	-37.35	0.02
18.25	17.52	64.42	-61.11	12.99	1.21	7.70	1.65	6.27	-6.27	0.00
19.04	19.34	64.42	-61.11	12.99	3.03	7.70	4.13	15.68	-15.69	0.00
20.91	20.35	64.42	-61.11	12.99	4.04	7.70	5.50	20.91	-20.91	0.00
										0.21

Table 8-47: Model output for Fe grades

-1000+106 µm		A	B	C	D	E	F	G	H	SOS
Actual (%)	Model (%)	55.63	-23.32	0.00	0.02	0.01	0.09	0.00	0.00	
		Constant	AX_1	AX_2	AX_3	AX_1X_2	AX_1X_3	AX_2X_3	$AX_1X_2X_3$	
51.94	51.98	55.63	-4.66	-0.81	1.82	5.14	1.83	10.46	-6.97	0.00
50.90	50.81	55.63	-5.83	-0.81	1.82	6.42	2.29	10.46	-8.71	0.00
50.42	49.65	55.63	-7.00	-0.81	1.82	7.71	2.75	10.46	-10.46	0.00
50.10	50.17	55.63	-7.00	-0.29	1.82	2.75	2.75	3.73	-3.73	0.00
48.78	48.87	55.63	-7.00	-1.59	1.82	15.14	2.75	20.54	-20.54	0.00
47.18	47.57	55.63	-7.00	-2.89	1.82	27.52	2.75	37.35	-37.35	0.00
50.25	48.92	55.63	-7.00	-0.81	1.09	7.71	1.65	6.27	-6.27	0.00
50.10	50.56	55.63	-7.00	-0.81	2.74	7.71	4.13	15.69	-15.69	0.00
52.30	51.47	55.63	-7.00	-0.81	3.65	7.71	5.50	20.91	-20.92	0.00
										0.00
-106+75 µm		A	B	C	D	E	F	G	H	SOS
Actual (%)	Model (%)	49.71	16.01	0.00	0.02	0.01	0.09	0.00	0.00	
		Constant	AX_1	AX_2	AX_3	AX_1X_2	AX_1X_3	AX_2X_3	$AX_1X_2X_3$	
52.10	50.51	49.71	3.20	-4.26	1.87	5.14	1.83	10.46	-6.97	0.00
51.06	51.31	49.71	4.00	-4.26	1.87	6.42	2.29	10.46	-8.71	0.00
51.70	52.11	49.71	4.80	-4.26	1.87	7.70	2.75	10.46	-10.46	0.00
51.60	54.85	49.71	4.80	-1.52	1.87	2.75	2.75	3.73	-3.73	0.00
47.47	48.01	49.71	4.80	-8.37	1.87	15.13	2.75	20.54	-20.54	0.00
40.80	41.16	49.71	4.80	-15.22	1.87	27.52	2.75	37.35	-37.35	0.00
54.40	51.37	49.71	4.80	-4.26	1.12	7.70	1.65	6.27	-6.27	0.00
54.55	53.05	49.71	4.80	-4.26	2.80	7.70	4.13	15.68	-15.69	0.00
54.45	53.98	49.71	4.80	-4.26	3.74	7.70	5.50	20.91	-20.91	0.00
										0.01
-75 µm		A	B	C	D	E	F	G	H	SOS
Actual (%)	Model (%)	47.02	-3.11	0.00	0.05	0.01	0.09	0.00	0.00	
		Constant	AX_1	AX_2	AX_3	AX_1X_2	AX_1X_3	AX_2X_3	$AX_1X_2X_3$	
49.70	50.11	47.02	-0.62	-1.24	4.94	5.14	1.83	10.46	-6.97	0.00
50.80	49.95	47.02	-0.78	-1.24	4.94	6.42	2.29	10.46	-8.71	0.00
49.90	49.80	47.02	-0.93	-1.24	4.94	7.70	2.75	10.46	-10.46	0.00
49.74	50.59	47.02	-0.93	-0.44	4.94	2.75	2.75	3.73	-3.73	0.00
48.36	48.60	47.02	-0.93	-2.43	4.94	15.13	2.75	20.54	-20.54	0.00
46.52	46.62	47.02	-0.93	-4.41	4.94	27.52	2.75	37.35	-37.35	0.00
48.30	47.82	47.02	-0.93	-1.24	2.97	7.70	1.65	6.27	-6.27	0.00
52.25	52.27	47.02	-0.93	-1.24	7.42	7.70	4.13	15.68	-15.69	0.00
55.00	54.74	47.02	-0.93	-1.24	9.89	7.70	5.50	20.91	-20.91	0.00
										0.00

Table 8-48: Model output for SiO_2 grades

-1000+106 µm		A	B	C	D	E	F	G	H	SOS
Actual (%)	Model (%)	5.89	22.24	0.00	-0.02	0.02	0.03	0.00	0.00	
		Constant	AX_1	AX_2	AX_3	AX_1X_2	AX_1X_3	AX_2X_3	$AX_1X_2X_3$	
8.53	8.89	5.89	4.45	0.14	-1.59	13.55	0.55	3.50	-8.34	0.13
10.71	10.00	5.89	5.56	0.14	-1.59	16.94	0.68	3.50	-10.43	0.51
10.50	11.11	5.89	6.67	0.14	-1.59	20.32	0.82	3.50	-12.52	0.37
10.73	11.02	5.89	6.67	0.05	-1.59	7.26	0.82	1.25	-4.47	0.08
11.00	11.24	5.89	6.67	0.27	-1.59	39.92	0.82	6.88	-24.59	0.06
12.00	11.46	5.89	6.67	0.49	-1.59	72.58	0.82	12.50	-44.70	0.29
10.51	11.75	5.89	6.67	0.14	-0.96	20.32	0.49	2.10	-7.51	1.53
10.14	10.31	5.89	6.67	0.14	-2.39	20.32	1.23	2.10	-18.78	0.03
9.11	9.52	5.89	6.67	0.14	-3.18	20.32	1.64	2.10	-25.03	0.17
										3.16
-106+75 µm		A	B	C	D	E	F	G	H	SOS
Actual (%)	Model (%)	0.10	22.73	0.00	0.07	-0.19	-0.04	0.00	0.00	
		Constant	AX_1	AX_2	AX_3	AX_1X_2	AX_1X_3	AX_2X_3	$AX_1X_2X_3$	
9.42	9.41	0.10	4.55	3.12	6.58	-106.96	-0.81	0.00	102.83	0.00
9.31	9.32	0.10	5.68	3.12	6.58	-133.69	-1.01	0.00	128.54	0.00
9.22	9.22	0.10	6.82	3.12	6.58	-160.43	-1.21	0.00	154.25	0.00
10.11	10.56	0.10	6.82	3.12	6.58	-5.73	-1.21	-54.20	55.09	0.00
17.18	14.56	0.10	6.82	3.12	6.58	-5.73	-1.21	-298.10	302.99	0.02
17.24	18.56	0.10	6.82	3.12	6.58	-5.73	-1.21	-542.00	550.89	0.01
10.19	10.29	0.10	6.82	3.12	-0.96	0.44	-0.73	-91.06	92.55	0.00
10.97	10.66	0.10	6.82	3.12	-2.39	1.09	-1.82	-227.64	231.37	0.00
10.67	10.86	0.10	6.82	3.12	-3.18	1.45	-2.42	-303.52	308.50	0.00
										0.03
-75 µm		A	B	C	D	E	F	G	H	SOS
Actual (%)	Model (%)	11.27	1.98	0.00	-0.01	0.02	-0.68	0.00	0.00	
		Constant	AX_1	AX_2	AX_3	AX_1X_2	AX_1X_3	AX_2X_3	$AX_1X_2X_3$	
11.29	10.63	11.27	0.40	0.31	-1.34	13.54	-13.54	-31.55	0.00	0.00
10.43	10.73	11.27	0.50	0.31	-1.34	16.92	-16.92	-31.55	0.00	0.00
11.30	10.83	11.27	0.59	0.31	-1.34	20.31	-20.31	-31.55	0.00	0.00
11.40	10.63	11.27	0.59	0.11	-1.34	0.73	-20.31	-11.27	7.21	0.00
11.00	11.13	11.27	0.59	0.61	-1.34	0.73	-20.31	-61.98	39.63	0.00
11.90	11.63	11.27	0.59	1.12	-1.34	0.73	-20.31	-112.68	72.06	0.00
10.83	11.37	11.27	0.59	0.31	-0.81	0.00	-12.19	-18.93	12.11	0.00
10.41	10.16	11.27	0.59	0.31	-2.02	0.00	-30.46	-47.33	30.27	0.00
9.23	9.49	11.27	0.59	0.31	-2.69	0.00	-40.62	-63.10	40.35	0.00
										0.02

Table 8-49: Model output for Fe recovery

-1000+106 µm		A	B	C	D	E	F	G	H	SOS
Actual (%)	Model (%)	100.88	-279.44	-0.01	-0.29	0.00	-0.13	0.00	0.00	
		Constant	AX_1	AX_2	AX_3	AX_1X_2	AX_1X_3	AX_2X_3	$AX_1X_2X_3$	
56.34	54.67	100.88	-55.89	-25.06	-28.91	-1.36	-2.64	38.96	28.69	2.79
43.53	46.87	100.88	-69.86	-25.06	-28.91	-1.70	-3.29	38.96	35.86	11.17
40.75	39.08	100.88	-83.83	-25.06	-28.91	-2.03	-3.95	38.96	43.03	2.79
13.80	17.11	100.88	-83.83	-8.95	-28.91	-0.73	-3.95	13.91	28.69	10.93
49.95	43.34	100.88	-83.83	-49.23	-28.91	-4.00	-3.95	76.52	35.86	43.74
66.26	69.57	100.88	-83.83	-89.51	-28.91	-7.27	-3.95	139.13	43.03	10.93
18.40	19.43	100.88	-83.83	-25.06	-17.35	-2.03	-2.37	23.37	25.82	1.05
31.44	28.57	100.88	-83.83	-25.06	-43.37	-2.03	-5.93	23.37	64.54	8.21
31.81	33.65	100.88	-83.83	-25.06	-57.83	-2.03	-7.91	23.37	86.06	3.39
										95.01
-106+75 µm		A	B	C	D	E	F	G	H	SOS
Actual (%)	Model (%)	0.10	1.00	0.01	0.10	0.02	0.10	0.00	0.00	
		Constant	AX_1	AX_2	AX_3	AX_1X_2	AX_1X_3	AX_2X_3	$AX_1X_2X_3$	
55.16	56.37	0.10	0.20	23.19	9.96	13.95	2.00	41.19	-34.21	0.00
54.19	51.86	0.10	0.25	23.19	9.96	17.44	2.50	41.19	-42.77	0.00
46.48	47.34	0.10	0.30	23.19	9.96	20.92	3.00	41.19	-51.32	0.00
18.80	18.77	0.10	0.30	8.28	9.96	0.75	3.00	14.71	-18.33	0.00
56.42	39.76	0.10	0.30	45.56	9.96	0.75	3.00	80.90	-100.81	0.09
56.92	60.75	0.10	0.30	82.83	9.96	0.75	3.00	147.09	-183.28	0.00
24.85	25.74	0.10	0.30	23.19	5.98	0.45	1.80	24.71	-30.79	0.00
28.81	28.95	0.10	0.30	23.19	14.94	1.12	4.49	61.78	-76.98	0.00
30.28	30.74	0.10	0.30	23.19	19.92	1.49	5.99	82.37	-102.64	0.00
										0.10
-75 µm		A	B	C	D	E	F	G	H	SOS
Actual (%)	Model (%)	-5.40	0.99	0.01	0.52	0.04	-1.68	0.00	0.00	
		Constant	AX_1	AX_2	AX_3	AX_1X_2	AX_1X_3	AX_2X_3	$AX_1X_2X_3$	
44.22	39.90	-5.40	0.20	20.59	51.80	23.02	-33.65	-16.66	0.00	0.01
42.64	37.29	-5.40	0.25	20.59	51.80	28.78	-42.06	-16.66	0.00	0.02
37.24	34.68	-5.40	0.30	20.59	51.80	34.54	-50.47	-16.66	0.00	0.00
11.15	11.15	-5.40	0.30	7.35	51.80	1.23	-50.47	-5.95	12.29	0.00
35.91	35.91	-5.40	0.30	40.45	51.80	1.23	-50.47	-32.72	30.73	0.00
52.47	52.47	-5.40	0.30	73.54	51.80	1.23	-50.47	-59.49	40.98	0.00
21.42	21.18	-5.40	0.30	23.19	31.08	0.00	-30.28	-10.00	12.29	0.00
24.91	25.81	-5.40	0.30	23.19	77.69	0.00	-75.71	-24.99	30.73	0.00
29.19	28.39	-5.40	0.30	23.19	103.59	0.00	-100.95	-33.32	40.98	0.00
										0.03

Table 8-50: Model output for SiO_2 recovery

-1000+106 µm		A	B	C	D	E	F	G	H	SOS
Actual (%)	Model (%)	50.33	-139.03	-0.01	-0.01	0.02	-0.26	0.00	0.00	
		Constant	AX_1	AX_2	AX_3	AX_1X_2	AX_1X_3	AX_2X_3	$AX_1X_2X_3$	
29.43	30.12	50.33	-27.81	-33.92	-0.86	10.19	0.07	19.79	12.34	0.47
30.19	28.82	50.33	-34.76	-33.92	-0.86	12.74	0.08	19.79	15.42	1.89
26.83	27.51	50.33	-41.71	-33.92	-0.86	15.29	0.10	19.79	18.50	0.47
9.70	16.68	50.33	-41.71	-12.12	-0.86	15.29	-7.93	7.07	6.61	48.65
36.32	23.69	50.33	-41.71	-66.64	-0.86	15.29	-7.93	38.87	36.34	159.32
53.75	30.71	50.33	-41.71	-121.16	-0.86	15.29	-7.93	70.67	66.08	530.74
6.01	7.69	50.33	-41.71	-33.92	-0.52	15.29	-4.76	11.87	11.10	2.82
21.12	16.42	50.33	-41.71	-33.92	-1.30	15.29	-11.90	11.87	27.75	22.08
18.25	21.27	50.33	-41.71	-33.92	-1.73	15.29	-15.87	11.87	37.01	9.12
										775.56
-106+75 µm		A	B	C	D	E	F	G	H	SOS
Actual (%)	Model (%)	0.09	0.99	0.01	0.21	-0.24	-0.34	0.00	0.00	
		Constant	AX_1	AX_2	AX_3	AX_1X_2	AX_1X_3	AX_2X_3	$AX_1X_2X_3$	
28.89	29.13	0.09	0.20	17.52	20.65	-136.50	-6.86	-0.01	134.05	0.00
27.28	26.85	0.09	0.25	17.52	20.65	-170.62	-8.57	-0.02	167.56	0.00
24.40	24.57	0.09	0.30	17.52	20.65	-204.75	-10.28	-0.02	201.07	0.00
12.55	8.38	0.09	0.30	6.26	20.65	-7.31	-10.28	-73.13	71.81	0.11
63.99	30.60	0.09	0.30	34.41	20.65	-7.31	-10.28	-402.21	394.96	0.27
70.61	52.82	0.09	0.30	62.57	20.65	-7.31	-10.28	-731.30	718.11	0.06
12.98	17.52	0.09	0.30	17.52	12.39	-4.39	-6.17	-122.86	120.64	0.12
16.68	16.94	0.09	0.30	17.52	30.97	-10.97	-15.42	-307.14	301.60	0.00
14.47	16.62	0.09	0.30	17.52	41.29	-14.62	-20.57	-409.53	402.14	0.02
										0.59
-75 µm		A	B	C	D	E	F	G	H	SOS
Actual (%)	Model (%)	0.09	0.99	0.00	0.12	-0.02	-0.29	0.00	0.00	
		Constant	AX_1	AX_2	AX_3	AX_1X_2	AX_1X_3	AX_2X_3	$AX_1X_2X_3$	
24.72	24.80	0.09	0.20	13.56	12.47	-8.75	-5.75	0.00	12.99	0.00
24.64	24.47	0.09	0.25	13.56	12.47	-10.94	-7.19	0.00	16.24	0.00
24.06	24.14	0.09	0.30	13.56	12.47	-13.13	-8.63	0.00	19.49	0.00
7.29	7.32	0.09	0.30	4.84	12.47	-0.47	-8.63	-8.24	6.96	0.00
23.93	23.33	0.09	0.30	26.63	12.47	-0.47	-8.63	-45.34	38.28	0.00
38.55	39.34	0.09	0.30	48.41	12.47	-0.47	-8.63	-82.43	69.60	0.00
14.07	14.09	0.09	0.30	13.56	7.48	0.00	-5.18	-13.85	11.69	0.00
14.37	14.31	0.09	0.30	13.56	18.71	0.00	-12.95	-34.62	29.23	0.00
14.40	14.44	0.09	0.30	13.56	24.94	0.00	-17.26	-46.16	38.98	0.00
										0.00